Water Vapour from Observations of the German Geodetic GPS Reference Network (GREF)

M. Becker, G. Weber
Bundesamt fur Kartographie und Geodäsie, Frankfurt a. M., Germany

C. Köpken
German Weather Service (DWD), Offenbach

SUMMARY

Since middle of 1996 the BKG computes daily solutions for a set of German and European permanent GPS stations using the Bernese software. The EUREF permanent network is to be densified by a set of up to twenty stations in Germany currently under installation. Presently about twelve stations are operating. Results for a subset of the EUREF network from the BKG processing center are submitted to the EUREF Analysis Center in Bern to be included to the European weekly EUREF solution. The BKG processing is used further to produce sets of tropospheric zenith delay parameters in two hour intervals. These are combined and compared to the Wettzell Water Vapour Radiometer of BKG operating since October 1997. In a joint research project with the German Weather Service the potential use of the vertically integrated water vapour (IWV) content as derived from the tropospheric zenith delay for the improvement of numerical weather forecasts is studied. As a first step, the derived GPS-IWV is compared to IWV derived from weather forecast models and the influence of ancillary numerical model data used in the derivation of GPS IWV is studied. This is a summary of the main objectives based on the slides of the IGS Analysis Center Workshop 1998, Darmstadt, 9-11 Feb. 1998

1. Verification of DWD Weather Forecasts

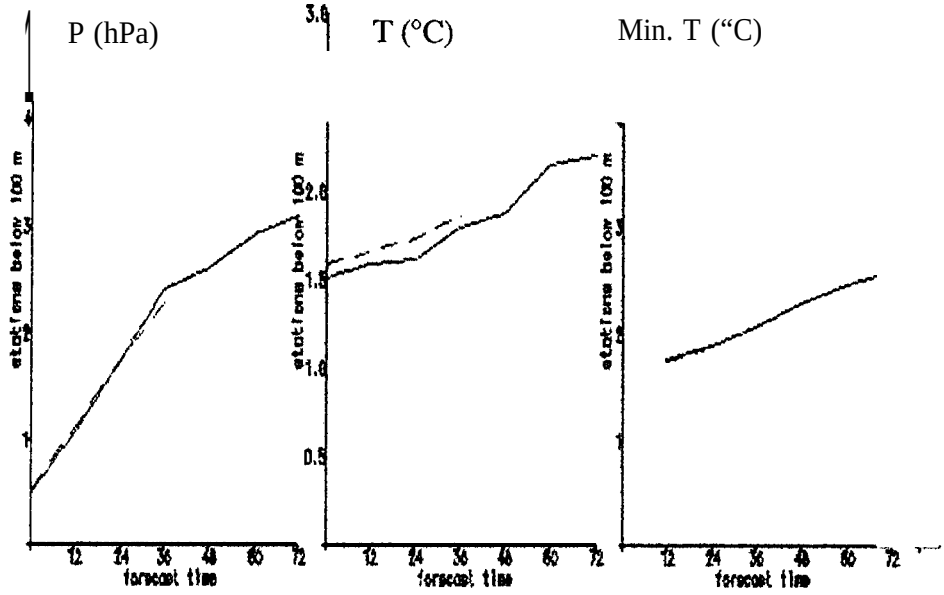

Fig. 1. RMS differences of predicted values to ground truth.

2. CALCULATION OF VERTICALLY INTEGRATED WATER VAPOUR

Integrated vertical water vapour from numerical weather prediction model (NWP):

$$IWV = \int_0^{ztop} \rho_{VAP} \cdot dz \quad [kg/nZ']; \qquad dp = -\rho_{WET} \cdot g \cdot dz$$

$$IWV = -\frac{1}{g} \int_{p_s}^{ptop} q \cdot dp \;;$$

ρ_{vap} = *density of water vapor;*

z_{top} = *height of upper model edge*

$\rho_{wet} = \rho_{DRY} + \rho_{VAP}$, *density of wet air*

ptop = pressure at upper edge of model;

p_s = *bottom pressure*

$q = \frac{\rho_{VAP}}{\rho_{WET}}$ *specific humidity of water vapor given in the model*

Integrated precipitable water:

$$IPW = \frac{1}{\rho_W} \cdot IWV \qquad [m]; \; \rho_w = \text{density of water}$$

3. GREF-*PERMANENT*

. Establishing of GPS permanent stations in Germany for daily analysis since 1996

. Currently 15 stations in Germany

. Intention

- Integration in European Reference System
- Densification for Germany
- Support of DGPS activities
- Near real time station control

4. WEEKLY BKG SOLUTION, EUREF PART, GPS-WEEK 0930

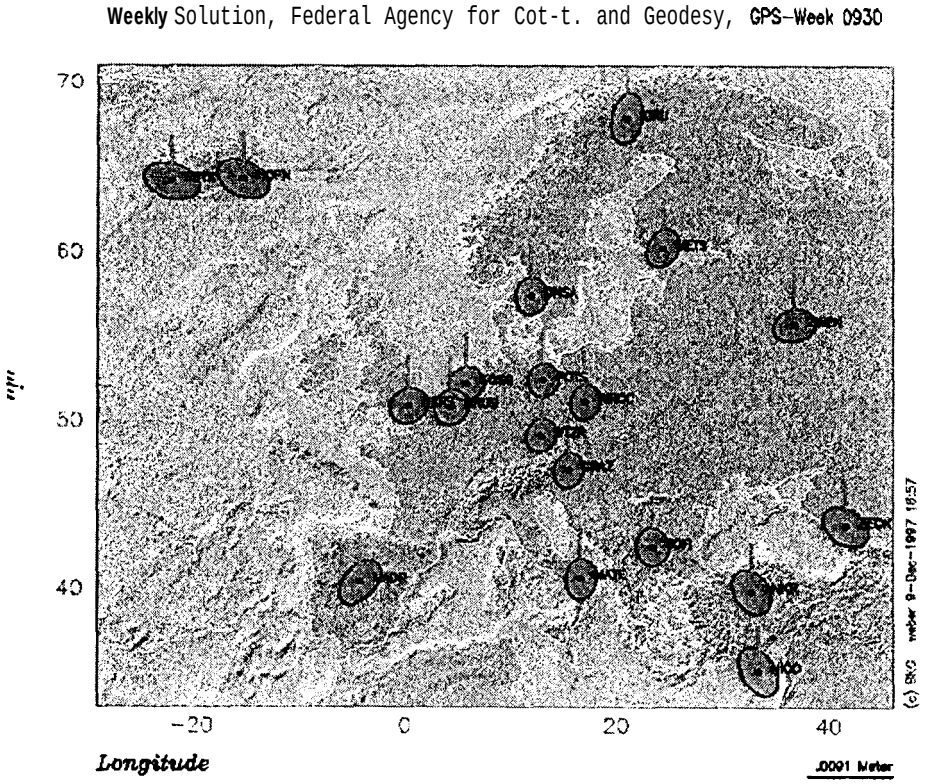

5. DAILY BKG SOLUTION, GREF PART, DAY 97306

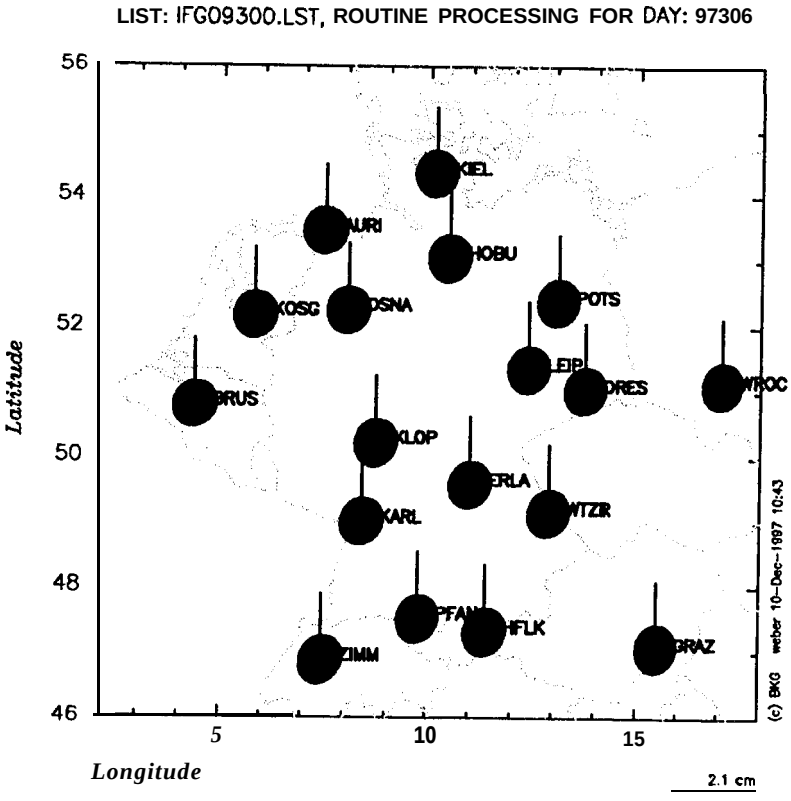

6. GREF PROCESSING FOR IPWV

- Presently 32 stations with 2 h interval Tropospheric Zenith Delay Estimation
  Problem: On] y few met-sensors

- Surface pressure and surface temperature from NWP

- GPS Zenith Path Delay:
  ZWD (GPS) = ZTD - ZHD = Total Delay - Hydrostatic Delay
  ZHD = $f(p_s)$, p,= Measured/Model

- Integrated Precipitable Water IPW
  IPW = Π * ZWD; $\Pi = f(T_m)$, T_m by Regression of Ts

- B KG routine processing problems before optimization of troposphere estimation:
  - bias
  - addition of global stations
  - use of WVR data

7. BKG WATER VAPOUR RADIOMETER

3 WVR'S supplied to BKG by ETH Zurich

. WVR recording permanently at WETTZELL
  - data provided to IGS after software revision
. WVR for experiments t.b.d.
• WVR for TIGO missions

8. ZPD FROM GPS AND WVR

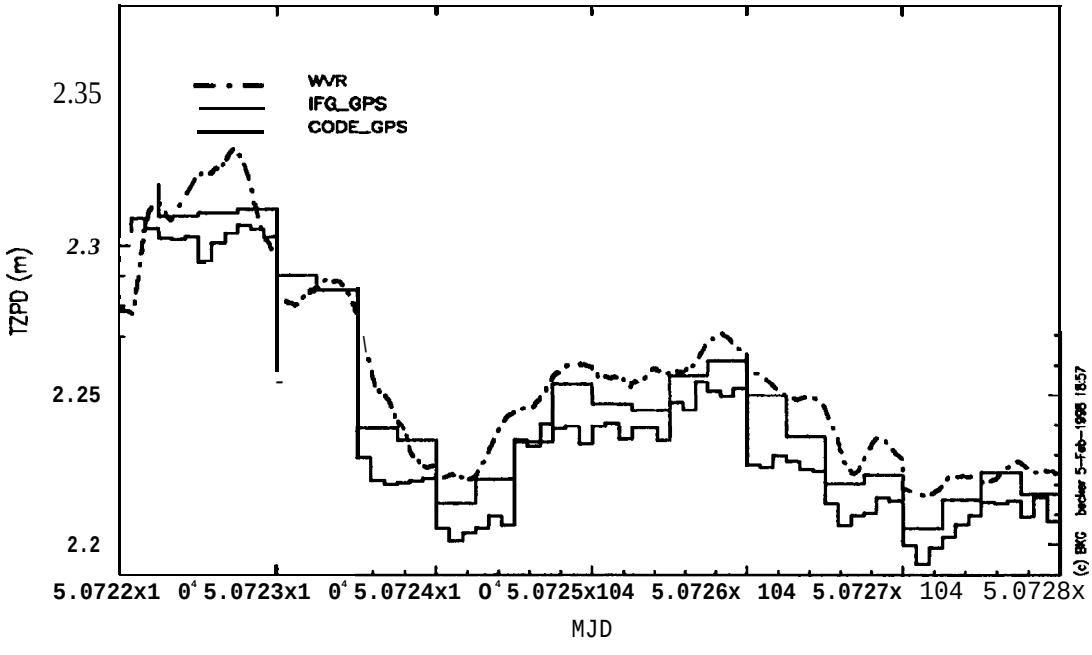

9. STATUS OF THE EXPERIMENT AND OUTLOOK

- Data extraction and formatting from NCM
- GPS test computations in the GREF Network
- Reprocessing of WVR Data with improved software
- Numerical results to be presented at EGS-98 conference

- Met-Packages for GREF stations
- Integration of WVR data and ZPD estimation procedures in routine analysis
- Study of numerical weather prediction with near real time requirements for ZPD availability

ESTIMATING HORIZONTAL GRADIENTS OF TROPOSPHERIC PATH DELAY WITH A SINGLE GPS RECEIVER

Yoaz E Bar-Sever[1], Peter M. Kroger[1] and Jorgen A. Borjesson[2]

'Jet Propulsion Laboratory, California Institute of Technology
[2]Onsala Space Observatory, Chalmers University of Technology, Sweden

(in press, ***Journal** of **Geophysical Research, 1998***)

ABSTRACT

We **present evidence that modeling troposphere delay gradients in precise GPS geodesy improves the accuracy and precision** of the estimated quantities, and that the estimated gradients resemble real atmospheric moisture gradients observed with a water vapor radiometer (WVR). Using a low elevation angle cutoff, combined with a model of the atmospheric delay gradient as a random walk process leads to 19.5% and 15% average improvement in radial and horizontal site position repeatabilities, respectively, relative to a current state-of-the-art estimation strategy that does not model horizontal gradients and imposes high elevation angle cutoff. The agreement between estimated values of zenith wet delay from collocated GPS receivers and WVRS was improved by at least 25%. Merely lowering the elevation angle cutoff improves the repeatability of the radial component of the site's position vector but tends to degrade the repeatability of the horizontal components of the position vector if troposphere gradients are not properly modeled. The estimates of wet delay gradients from a collocated GPS receiver and a WVR at Onsala, Sweden, seem to be correlated over timescales as short as 15 min (Figure 1). The agreement in azimuth between the GPS-based and the WVR- based gradients was at the 10° level, for significant gradients. The GPS was found to under-estimate the magnitude of the gradients by about 60% relative to the WVR-based gradients. The ability to sense atmospheric moisture gradients from a single GPS receiver increases the useful information content from networks of GPS receivers by providing additional spatial information for weather forecasting applications.

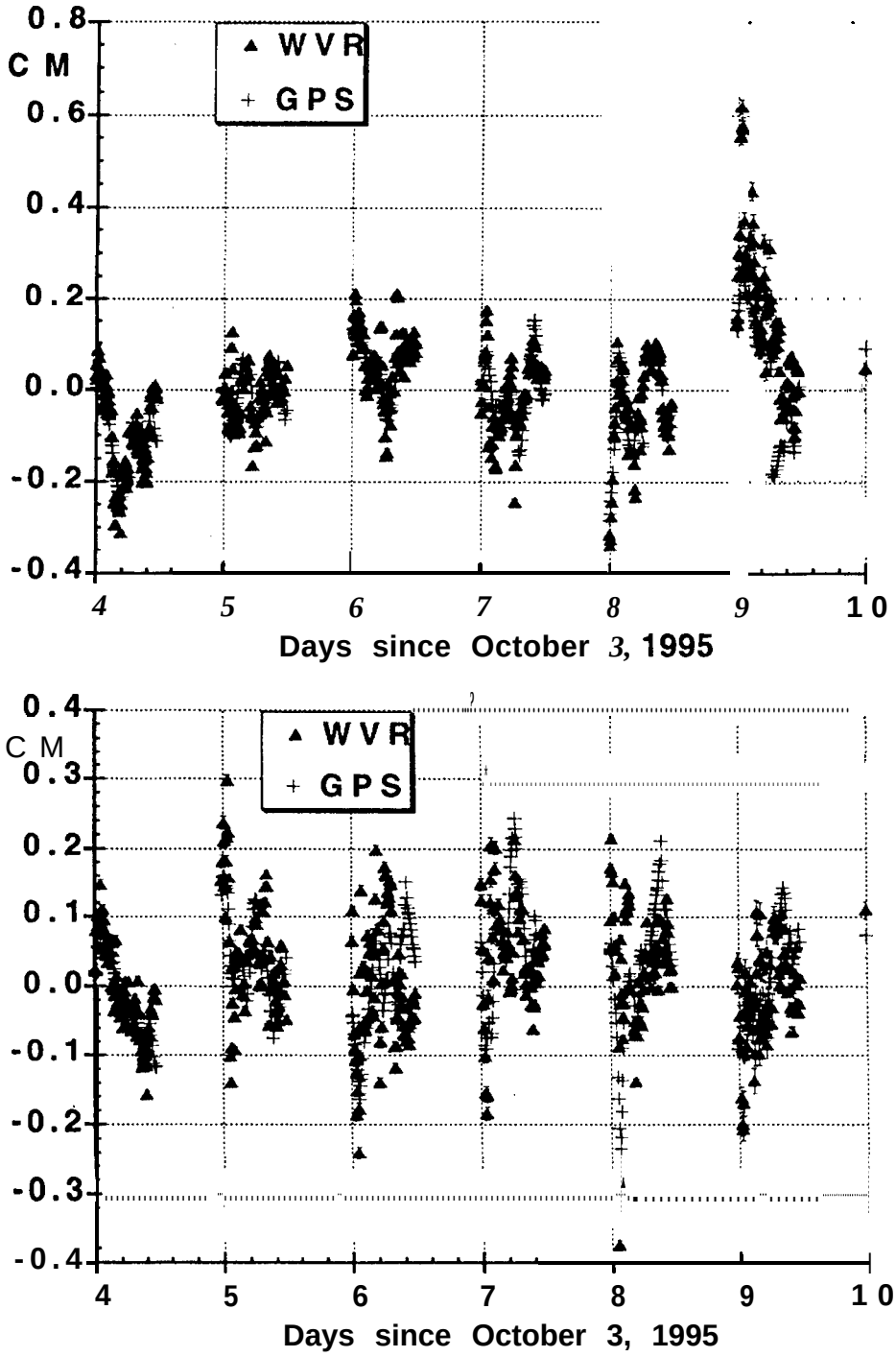

Figure 1. GPS- and WVR-based estimates of north component of the gradient vector, G_N (top), and the east component, G_E(bottom), for 6 12-hour segments during October 1995. Note, the bias between the GPS and the WVR estimates for each segment was removed. Only 6 segments are shown for clarity. Other segments are similar.

IGS PRODUCTS FOR THE IONOSPHERE

J. Feltens
EDS Industrien (Deutschland) GmbH, based at
Flight Dynamics Division,
ESA, European Space Operations Centre,
Robert-B osch-Str. 5, D-64293 Darrnstadt, Germany

S. Schaer
Astronomical Institute, University of Berne,
Sidlerstr. 5, CH-3012 Berne, Switzerland

ABSTRACT

In June 1992 the International GPS Service for Geodynamics (IGS) started with the routine provision of precise GPS orbits and earth orientation parameters. In the meantime other products were included into the product palette: rapid orbits, predicted orbits, GPS satellite clock information, station coordinates and velocities (SINEX), and station-specific tropospheric zenith delays.

For a long time the IGS community has been well aware of the fact that the world-wide IGS network offers a unique opportunity to extract ionospheric information on a global scale. At the IGS workshops held in Potsdam in May 1995 and in Silver Spring in March 1996, sub-sessions were dedicated to the ionosphere. Main subject of the ionosphere sub-session in Silver Spring in March 1996 was an intercomparison of ionosphere products provided by several Analysis Centers in order to get an idea of the accuracies that can be achieved. In addition it was identified for the first time, which Analysis Centers are interested to contribute to an IGS ionosphere product.

Since 1996 considerable progress in ionosphere modeling has been achieved at the different Analysis Centers. Today most centers are able (or close to that state) to provide ionosphere information on a routine basis. An official format for the exchange of ionosphere maps, called IONEX, has been developed and approved. It was the main task of the 1998 IGS Workshop to prepare the start of a coordinated routine processing and a combination of future IGS ionosphere products,

INTRODUCTION AND MOTIVATION

Since mid 1996 we are approaching the next solar maximum. Therefore good and fast knowledge about the ionosphere's actual state becomes increasingly important: Users of satellite navigation systems need accurate corrections to remove signal degradation caused by the ionosphere, information on the ionosphere's behavior is of great importance for radio

signal propagation applications, scientists will benefit from up-to-date and long-term ionosphere information, as well. ESOC is, for instance, interested to use IGS ionosphere maps to support other ESA missions, like ERS and ENVISAT.

As part of the IGS activities GPS dual-frequency data are collected from a global net of ground stations for years. Due to the fact that the ionosphere is a dispersive medium for microwave signals, dual-frequency GPS data provides thus a direct measure of the ionosphere's activity and can be used to extract global ionospheric information.

Since 1992 the IGS Analysis Centers demonstrate that they are capable to routinely determine orbits, earth orientation and rotation parameters, and other parameters of geophysical interest. In principle, it is a small step for them to derive ionospheric parameters on a regular basis - provided special software for ionosphere modeling is available.

The main motivation for the IGS to get involved in regular ionosphere modeling and mapping is a continuous monitoring of the ionosphere for (at least) the next period of high solar activity and to study in particular the impact of the ionosphere on the "traditional" IGS products (IGS core products).

REVIEW OF IONOSPHERE IGS ACTIVITIES SINCE MARCH 1996

Several of the Analysis Centers participating in the IGS have experience with the evaluation of ionospheric parameters from dual-frequency GPS data and develop corresponding software. Institutions, which do currently not contribute to the IGS with products (like orbits, etc.) but indicated their willingness to contribute routinely to IGS ionosphere products, will be denoted as "Analysis Centers", as well, below. Table 1 gives an overview over all Analysis Centers involved and provides detailed information about their ionosphere modeling.

Looking back over the preceding two years, it can be noticed positively that some of the Analysis Centers have achieved considerable progress and improvement in their ionosphere processing. And, as reaction on an e-mail inquiry initiated in preparation to this 1998 workshop, new Analysis Centers have manifested their interest to enter into future IGS ionosphere activities. It must be noticed, however, that most ionosphere-related efforts of the Analysis Centers dealt with internal improvements. Apart from the intercomparison of ionosphere maps and differential code biases, performed as a part of the 1996 IGS workshop session, and the definition and approval of the so-called Ionosphere Map EXchange Format (IONEX) (Schaer et al., 1997), no significant contributions to a common IGS activity could be registered.

Many Analysis Centers are ready to participate in a routine IGS ionosphere service or are being very close to do so. Therefore, in principle it should only be a small step to start with a routine provision of ionosphere products within the IGS.

POTENTIAL PARTICIPANTS IN A ROUTINE IGS SERVICE FOR IONOSPHERE PRODUCTS

In order to get an overview over the possible participants and their individual ionosphere products, an inquiry via e-mail was initiated prior to the 1998 workshop. The reactions on this inquiry are condensed in the following table:

Analysis Center	CODE	DLR	ESOC	JPL	NOAA	NRCan	ROB	UNB	UPC	WUT
IGS Analysis Center ?	yes	no	yes	yes	yes	yes	no	no	no	no
Extent of ionosphere maps	global & regional (Europe)	regional (Europe)	global	global	regional (US) + global (planned)	regional (Canada) + global (planned)	regional (Belgium)	regional + global (planned)	global	regional
Temporal resolution	24h/2h in preparation	1h	24h	15m	24h	24h	15m		1h	
Observable(s) used	doubly differenced phase or carrier phase leveled to code	carrier phase leveled to code	carrier phase leveled to code	carrier phase leveled to code	GPS phase information	carrier phase leveled to code	carrier phase leveled to code	carrier phase leveled to code	carrier phases and differences	doubly differenced phase
Shell height	400 km	400 km	450 km for 2-d models	450 km		350 km		400 km and calculated from IRI		400 km
Elevation Swell angle	10°	10°	20"	10°		15°				15°
evati ependent observation weighting			yes	yes		yes				
TEC representation	spherical harmonics, n= 12, m = 8	NTCM model	2-d GE-functtions & 3-d Chapman profile models	composition of local basis functions	specific models		Station-specific profil	spatial linear approximation	3-d tomography models	spherical harmonics, n,m = 3
Grid width	2.5°	2.5°/5°	2.5°			3°				2.5°
Differential sods biases	yes	yes	yes	yes	no	yes	yes	lsa	no	no
Reference frame internally used	sun-fixed / geographic		sun-fixed / geomagnetic	sun-fixed / geomagnetic		sun-fixed / geographic		sun-fixed / geomagnetic	sun-fixed	sun-find
Mapping function	1/cosZ	1/cosZ	1/cosZ, integrated in Chapman profile models	elevation scaling function based on extended slab model		1/cosZ		1/cosZ		1/cosZ
Single layer shape	spherical		spherical for 2-d models			spherical		spherical		spherical
IONEX format implemented ?	yes	in preparation	yea	in preparation		planned		planned		yes
Ready for routine processing ?	yes	yes	yes	yes	planned	regional: yes global: planned				yes

Analysis Center	CODE	DLR	ESOC	JPL	NOAA	NRCan	ROB	UNB	UPC	WUT
RMS maps provided ?	yes		planned							no
Delay of availability	rapid: 12^h, final: 4^d	2^d	final: 11^d rapid: planned	3^d						

Table 1: Potential participants and their ionosphere products.

The Analysis Center identifiers are in alphabetical order:
CODE (AIUB): Center for Orbit Determination in Europe, Berne, Switzerland,
DLR: DLR/DFD Femerkundungsstation Neustrelitz, Germany,
ESOC: ESA/European Space Operations Centre, Darmstadt, Germany,
JPL: Jet Propulsion Laboratory, Pasadena, CA, U.S.A.,
NOAA: National Oceanic and Atmospheric Admiitration, Silver Spring, U.S.A.,
NRCan (EMR): Natural Resources Canada, Ottawa, Ontario, Canada,
ROB: Royal Observatory of Belgium, Brussels, Belgium,
UNB: University of New Brunswick Fredericton, N.B., Canada,
UPC: Politechnical University of Catalonia, Barcelona, Spain,
WUT: Warsaw University of Technology, Warsaw, Poland.

A blank field indicate-s that no information is available for the Analysis Center.
The University of New Brunswick (uN'B), Fredericton, N. B., Canada, intends (at least in the near future) to contribute with intercomparisons of technique-s and scientific findings rather than with routine ionosphere products.

Table 1 shows that the number of methods of ionospheric modeling corresponds to the number of Analysis Centers!

POTENTIAL USERS OF IGS IONOSPHERE PRODUCTS

When developing IGS ionosphere products, potential users of such ionosphere products should be specified. Ionospheric electron density models are of greatest interest to GPS/GLONASS users with single-frequency receivers. The same information may of course be used for other than GPS/GLONASS satellite tracking data, too. Regular information on ionospheric conditions may also be helpful in other fields of radio signal propagation and for scientific interpretation of phenomena in the high atmosphere, the magnetosphere, and solar activity.

Depending on the interests of different users, different kinds of ionosphere products are required. Users may be grouped into two categories:

1) Users interested in fast access to up-to-date ionosphere information, but do not require highest accuracy. We think, e.g., of geodetic survey, navigation applications, road and shipping transport companies. Ionosphere models are only of interest to obtain reasonable corrections for tracking data.

TOWARDS A COMBINED IGS IONOSPHERE PRODUCT

From Table 1 we can see that ten Analysis Centers are prepared to contribute with ionosphere products to the IGS. The analysis procedures are well established at each center, and they differ considerably. We conclude that it does not make sense for the IGS to come up with very stringent requirements concerning the generation of such products. The IGS should, however, define minimum standards, formats, and deadlines for product delivery. These are the basic considerations underlying the following recommendations which emerged from the Darmstadt workshop:

Recommendations

(1) Initially, the IGS should focus on two kinds of products:
(a) TEC maps in grid form and
(b) differential code biases (DCBs).

(2) IGS TEC maps are global maps. Only global maps will be compared and perhaps combined. This policy may be reviewed after one year of pilot operations.

(3) All TEC maps must be delivered to the IGS in the IONEX format [Schaer et al., 1998]. TEC maps delivered to the IGS thus are "snapshots" of the electron density referring to a particular epoch and to an earth-fixed reference frame.

(4) Global TEC maps from each contributing Analysis Center are given the name *cccGddd0.yyI*, where ccc is a 3-figure acronym for the AC (in uppercase), " G" says that this file contains global maps, *ddd* is the day of the year, " O" indicates a daily file, *yy* specifies the 2-digit year, and the last letter "1" stands for "ionosphere maps". Example: *CODG0410*.981 (or *CODG0410.98I.Z*). These files are {compressed} and sent to the IGS Global Data Centers and are available to the interested user. Access Fortran routines are also made available.

(5) The daily IONEX file, as produced by an IGS Analysis Center, should have a 2-hour resolution referring to the epochs *01*, 03, ... 23 *hours UT*. RMS files corresponding to the 2-hourly TEC maps may be included in the IONEX files. TEC/RMS maps refer to a two-dimensional grid in a single layer. The height of the single layer should be 450 *km* adopting a base radius of *6371 km*. The latitude ranges from 87.5 to -87.5 degrees in steps of -2.5 degrees; the longitude ranges from -180 **to** *180 degrees in* steps of **5** *degrees*. TEC/RMS values have to be given in units of 0.1 *TECU*.

(6) Daily sets of differential code biases (DCBs) for the GPS satellites are recommended to be included in IONEX files. The exchange of satellite-specific DCBS is IONEX-supported, too. Note that the DCB reference may be chosen arbitrarily and can be taken into account in the combination procedure.

2) Scientists interested in highly accurate ionosphere models. To get precise ionosphere information, this group will accept time delays in having ionosphere products available. Scientists have already signalized their interest in an IGS ionosphere product.

We assume that the majority of potential users will belong to the first category.

PROGRESS MADE AT THE 1998 WORKSHOP

The ionosphere sub-session started with the presentation of the position paper prepared by S. Schaer and J. Feltens. Thereafter contributions covering different aspects relevant for the development of an IGS ionosphere product followed:

- R. Warnant from ROB presented results of a study dealing with the short-term resolution of TEC and its irregularities from GPS data in a regional network.

- N. Jakowski from DLR Neustrelitz reported about their monitoring of the ionosphere over Europe using a model developed at Neustrelitz and discussed its applicability to related ionosphere studies.

- J. Feltens from ESOC presented the basics of a mathematical model to describe the TEC with a 3-d "Chapman profile approach", together with first results obtained - a first attempt in the direction of a 3-d TEC map establishment.

- R. Leitinger from TU Graz pointed out the importance of GPS in ionospheric monitoring, mapping, and nowcasting for atmospheric research. He also pointed out that regional differences are considerable. Nevertheless there is a clear interest in global ionospheric models.

- **S. Schaer from AIUB showed long-time series of global TEC parameters and demonstrated that it is possible to predict the parameters of CODE ionosphere maps.**

The above presentations and the subsequent discussion revealed that there is a great interest of the ionosphere community in a continuous series of global IGS ionosphere models. However, some of the above presentations indicated that many activities in the ionosphere community are regional in nature. Nevertheless, it was decided that the IGS (at least in a first phase) should stay out of regional ionosphere modeling, but should rather focus on global aspects.

In summary it can be said that the authors and the interested institutions are convinced that the development of an IGS ionosphere product is an important task. A continuous series of IGS TEC maps should be produced at least over one full 1 l-year cycle of solar activity. It is of particular importance that the IGS TEC maps are covering the next period of maximum solar activity (years 2000-2003).

GOALS AND NEXT STEPS

For the near future (about two years) we see the following goals:

(1) Global ionosphere maps (TEC maps) including satellite-specific differential code biases (DCBs) from contributing Analysis Centers are made available in IONEX format through the IGS Global Data Centers. The start of the pilot ionosphere service is scheduled for June 28, 1998 (GPS week 964).

(2) Minimum analysis and performance standards are prescribed:
- **Minimum analysis standards are listed in recommendation (5), above.**
- **Ionosphere products are made available not later than the IGS Final Orbits and EOPS, i.e., 11 days after the observations.**

(3) TEC maps and DCB values as produced by individual Analysis Centers are compared by the "IGS Ionosphere Coordinating Center". A weekly report has to be produced.

(4) Individual TEC maps and DCB sets are combined into a preliminary "IGS Combined Ionosphere Product". The weekly report now contains also "rms values" relative to the combined product.

(5) Deadlines for ionosphere product delivery after at least six months of pilot service are reviewed. Define an "IGS Rapid Ionosphere Product".

(6) An "IGS Ionosphere Model" based on the available combined (or individual) time series of IGS ionosphere maps (IGS TEC maps) is developed.

In order to accomplish these goals we propose to establish an "IGS Ionosphere Working Group" proceeding as follows:

- Terms of Reference for the "IGS Ionosphere Working Group":

  A draft for these Terms of Reference will be developed jointly by the authors of this position paper, and, as agreed upon at the Darmstadt Governing Board Meeting, by Gerhard Beutler and John Dow.

- Membership:

  This group should contain representatives of those Analysis Centers which will (with utmost certainty) contribute to the "IGS Ionosphere Service". The list of names will be provided by those IGS parties which intend to participate in the "ionosphere club".

  From the ionosphere research community representatives will be

  Norbert Jakowski (DLR Neustrelitz),

  Reinhard Leitinger (TU Graz),

  and, as IGS Analysis Center Coordinator,

  Jan Kouba.

  Further participation will be called for through an IGS-mail message (see below).

- Chairperson:

The **IGS** Governing Board will appoint the first chairperson for the IGS Ionosphere Working Group.

- Announcement, call for participation:

  The establishment of the IGS Ionosphere Working Group containing the Terms of Reference, the goals, the next steps, and the list of WG members is published through IGS mail. Further participation is sought in this message. The working group should not have more than 20 members.

- Time frame:

  The IGS Ionosphere Working Group should be formally established at the IGS GB Meeting of May 28, 1998 in Boston. This implies that

  - draft Terms of Reference for the IGS Ionosphere Working Group and

  - draft IGS message containing information and a call for further participation

  must be available not later than May 7, 1998 for distribution to the IGS Governing Board.

REFERENCES

Feltens, J., 1996a, Ionosphere Models - A New Product of IGS ? IGS Position Paper, IGS Analysis Center Workshop, Silver Spring, MD, U. S.A., March 19-21, 1996.

Feltens, J., 1996b, Ionosphere Maps - A New Product of IGS ? IGS Summary, in ***Proceedings of the 1996 IGS Analysis Center Workshop,*** Silver Spring, MD, U.S.A., March 19-21, 1996, pp 177-180.

Schaer, S., W. Gurtner, and J. Feltens, 1997, IONEX: The Ionosphere Map EXchange Format Version 1, February 25, 1998, in ***Proceedings of the 1998 IGS Analysis Centers Workshop,*** **ESOC, Darmstadt,** Germany, February 9-11, 1998.

IONEX: The ionosphere Map EXchange Format Version 1

Stefan Schaer, Werner Gurtner
Astronomical Institute, University of Berne, Switzerland
stef an. schaer@aiub. unibe. ch

Joachim Feltens
ESA/ESOC, Darmstadt, Germany

February 25, 1998

Introduction

The International GPS Service for Geodynamics (IGS) provides precise GPS orbits, earth orientation parameters (EOPs), station coordinates, satellite clock information, and – on a test basis – tropospheric zenith delays. The IGS community is well aware of the fact that the IGS network can also be used to extract information about the total electron content (TEC) of the ionosphere on a global scale. One may expect that the IGS will include TEC maps into its product palette in the near future.

As part of the 1996 IGS Workshop in Silver Spring, a first effort has been made to compare GPS-derived TEC maps produced by IGS Analysis Centers (CODE and ESA/ESOC) as well as external processing centers (DLR Neustrelitz and University of New Brunswick) [Feltens, 1996a]. For this purpose, a very simple data exchange format proposed by Wilson (JPL) has been used.

One essential conclusion of the ionosphere-related discussion was that a common data format to exchange, compare, or combine TEC maps has to be defined. Based on a first format proposal by [Schaer, 1996], which strongly follows the Receiver INdependent EXchange format (RINEX) [Gurtner and Mader, 1990], [Schaer and Gurtner, 1996], and [Feltens, 1996b], we present a revised version of the so-called Ionosphere map EXchange format (1 ONEX) that supports the exchange of 2- and 3-dimensional TEC maps given in a geographic grid.

The most important modifications with respect to [Schaer and Gurtner, 1996] are:

- Ionosphere maps given in an earth-fixed reference frame are supported only.
- Ionosphere maps are epoch-specific, i. e., they have to be interpreted as "snapshots" at certain epochs. Guidelines how to use IONEX TEC maps are formulated in the next sect ion.
- in addition to TEC and RMS error maps, single-layer height maps are allowed, too.
- The option of 3-dimensional TEC maps has been included into IONEX, i. e., multi-layer models may be handled very easily by performing an additional loop over an equidistant height grid.
- TEC values are written using format m15 instead of m (Xl, 14). The definition of an exponent (see "EXPONENT") should help to cover the necessary dynamic range of electron density.
- Further satellite systems and techniques have been added to the list (see "IONEX VERSION / TYPE").
- A general escape sequence has been defined to include technique-related auxiliary data blocks in the header part of IONEX files.

Application of IONEX TEC Maps

We may use three different procedures to compute the TEC E as a function of *geocentric* latitude β, longitude λ, and universal time t, when we have the TEC maps $E_i = E(T_i)$, i = 1,2,... ,nat our disposal:

- Simply take the nearest TEC map $E_i = E(T_i)$ at epoch T_i:

$$-?3(/3, \lambda, t) = E_i(\beta, \lambda), \tag{1}$$

  where $|t - T_i|$ = min.

- Interpolate between consecutive TEC maps $E_i = E(T_i)$ and $E_{i+1} = E(T_{i+1})$:

$$E(\beta, \lambda, t) = \frac{T_{i+1} - t}{T_{i+1}} T_i E_i(\beta, \lambda) + \frac{t - T_i}{T_{i+1} - T_i} E_{i+1}(p, \lambda), \tag{2}$$

  where $T_i \leq t < T_{i+1}$.

- Interpolate between consecutive *rotated* TEC maps:

$$E(\beta, \lambda, t) = \frac{T_{i+1} - t}{T_{i+1} - T_i} E_i(\beta, \lambda_i') + \frac{t - T_i}{T_{i+1} - T_i} E_{i+1}(\beta, \lambda_{i+1}'), \tag{3}$$

  where $T_i \leq t < T_{i+1}$ and $\lambda_i' = \lambda + (t - T_i)$. The TEC maps are rotated by $t - T_i$ around the Z-axis in order to compensate to a great extent the strong correlation between the ionosphere and the Sun's position. Note that method (1) can be refined accordingly by taking the nearest *rotated* map: $E(\beta, \lambda, t) = E_i(\beta, \lambda')$.

From method (1) to method (3), one may expect an improvement of the interpolation results, therefore we recommend to use the last approach (3).

Grid interpolation algorithms to be used are not discussed in detail here. However, a simple 4-point formula should be adequate, if the IONEX grid is dense enough:

$$E(\lambda_0 + p\,\Delta\lambda, \beta_0 + q\,\Delta\beta) = (1-p)(1-q)\,E_{0,0} + p\,(1-q)\,E_{1,0} + q\,(1-p)\,E_{0,1} + p\,q\,E_{1,1},$$

where $0 \leq p < 1$ and $0 \leq q < 1$. $\Delta\lambda$ and $\Delta\beta$ denote the grid widths in longitude and latitude.

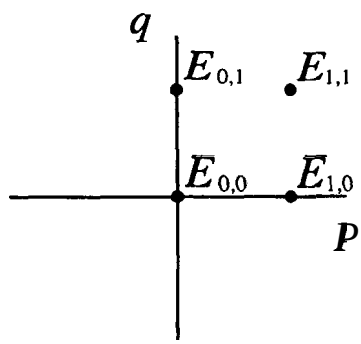

Figure 1: Bivariate interpolation using the nearest 4 TEC values $E_{i,j}$

General Format Description

Each IONEX file consists of a header section and a data section. The header section contains global information for the entire file and is placed at the beginning of the file. The header section cent ains header labels in columns 61-80 for each line contained in the header section. These labels are mandatory and must appear exactly as given in the 10NEX descriptions. Note that the maximum record length is 80 bytes per record.

As record descriptors in columns 61-80 are mandatory, the programs reading an IONEX file should be able to decode the header records with formats according to the record descriptor, provided the records have been first read into an internal buffer.

We propose to allow free ordering of the header records, with the following exception:

- The "IONEX VERSION / TYPE" record must be the first record in a file.

There are further rules to be considered:

- Each value remains valid until changed by an additional header record!
- Fields of lines with formatted numbers must contain at least a "0" to facilitate reading with C language routines, i. e., empty fields are not permitted here.

- In principle there should be no blank lines. We recommend however to anticipate blank line skipping by the reading routines.

Writing and reading IONEX files one has to perform loops over up to a maximum of five arguments, namely: time (EPOCH), latitude (LAT), longitude (LON), height (HGT), and map type. Possible loops are:

(a) map type, EPOCH, HGT, LAT, LON,

(b) EPOCH, map type, HGT, LAT, LON.

Both enclosed examples have been created according to loop (a).

The proposed format descriptions as well as examples are given in the tables at the end of this paper.

Exchange of IONEX Files

We recommend to use the following naming convention for IONEX files:

cccedddh.yyI,

where

ccc: 3-figure Analysis Center (AC) designator
e: extension or region code ("G" for Global ionosphere maps)
ddd: day of the year of first record
h: file sequence number (1, 2,...) or hour (A, B,...) within day;
O: file contains all existing data of the current day
yy: 2-digit year
I: file type ("I" for Ionosphere maps).

Example: CODG2880. 951. It is recommended to specify IONEX file names in uppercase.

When data transmission time or storage volume are critical we recommend to compress the files prior to storage or transmission using the UNIX compress und decompress programs. Compatible routines are available for VAX/VMS and PC/DOS systems.

Proposed naming conventions for compressed files:

System	Ionosphere files
UNIX	cccedddh.yyI.Z
VMS	cccedddh.yyI_Z
DOS	cccedddh.yyJ

Reading and Writing IONEX Modules

Fortran-77 routines to read and write IONEX files are available, for instance, via AIUB's anonymous ftp server ubeclu.unibe.ch (or 130.92.6.18) — type "cd aiub$f tp" after login — in the directory [IONEX.SOURCE]. The main modules are RDIXFL (read IONEX file) and WTIXFL (write IONEX file). They use the subroutines RDIXHD/WTIXHD (read/write IONEX header) and RDIXDT/WTIXDT (read/write IONEX data). Auxiliary subroutines are: DJUL (date-to-MJD conversion), JMT (MJD-to-date conversion), and RADGMS (converts a day-fraction into hours-minutes-seconds). Note that the OPNFIL-OPNERR sequence must be replaced by an own file opening sequence.

References

Feltens, J. (1996a): *Ionosphere Maps — A New Product of IGS?* Summary of the Ionosphere Session, IGS Workshop, Silver Spring, MD, USA, March 19–21, 1996.

Feltens, J. (1996b): *IONEX Format,* GPS-IONO mail, October 30, 1996.

Gurtner, W., G. Mader (1990): *Receiver Independent Exchange Format* Version 2. CSTG GPS Bulletin, Vol. 3, No. 3, September/October 1990, National Geodetic Survey, Rockville.

Schaer, S. (1996): *Proposal Concerning VTEC Data Format.* GPS-IONO mail, February 6, 1996.

Schaer, S., W. Gurtner (1996): *IONEX: The Ionosphere Map EXchange Format Version O (Proposal, August 1996).* GPS-IONO mail, September 3, 1996.

Table 1: Ionosphere map file — header section description

HEADER LABEL (columns 61-80)	DESCRIPTION	FORMAT
IONEX VERSION / TYPE	o Format version (1.0) o File type ('1' for Ionosphere maps) o Satellite system or theoretical model: - 'BEN': BENt - 'ENV': ENVisat - 'ERS': ERS + 'GEO': GEOstationary satellite(s) - 'GLO': GLOnass - 'GNS': GNSS (gps/glonass) -'GPS': GPS - 'IRI': IRI + 'MIX': MIXed/combined - 'NNS': NNSS (transit) - 'TOP': TOPex/poseidon This record has to be the first one in en IONEX file! For techniques marked by a '+', description lines should be added identifying the satellite(s) or roughly specifying the technique used.	F8.1,12X, A1,19X, A3,17X
PGM / RUN BY / DATE	o Name of program creating current file o Name of agency creating current file o Date and time of file creation	A20, A20, A20
* IDESCRIPTION	It is highly recommended to give a brief description of the technique, model, . . . Please distinguish between description and pure comment.	A60 *
* COMMENT	Comment line(s). Note that comment lines are not allowed right at the beginning of a file or within TEC/RMS/HGT data blocks (see 'LAT/LON1/LON2/DLON/H').	A60 *
EPOCH OF FIRST MAP	Epoch of first TECmap (UT): year (4 digits), month, day, hour, rein, sec (integer)	616,24X
EPOCH OF LAST MAP	Epoch of last TEC map (UT): year (4 digits), month, day, hour, rein, sec (integer)	616,24X
INTERVAL	Time interval between the TEC maps, in seconds (integer). If '0' is specified, 'INTERVAL' may be variable.	16,54X
# OF MAPS IN FILE	Total number of TEC/RMS/HGT maps	16,54X

	contained *in* current file.	
MAPPING FUNCTION	Mapping function adopted for TEC determination: 'NONE' : no MF used (e.g. altimetry), 'COSZ' : 1/cos(z), 'QFAC': Q-factor. Others might be introduced.	2X,A4,54X
IELEVATION CUTOFF	Minimum elevation angle in degrees. '0.0', if unknown; '90.0' for altimetry.	F8.1,52X
OBSERVABLES USED	One-line specification of the observable(s) used in the TEC computation (or blank line for theoretical models).	A60
# OF STATIONS	Number of contributing stations.	16,54X
# OF SATELLITES	Number of contributing satellites.	16,54X
IBASE RADIUS	Mean earth radius or bottom of height grid (in km), e.g.: 6371 km or 6771 km.	F8.1,52X
MAP DIMENSION	Dimension of TEC/RMS maps: 2 or 3. See also 'TEC VALUES'.	16,54X
HGT1 / HGT2 / DHGT	Definition of an equidistant grid in height: 'HGT1' to 'HGT2' with increment 'DHGT' (in km), e.g.: ' 200.0 800.0 50.0'. For 2-dimensional maps, HGT1=HGT2 and DHGT=0, e.g.: ' 400.0 400.0 0.0' or ' 0.0 0.0 0.0' (see also 'BASE RADIUS').	2X,3F6.1, 40X
LAT1 / LAT2 / DLAT	Definition of the grid in latitude: 'LAT1' to 'LAT2' with increment 'DLAT' (in degrees). 'LAT1' and 'LAT2' always have to be multiples of 'DLAT'. Example: ' 87.5 -87.5 -2.5'.	2X,3F6.1. 40X
LON1 / LON2 / DLON	Definition of the grid in longitude: 'LON1' to 'LON2' with increment 'DLON' (in degrees), where LON equals east longitude. 'LON1' and 'LON2' always have to be multiples of 'DLON'. Example: ' 0.0 357.5 2.5' or ' -180.0 177.5 2.5'.	2X,3F6.1, 40X
EXPONENT	Exponent defining the unit of the *values* listed in the following data block(s). Default exponent is -1. See also 'TEC VALUES', 'RMS VALUES', and 'HGT VALUES',	16,54X
START OF AUX DATA	Record opening general escape sequence	A60

	that contains technique-related auxiliary data (e.g. differential code biases for GPS). Note that such data blocks may be skipped if you are interested in ionospheric information only. Format definitions end examples are given in Appendix B.		
END OF AUX DATA	Record closing auxiliary data block.	A60	*
END OF HEADER	Last record of the header section.	60X	
START OF TEC MAP	Record indicating the start of the i-th TEC map, where i=1,2, . . .,n denotes the internal number of the *current* map. All maps have to be ordered chronologically.	16,54X	
EPOCH OF CURRENT MAP	Epoch of current map (UT): year (4 digits), month, day, hour, rein, sec (integer). 'EPOCH OF CURRENT MAP' must be specified at the first occurrence of the associated map!	616,24X	
LAT/LON1/LON2/DLON/H	Record initializing a new TEC/RMS/HGT data block for latitude 'LAT' (end height 'H(GT)'), from 'LON1' to 'LON2 (with increment 'DLON'). In case of 2-dimensional maps, it is recommended to define H=HGT1. Neither other types of records nor comment lines are allowed after this record and within the subsequent data block!	2X,5F6.1, 28X	
END OF TEC MAP	Record indicating the end of the i-th TEC map (see also 'START OF TEC MAP').	16,54X	
START OF RMS MAP	Record indicating the start of an RMS map related to the i-th TEC map (see also 'START OF TEC MAP').	16,54X	*
END OF RMS MAP	Record indicating the end of an RMS map.	16,54X	*
START OF HEIGHT MAP	Record indicating the stint of a HEIGHT map related to the i-th TEC map (see also 'START OF TEC MAP').	16,54X	*
END OF HEIGHT MAP	Record indicating the end of a HGT map.	16,54X	*
END OF FILE	Last record closing the IONEX file.	60X	

(Records marked with "*" are optional)

Table 2: Ionosphere map file — data record description

OBS. RECORD I DESCRIPTION	FORMAT
TEC VALUES	TEC values in 0.1 TECU. After 16 values (per latitude band) continue values in next data record. Non-available TEC values are written as '9999'. If an exponent k is specified, the TEC values are given in units of 10**k TECU. The default exponent is -1. See also 'EXPONENT'. If 3-dimensional maps are provided, TEC values should correspond to the surface electron densities at the grid points times 'DHGT' (again in 10**k TECU), that means, you can derive the surface electron densities by simply dividing the TEC values by 'DHGT'. However, if you estimate electron densities integrated over voxels (volume elements), you should ensure that the height grid specified in 'HGT1 / HGT2 / DHGT' refers to the heights of the voxel centers.	m15
* RMS VALUES	RMS values are formatted exactly in the same way as TEC values (see above).	mI5 *
* HGT VALUES	HGT values are formatted exactly in the same way as TEC values (see above). If an exponent k is specified, the HGT values are given in units of 10**k km. The default exponent is -1, too, i.e. in this case the unit corresponds to 0.1 km. The actual heights (with respect to the 'BASE RADIUS') are computed as the sum of 'HGT1' and 'HGT VALUES'.	mI5 *

(Records marked with "*" are optional)

Table 3: Ionosphere map file-example 1: 2-d TEC maps

```
----1---110---1---210---1  ---310---4---4 |0---|---5|0--- |---6|0---|---7 |0---|---8|

     1.0            IONOSPHERE  MAPS     GPS                 IONEX VERSION / TYPE
ionpgm v1.0         aiub                 29-jan-96 17:29     PGM / RUN BY / DATE
example of an ionex file containing 2-dimensional tec maps  COMMENT
global ionosphere maps for day 288, 1995                    DESCRIPTION
modeled by spherical harmonics . . .                        DESCRIPTION
  1995   10   15     0     0     0                          EPOCH OF FIRST MAP
  1995   10   16     0     0     0                          EPOCH OF LAST MAP
 21600                                                      INTERVAL
     5                                                      # OF MAPS IN FILE
```

```
  COSZ                                                    MAPPING FUNCTION
    20.0                                                  ELEVATION CUTOFF
double-difference carrier phase                           OBSERVABLE USED
    80                                                    # OF STATIONS
    24                                                    # OF SATELLITES
  6371.0                                                  BASE RADIUS
     2                                                    MAP DIMENSION
   400.0400.0 0.0                                         HGT1 / HGT2 / DHGT
    85.0 -85.0 -5.0                                       LAT1 / LAT2 / DLAT
     0.0355.0  5.0                                        LON1 / LON2 / DLON
    -1                                                    EXPONENT
tec values in 0.1 tec units; 9999, if no value available  COMMENT
height values in 0.1 km                                   COMMENT
                                                          END OF HEADER
     1                                                    START OF TEC NAP
  1995   10   15     0     0     0                       EPOCH OF CURRENT NAP
    85.0   0.0 355.0   5.0 400.0                          LAT/LON1/LON2/DLON/H
 1000 1000 1000 1000 1000 1000 1000 1000 1000 1000 1000 1000 1000 1000 1000 1000
 1000 1000 1000 1000 1000 1000 1000 1000 1000 1000 1000 1000 1000 1000 1000 1000
 1000 1000 1000 1000 1000 1000 1000 1000 1000 1000 1000 1000 1000 1000 1000 1000
 1000 1000 1000 1000 1000 1000 1000 1000 1000 1000 1000 1000 1000 1000 1000 1000
 1000 1000 1000 1000 1000 1000 1000 1000
    80.0   0.0 355.0   5.0 400.0                          LAT/LON1/LON2/DLON/H
 1000 1000 1000 1000 1000 1000 1000 1000 1000 1000 1000 1000 1000 1000 1000 1000
 1000 1000 1000 1000 1000 1000 1000 1000 1000 1000 1000 1000 1000 1000 1000 1000
 1000 1000 1000 1000 1000 1000 1000 1000 1000 1000 1000 1000 1000 1000 1000 1000
 1000 1000 1000 1000 1000 1000 1000 1000 1000 1000 1000 1000 1000 1000 1000 1000
 1000 1000 1000 1000 1000 1000 1000 1000
...
   -85.0   0.0 355.0   5.0 400.0                          LAT/LON1/LON2/DLON/H
 1000 1000 1000 1000 1000 1000 1000 1000 1000 1000 1000 1000 1000 1000 1000 1000
 1000 1000 1000 1000 1000 1000 1000 1000 1000 1000 1000 1000 1000 1000 1000 1000
 1000 1000 1000 1000 1000 1000 1000 1000 1000 1000 1000 1000 1000 1000 1000 1000
 1000 1000 1000 1000 1000 1000 1000 1000 1000 1000 1000 1000 1000 1000 1000 1000
 1000 1000 1000 1000 1000 1000 1000 1000
     1                                                    END OF TEC NAP
     2                                                    START OF TEC NAP
  1995   10   15     6     0     0                       EPOCH OF CURRENT MAP
    85.0   0.0 355.0   5.0 400.0                          LAT/LoNl/LoN2/DLoN/H
 1000 1000 1000 1000 1000 1000 1000 1000 1000 1000 1000 1000 1000 1000 1000 1000
 1000 1000 1000 1000 1000 1000 1000 1000 1000 1000 1000 1000 1000 1000 1000 1000
 1000 1000 1000 1000 1000 1000 1000 1000 1000 1000 1000 1000 1000 1000 1000 1000
 1000 1000 1000 1000 1000 1000 1000 1000 1000 1000 1000 1000 1000 1000 1000 1000
 1000 1000 1000 1000 1000 1000 1000 1000
...
     5                                                    END OF TEC NAP
     1                                                    START OF RMS MAP
    85.0   0.0 355.0   5.0 400.0                          LAT/LON1/LON2/DLON/H
 1000 1000 1000 1000 1000 1000 1000 1000 1000 1000 1000 1000 1000 1000 1000 1000
 1000 1000 1000 1000 1000 1000 1000 1000 1000 1000 1000 1000 1000 1000 1000 1000
 1000 1000 1000 1000 1000 1000 1000 1000 1000 1000 1000 1000 1000 1000 1000 1000
 1000 1000 1000 1000 1000 1000 1000 1000 1000 1000 1000 1000 1000 1000 1000 1000
 1000 1000 1000 1000 1000 1000 1000 1000
    80.0   0.0 355.0   5.0 400.0                          LAT/LON1/LON2/DLON/H
 1000 1000 1000 1000 1000 1000 1000 1000 1000 1000 1000 1000 1000 1000 1000 1000
 1000 1000 1000 1000 1000 1000 1000 1000 1000 1000 1000 1000 1000 1000 1000 1000
 1000 1000 1000 1000 1000 1000 1000 1000 1000 1000 1000 1000 1000 1000 1000 1000
 1000 1000 1000 1000 1000 1000 1000 1000 1000 1000 1000 1000 1000 1000 1000 1000
```

```
 1000 1000 1000 1000 1000 1000 1000 1000

...
   -85.0   0.0 355.0   5.0 400.0                                  LAT/LON1/LON2/DLON/H
 1000 1000 1000 1000 1000 1000 1000 1000 1000 1000 1000 1000 1000 1000 1000 1000
 1000 1000 1000 1000 1000 1000 1000 1000 1000 1000 1000 1000 1000 1000 1000 1000
 1000 1000 1000 1000 1000 1000 1000 1000 1000 1000 1000 1000 1000 1000 1000 1000
 1000 1000 1000 1000 1000 1000 1000 1000 1000 1000 1000 1000 iooo 1000 1000 1000
 1000 1000 1000 1000 1000 1000 1000 1000
     1                                                          END OF RMS NAP
     2                                                          START OF RMS NAP
    85.0   0.0 355.0   5.0 400.0                                 LAT/LON1/LON2/DLON/H
 1000 1000 1000 1000 1000 1000 1000 1000 1000 1000 1000 1000 1000 1000 1000 1000
 1000 1000 1000 1000 1000 1000 1000 1000 1000 1000 1000 1000 1000 1000 1000 1000
 1000 1000 1000 1000 1000 1000 1000 1000 1000 1000 1000 1000 1000 1000 1000 1000
 1000 1000 1000 1000 1000 1000 1000 1000 1000 1000 1000 1000 1000 1000 1000 1000
 1000 1000 1000 1000 1000 1000 1000 1000
...
     5                                                          END OF RMS MAP
     1                                                          START OF HEIGHT MAP
    85.0   0.0 355.0   5.0 400.0                                 LAT/LON1/LON2/DLON/H
    0    0    0    0    0    0    0    0    0    0    0    0    0    0    0    0
    0    0    0    0    0    0    0    0    0    0    0    0    0    0    0    0
    0    0    0    0    0    0    0    0    0    0    0    0    0    0    0    0
    0    0    0    0    0    0    0    0    0    0    0    0    0    0    0    0
    0    0    0    0    0    0    0    0
    80.0   0.0 355.0   5.0 400.0                                 LAT/LON1/LON2/DLON/H
    0    0    0    0    0    0    0    0    0    0    0    0    0    0    0    0
    0    0    0    0    0    0    0    0    0    0    0    0    0    0    0    0
    0    0    0    0    0    0    0    0    0    0    0    0    0    0    0    0
    0    0    0    0    0    0    0    0    0    0    0    0    0    0    0    0
    0    0    0    0    0    0    0    0
...
   -85.0   0.0 355.0   5.0 400.0                                 LAT/LON1/LON2/DLON/H
    0    0    0    0    0    0    0    0    0    0    0    0    0    0    0    0
    0    0    0    0    0    0    0    0    0    0    0    0    0    0    0    0
    0    0    0    0    0    0    0    0    0    0    0    0    0    0    0    0
    0    0    0    0    0    0    0    0    0    0    0    0    0    0    0    0
    0    0    0    0    0    0    0    0
     1                                                          END OF HEIGHT MAP
     2                                                          START OF HEIGHT NAP
    85.0   0.0 355.0   5.0 400.0                                 LAT/LON1/LON2/DLON/H
    0    0    0    0    0    0    0    0    0    0    0    0    0    0    0    0
    0    0    0    0    0    0    0    0    0    0    0    0    0    0    0    0
    0    0    0    0    0    0    0    0    0    0    0    0    0    0    0    0
    0    0    0    0    0    0    0    0    0    0    0    0    0    0    0    0
    0    0    0    0    0    0    0    0
..
     5                                                          END OF HEIGHT NAP
                                                                END OF FILE

----1--1]0--1---2 IO---I---310---! ---4|0---|---5|0--- 1---610---1---710---1---81
```

Table 4: Ionosphere map file — example 2: 3-d TEC maps

```
'---1---110---1---2 |0---|---3|0---|---4  10---1---510---1---610---  |---7|0---|---8|

     1.0            IONOSPHERE  MAPS     GPS                 IONEX VERSION / TYPE
ionpgm v1.0         aiub                 29-jan-96 17:29     PGM / RUN BY / DATE
example of an ionex file containing 3-dimensional tec maps  COMMENT
global ionosphere maps for day 288, 1995                    DESCRIPTION
modeled by spherical harmonics . . .                        DESCRIPTION
  1995   10   15     0     0     0                          EPOCH OF FIRST MAP
  1995   10   16     0     0     0                          EPOCH OF LAST MAP
 21600                                                      INTERVAL
     5                                                      # OF MAPS IN FILE
  COSZ                                                      MAPPING  FUNCTION
    20.0                                                    ELEVATION  CUTOFF
double-difference  carrier  phase                           OBSERVABLE USED
    80                                                      # OF STATIONS
    24                                                      # OF SATELLITES
  6371.0                                                    BASE RADIUS
     3                                                      MAP DIMENSION
   200.0 800.0 50.0                                         HGT1 / HGT2 / DHGT
    85.0 -85.0 -5.0                                         LAT1 / LAT2 / DLAT
     0.0355.0 5.0                                           LON1 / LON2 / DLON
                                                            END OF HEADER
     1                                                      START OF TEC MAP
  1995   10   15     0     0     0                          EPOCH OF CURRENT MAP
    -3                                                      EXPONENT
    85.0   0.0 355.0   5.0  200.0                          LAT/LON1/LON2/DLON/H
 1000 1000 1000 1000 1000 1000 1000 1000 1000 1000 1000 1000 1000 1000 1000 1000
 1000 1000 1000 1000 1000 1000 1000 1000 1000 1000 1000 1000 1000 1000 1000 1000
 1000 1000 1000 1000 1000 1000 1000 1000 1000 1000 1000 1000 1000 1000 1000 1000
 1000 1000 1000 1000 1000 1000 1000 1000 1000 1000 1000 1000 1000 1000 1000 1000
 1000 1000 1000 1000 1000 1000 1000 1000
    80.0   0.0 355.0   5.0  200.0                          LAT/LON1/LON2/DLON/H
 1000 1000 1000 1000 1000 1000 1000 1000 1000 1000 1000 1000 1000 1000 1000 1000
 1000 1000 1000 1000 1000 1000 1000 1000 1000 1000 1000 1000 1000 1000 1000 1000
 1000 1000 1000 1000 1000 1000 1000 1000 1000 1000 1000 1000 1000 1000 1000 1000
 1000 1000 1000 1000 1000 1000 1000 1000 1000 1000 1000 1000 1000 1000 1000 1000
 1000 1000 1000 1000 1000 1000 1000 1000
'''
   -85.0   0.0 355.0   5.0  200.0                          LAT/LON1/LON2/DLON/H
 1000 1000 1000 1000 1000 1000 1000 1000 1000 1000 1000 1000 1000 1000 1000 1000
 1000 1000 1000 1000 1000 1000 1000 1000 1000 1000 1000 1000 1000 1000 1000 1000
 1000 1000 1000 1000 1000 1000 1000 1000 1000 1000 1000 1000 1000 1000 1000 1000
 1000 1000 1000 1000 1000 1000 1000 1000 1000 1000 1000 1000 1000 1000 1000 1000
 1000 1000 1000 1000 1000 1000 1000 1000
    -2                                                      EXPONENT
    85.0   0.0 355.0   5.0 250.0                          LAT/LON1/LON2/DLON/H
 1000 1000 1000 1000 1000 1000 1000 1000 1000 1000 1000 1000 1000 1000 1000 1000
 1000 1000 1000 1000 1000 1000 1000 1000 1000 1000 1000 1000 1000 1000 1000 1000
 1000 1000 1000 1000 1000 1000 1000 1000 1000 1000 1000 1000 1000 1000 1000 1000
 1000 1000 1000 1000 1000 1000 1000 1000 1000 1000 1000 1000 1000 1000 1000 1000
 1000 1000 1000 1000 1000 1000 1000 1000
    80.0   0.0 355.0   5.0  250.0                          LAT/LON1/LON2/DLON/H
 1000 1000 1000 1000 1000 1000 1000 1000 1000 1000 1000 1000 1000 1000 1000 1000
 1000 1000 1000 1000 1000 1000 1000 1000 1000 1000 1000 1000 1000 1000 1000 1000
 1000 1000 1000 1000 1000 1000 1000 1000 1000 1000 1000 1000 1000 1000 1000 1000
 1000 1000 1000 1000 1000 1000 1000 1000 1000 1000 1000 1000 1000 1000 1000 1000
```

```
 1000 1000 1000 1000 1000 1000 1000 1000
...
  -85.0   0.0 355.0   5.0 250.0                          LAT/LoNl/LoN2/DLoN/H
 1000 1000 1000 1000 1000 1000 1000 1000 1000 1000 1000 1000 1000 1000 1000 1000
 1000 1000 1000 1000 1000 1000 1000 1000 1000 1000 1000 1000 1000 1000 1000 1000
 1000 1000 1000 1000 1000 1000 1000 1000 1000 1000 1000 1000 1000 1000 1000 1000
 1000 1000 1000 1000 1000 1000 1000 1000 1000 1000 1000 1000 1000 1000 1000 1000
 1000 1000 1000 1000 1000 1000 1000 1000
...
    -4                                                   EXPONENT
   85.0   0.0 355.0   5.0 800.0                          LAT/LON1/LON2/DLON/H
 1000 1000 1000 1000 1000 1000 1000 1000 1000 1000 1000 1000 1000 1000 1000 1000
 1000 1000 1000 1000 1000 1000 1000 1000 1000 1000 1000 1000 1000 1000 1000 1000
 1000 1000 1000 1000 1000 1000 1000 1000 1000 1000 1000 1000 1000 1000 1000 1000
 1000 1000 1000 1000 1000 1000 1000 1000 1000 1000 1000 1000 1000 1000 1000 1000
 1000 1000 1000 1000 1000 1000 1000 1000
   80.0   0.0 355.0   5.0 800.0                          LAT/LON1/LON2/DLON/H
 1000 1000 1000 1000 1000 1000 1000 1000 1000 1000 1000 1000 1000 1000 1000 1000
 1000 1000 1000 1000 1000 1000 1000 1000 1000 1000 1000 1000 1000 1000 1000 1000
 1000 1000 1000 1000 1000 1000 1000 1000 1000 1000 1000 1000 1000 1000 1000 1000
 1000 1000 1000 1000 1000 1000 1000 1000 1000 1000 1000 1000 1000 1000 1000 1000
 1000 1000 1000 1000 1000 1000 1000 1000
...
  -85.0   0.0 355.0   5.0 800.0                          LAT/LON1/LON2/DLON/H
 1000 1000 1000 1000 1000 1000 1000 1000 1000 1000 1000 1000 1000 1000 1000 1000
 1000 1000 1000 1000 1000 1000 1000 1000 1000 1000 1000 1000 1000 1000 1000 1000
 1000 1000 1000 1000 1000 1000 1000 1000 1000 1000 1000 1000 1000 1000 1000 1000
 1000 1000 1000 1000 1000 1000 1000 1000 1000 1000 1000 1000 1000 1000 1000 1000
 1000 1000 1000 1000 1000 1000 1000 1000
     1                                                   END OF TEC MAP
     2                                                   START OF TEC MAP
  1995    10    15     6     0     0                     EPOCH OF CURRENT MAP
    -3                                                   EXPONENT
   85.0   0.0 355.0   5.0 200.0                          LAT/LON1/LON2/DLON/H
 1000 1000 1000 1000 1000 1000 1000 1000 1000 1000 1000 1000 1000 1000 1000 1000
 1000 1000 1000 1000 1000 1000 1000 1000 1000 1000 1000 1000 1000 1000 1000 1000
 1000 1000 1000 1000 1000 1000 1000 1000 1000 1000 1000 1000 1000 1000 1000 1000
 1000 1000 1000 1000 1000 1000 1000 1000 1000 1000 1000 1000 1000 1000 1000 1000
 1000 1000 1000 1000 1000 1000 1000 1000
...
     5                                                   END OF TEC NAP
     1                                                   START OF RMS MAP
    -3                                                   EXPONENT
   85.0   0.0 355.0   5.0 200.0                          LAT/LON1/LON2/DLON/H
 1000 1000 1000 1000 1000 1000 1000 1000 1000 1000 1000 1000 1000 1000 1000 1000
 1000 1000 1000 1000 1000 1000 1000 1000 1000 1000 1000 1000 1000 1000 1000 1000
 1000 1000 1000 1000 1000 1000 1000 1000 1000 1000 1000 1000 1000 1000 1000 1000
 1000 1000 1000 1000 1000 1000 1000 1000 1000 1000 1000 1000 1000 1000 1000 1000
 1000 1000 1000 1000 1000 1000 1000 1000
...
     5                                                   END OF RMS MAP
                                                         END OF FILE

----|---1|0---|---2 |0---|---3|0---|---4| 0---1---5]0---1---610--- |---7|0---|---8|
```

GPS/GLONASS-Related Data Block

If single-frequency GPS users apply precise ephemerides and precise satellite clock information — which always refers to the ionosphere-free linear combination (LC) — as well as IONEX TEC maps to eliminate or greatly reduce ionosphere-induced errors, they may also be interested in having a set of differential code biases (DCBs) of the satellites to correct their C/A- or Pi-code measurements accordingly (to make them consistent to the LC satellite clocks — or vice versa). The DCBS b are estimated simultaneously with the TEC parameters using the relationship

$$c\,b = (P1 - P2)_{observed} - (P1 - P2)_{corrected},$$

where P1 and P2 denote the C/A- or P-code observable in meters on L1 (under AS or non-AS conditions) and L2, respectively. The DCB correction for the P1 measurements *or* for the LC satellite clock values T_{LC} (from SP3 orbit file) are given by

$$P1_{corrected} = P1_{observed} - \kappa_2\, c\, b$$

and

$$T_{corrected} = T_{LC} + \kappa_2\, b,$$

where $\kappa_2 = -\nu_2^2/(\nu_1^2 - \nu_2^2) = -1.55$ is the second LC factor, ν_i is the frequency of the i-th carrier, c is the vacuum speed of light, and $b = b_1 - b_2$ is the (geometry-free) DCB of the SV considered (usually in nanoseconds).

Since the DCB information is a by-product of the TEC determination when analyzing dual-band code measurements, DCB estimates may be included in IONEX files. The *GPS/GLONASS*-related data block has to be labelled with "DIFFERENTIAL CODE BIASES" (see example in Table 2).

Table 1: Differential code biases — format definitions

	HEADER LABEL (columns 61-80)	DESCRIPTION	FORMAT
	PRN / BIAS / RMS	Pseudo Random Number (PRN), differential (L1-L2) code bias, and its RMS error in nanoseconds. Note that the PRN consists of a character indicating the satellite system ('G' or blank for GPS and 'R' for GLONASS) and the actual PRN (2 digits).	3X, A1, 12.2, 2F10.3, 34X
*	COMMENT	Comment lines are allowed.	A60

(Records marked with "*" are optional)

Table 2: Differential code biases — example

```
‘---1---110---1---2 10¯1-¯310---1---4{0---  1---510---1---610---  |---7|0---|---8|

DIFFERENTIAL CODE BIASES                                    START OF AUX DATA
    01     0.000     0.000                                  PRN / BIAS / RMS
    02     0.000     0.000                                  PRN / BIAS / RMS
' ' '
    31     0.000     0.000                                  PRN / BIAS / RMS
11-12 biases and rms in ns                                  COMMENT
sum of biases constrained to zero                           COMMENT
DIFFERENTIAL CODE BIASES                                    END OF AUX DATA

----1---110---1---2  10---1---310---1---410---  1---510---1---610---1---710---1---81
```

THE STUDY OF THE TEC AND ITS IRREGULARITIES USING A REGIONAL NETWORK OF GPS STATIONS.

Rene Warnant

Royal Observatory of Belgium
Avenue Circulaire, 3
B-1 180 Brussels
Belgium

ABSTRACT

In this paper, we outline the procedure used at the Royal Observatory of Belgium in order to compute the TEC using GPS measurements with a precision of 2-3 TECU. This procedure requires the determination of the so-called receiver and satellite differential group delays. The combined biases (receiver + satellite) are determined using the geometry-free combination of code observations where the TEC is modelled using a simple polynomial in latitude and local time; the long-term behaviour of the biases is studied. In addition, the reliability of the computed TEC is discussed.

The paper also presents a very simple method allowing to detect medium-scale Traveling Ionospheric Disturbances and scintillation effects by observing the high frequency changes in the geometry-free combination of GPS phase measurements. The method has been applied to the GPS measurements gathered at Brussels (mid-latitude European station) during more than 8 years: only a few scintillations were detected during this period but TIDs were very regularly observed. Statistics concerning the occurrence of Traveling Ionospheric Disturbances at Brussels are presented.

COMPUTING THE TEC USING GPS MEASUREMENTS

The Global Positioning System has already proved to be a very useful tool to study the ionosphere. Indeed, GPS code and carrier phase measurements can be processed in order to determine the Total Electron Content (Lanyi and Roth (1988), Wamant (1996)).
In practice, the TEC can be obtained from:

1) the so-called geometry-flee combination of dual frequency code measurements, $P^{i}_{p,GF}$;

$$P^{i}_{p>GF} = P^{i}_{p,L1} - P^{i}_{p,L2} \qquad (1)$$

This equation can be rewritten in function of the Total Electron Content, TEC_p^i:

$$P'_{p,\,GF} = -1.0510\text{-}17\ TEC_p^i + (DG_p - DG^i) \qquad (2)$$

with TEC_p^i slant TEC measured along the path going from satellite i to receiver p;
DG^i, DG_p the satellite i and receiver p differential group delays;
$P_{p,L1}^i$, $P_{p,L2}^i$ the $L1, L2$ P-code measurements made by receiver p on satellite i.

When the Anti-spoofing is active (as it is the case since January 31 1994), the code observations have a precision ranging from a few decimeters to more than one metre. These measurements are not ambiguous but contain biases called receiver and satellite ***differential group delays.*** The existence of these biases is due to the fact that the two GPS frequencies undergo different propagation delays inside the receiver and satellite hardware.

2) the geometry-free combination of dual frequency phase measurements $\Phi_{p,GF}^i$;

$$\Phi_{p,GF}^i = \Phi_{p,L1}^i - \frac{f_{L1}}{f_{L2}}\,\Phi_{p,L2}^i \qquad (3)$$

or rewritten in function of the TEC:

$$\Phi_{p,GF}^i = -5.5210\text{-}17\ TEC_p^i + N'_{p,\,GF} \qquad (4)$$

with f_{L1}, f_{L2} the frequency of the $Ll, L2$ carriers;
$\Phi_{p,L1}^i$, $\Phi_{p\ L2}^i$ the $L1, L2$ carrier phase measurements made by receiver p on satellite i;
$N_{P,GF}^i$ a real ambiguity.

Phase measurements usually have a precision better than one millimetre but contain an initial ambiguity which is real in the case of the geomet~-free combination. In the absence of cycle slips, $N_{P,GF}^i$ has to be solved for every satellite pass.

3) a combination of geometry-free code and phase measurements.

$$P_{p,GF}^i - \lambda_{L1}\,\Phi_{p,GF}^i = (DG_p - DG^i) - \lambda_{L1}\,N_{p,GF}^i \qquad (5)$$

with λ_{L1} the L1 carrier wavelength.

This combination is used to solve the ambiguity $N_{P,GF}^i$ which is injected in equation (4) in order

to determine the TEC. This third method which is applied at the Royal Observatory of Belgium allows to combine the advantages of both measurement types: the TEC is obtained from the precise phase measurements but the information contained in the code observations is used to solve the ambiguity. Nevertheless, the procedure requires the determination of the receiver and satellite differential group delays. In most of the cases, these biases have to be computed:

- ***the satellite biases:*** they are measured by the manufacturer before the satellites are launched but inmost of the cases, these values are not valid anymore when the satellites are on their orbit (see, for example, Wilson and Mannucci (1 993), Wanninger et al. (1994), Wamant (1996)).

- *the receiver* ***biases:*** in the past, the old Rogue receivers (the so-called Big-Rogue and Mini-Rogue) had an auto-calibration function allowing to measure the receiver bias. Unfortunately, this function does not exist any more on the Turbo Rogue receiver. To our knowledge, no other receiver has this capability.

THE HARDWARE BIASES

The Royal Observatory of Belgium has a network of 7 permanent GPS stations (figure 1). The station of Brussels is in continuous operation since April 1993. Dentergem, Dourbes and Waremme were installed in January 1994; Bree, Meeuwen and Membach were installed in 1997. All the stations are equipped with Turbo Rogue receivers. In this section, we outline the method we have developed to study the hardware biases. The method has been applied to our Turbo Rogue network. In fact, the error made in the determination of the differential group delays is the largest error source when computing the **TEC** using **GPS** measurements. It is clear that these biases cannot be neglected: for example the bias of one of our receivers (serial number 238) is +5 .33 ns. The fact to neglect it would give an error of 16 TECU on the computed TEC.

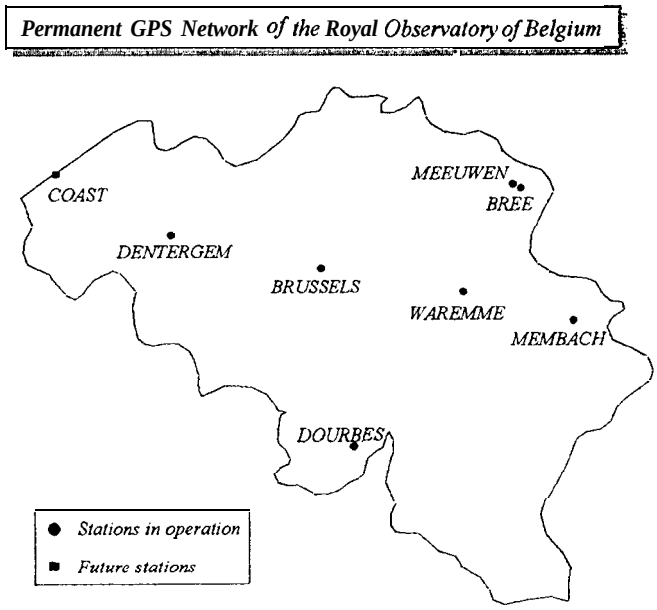

Figure *1. The permanent network of the Royal Observatory* ***of Belgium.***

In practice, the combined biases (receiver+ satellite) are determined using equation (2) where the ionosphere is modelled by means of a simple polynomial in latitude and local time. Every model (i.e. polynomial) is computed using periods of about 6 hours of data. During this procedure, the "usual" assumptions are made:

- the ionosphere is concentrated in a spherical shell of infinitesimal thickness located at a height of 350 km; the intersection between this layer and the satellite line of sight is called the *ionospheric point;*
- "static" behaviour of the ionosphere on short periods (6 hours): the TEC only depends on latitude and local time;
- the receiver and satellite biases are constant on short periods. In the case of the Turbo Rogue biases, we have verified this assumption: during a period of a few hours, the biases remain constant within 0.2 ns(Wamant(1996)).

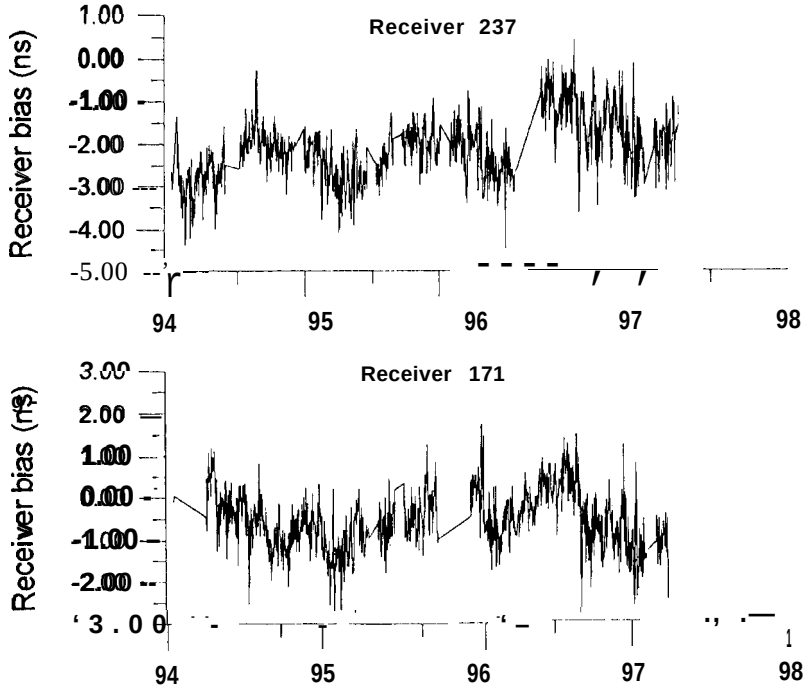

Figure 2. Computed biases for Turbo Rogue receivers237 and 171.

The combined biases are determined on a daily basis (i.e. one solution a day). We only process night-time observations with an elevation mask of 20°: in most of the cases, the ionosphere is "quieter" during the night. This procedure which has been applied to our 7 Turbo Rogue GPS receivers has allowed us to study the long-term behaviour of the computed biases. The main results obtained with this network can be summarized as follows:

- The Turbo Rogue bias changes according as the Anti-Spoofing is activated or not: we have observed that, inmost of the cases, the difference between the two values (i.e with Anti-Spoofing on or off) is about ± 0.5 ns. Since January 31 1994, the Anti-spoofing is activated but sometimes, it is turned off on a few or all the satellites.

- the biases of two "identical" receivers even with two consecutive serial numbers can be very different from each other: for example, the biases of receivers 237 and 238 are respectively -2.37 ns and +5.33 ns;

- the bias depends on the temperature; the effect is visible during hot summer days;

- Figure 2 shows the computed differential group delays for 2 receivers (serial numbers 237 and 171) on a period of about 3 years. By looking at this figure, it can be seen that the bias changes (sometimes much) as soon as a little change is made to the hardware (after a repair, for example): in June 1996, we have replaced the microprocessor of receiver237: you can see very clearly a jump in the computed biases after this change; a similar upgrade has been applied to receiver 171 at the end of December 1995 and a repair has been performed in September 1996.
In addition, the computed biases have a (short-term) day-to-day repeatability of about 1 ns and have a periodic (seasonal) behaviour. Which is the origin of these variations in the **computed biases ? There are 2 possible explanations: the variations are due to a real change of the receiver** bias or they are due to the fact that the use of our simple polynomial to model the ionosphere **gives rise** to residual errors which vary from day to day, from season to season, . . . as it is the case for the ionosphere. If this last explanation is true, then we would expect that the residual errors would be similar for the different receivers: from figure 2, it is clear that the seasonal behaviors of receivers 171 and 237 are very similar; it is also the case of the other Belgian receivers. If these seasonal variations were real changes of the biases, the effect would be different for the different receivers. It could be argued that this seasonal trend could be due to the environmental parameters in which the receivers are placed: the external temperature also depends on the season. Nevertheless, in our case, this explanation cannot be true: the receiver installed at Brussels which is placed in a room where the temperature remains constant within 2 or 3 'K undergoes the same seasonal variations as the other receivers.

For these reasons, the value of the bias adopted to determine the TEC is obtained by computing the mean of all the daily solutions on a period of which the duration depends on data availability: it ranges from one month to more than one year. This technique has the advantage to reduce the influence of the ionospheric residual errors: most of the effects are cancelled in the mean,

- in addition to these "artificial" variations, the receiver biases also undergo real (sometimes unexplained) changes; such variations can be detected by forming the difference between the bias computed for 2 different receivers: the difference has the advantage to remove the common seasonal effects; figure 3 shows the difference between the delays computed for receivers 238 and 321. Receiver 321 was installed at Brussels in a room where the temperature remains stable. In March 96, the difference suddenly increases of about 2 ns, remains stable during a few days and then goes back to the original value, In fact, the bias of receiver 238 has changed: we have seen it by forming differences with other receivers. We have no idea about the origin of this problem.

We have explained in the previous paragraph that we adopt the long-term mean of all the daily computed biases to determine the TEC in order to reduce the residual ionospheric errors. In the case of receiver238, the bias variation was real; as a consequence, we have seen a corresponding jump in the TEC coming from receiver 238 as compared with the other Belgian receivers (figure 3). For this reason, it is clear that the receiver bias has to be very regularly controlled.

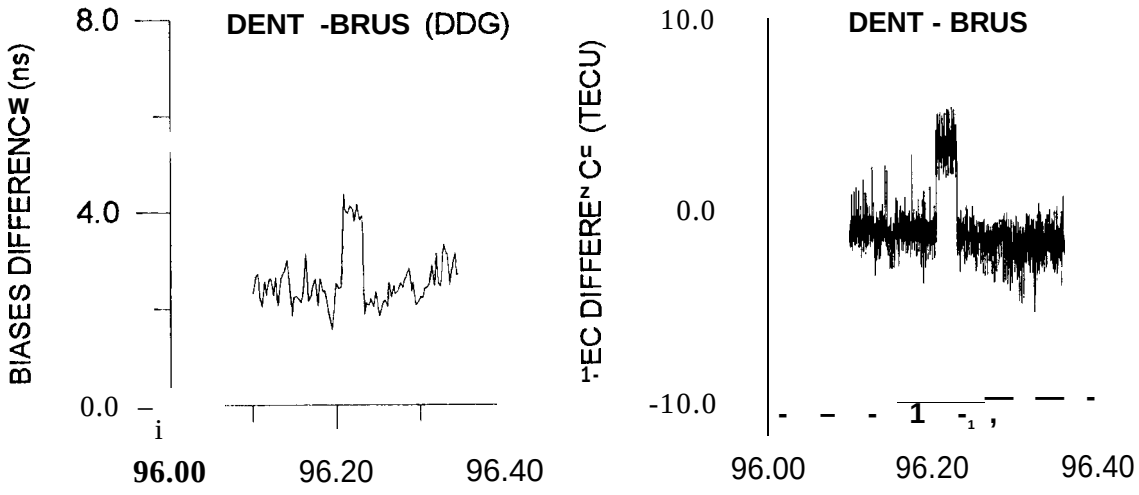

Figure **3.** *Difference between the biases* ***(left)*** *and the* ***TEC (right)*** *computed for the receivers installed at* ***Dentergem*** *(sn 238) and Brussels (sn 321).*

TEC ABOVE THE OBSERVING STATION

When the biases have been determined, the TEC is computed in function of latitude and local time (or longitude) of the ionospheric point. For example, the data collected at Brussels (latitude= 50.8 "N, longitude = 4.40 E) allow to compute the TEC from about 35 "N to 60° N in latitude and from -20 "W to 25° E in longitude.

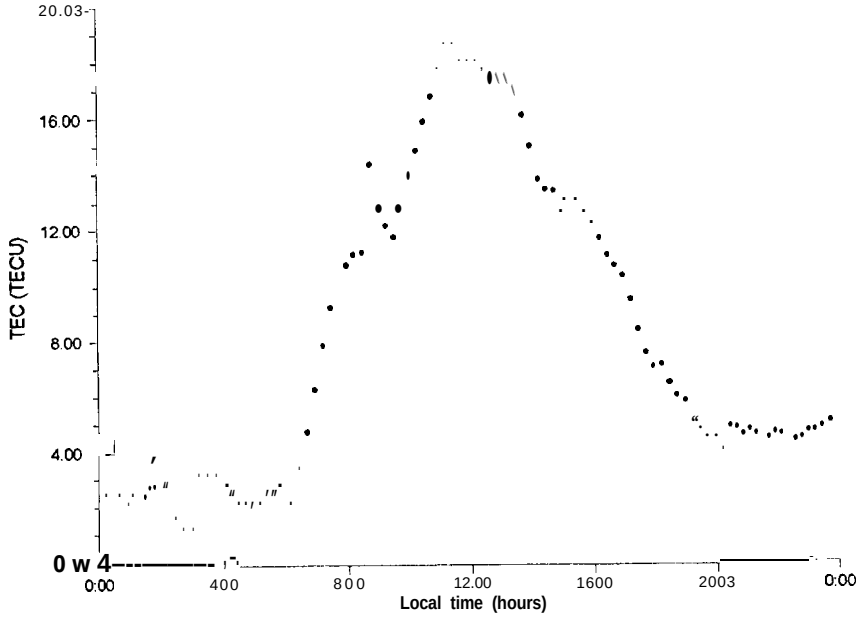

Figure 4. ***TEC*** *at Brussels on October 301994.*

To obtain TEC profiles representative of the ionosphere above the observing station, we apply the following procedure:

- we select all the TEC values corresponding to an ionospheric latitude, L_{iono}, given by :

$$L_{sta} - 1.50 < L_{iono} \leq L_{sta} + 1.5°$$

where L_{sta} is the latitude of the observing station;

- we compute the mean of these TEC values on 15 minute periods.

Figure 4 shows the TEC profile above Brussels on October 301994 obtained by this method. The procedure outlined here above has been applied to a data set covering a period of more than 8 years.

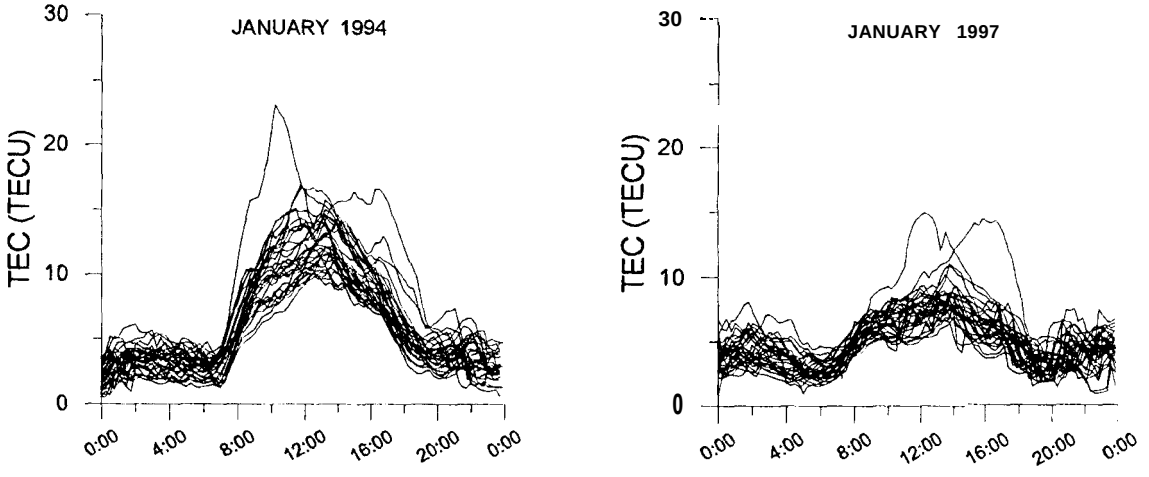

Figure 5. TEC at Brussels during 2 month (January 94 and January 97).

Figure 5 shows, as example, the results obtained at Brussels for two months (January 94 and January 97): in this figure, all the TEC profiles corresponding to the same month are represented on the same graph.

To verify the reliability (precision and accuracy) of the TEC determined by the method developed at ROB, two experiments have been performed:

1. **Precision: we have compared the TEC obtained at Brussels with the TEC computed at Dentergem, Dourbes and Waremme (the typical station inter-distance is about 70 km) during a period of more than 3 years: in most of the cases, the difference between the TEC at Brussels and the TEC in the other Belgian stations remains within 2-3 TECU (figure 6).**

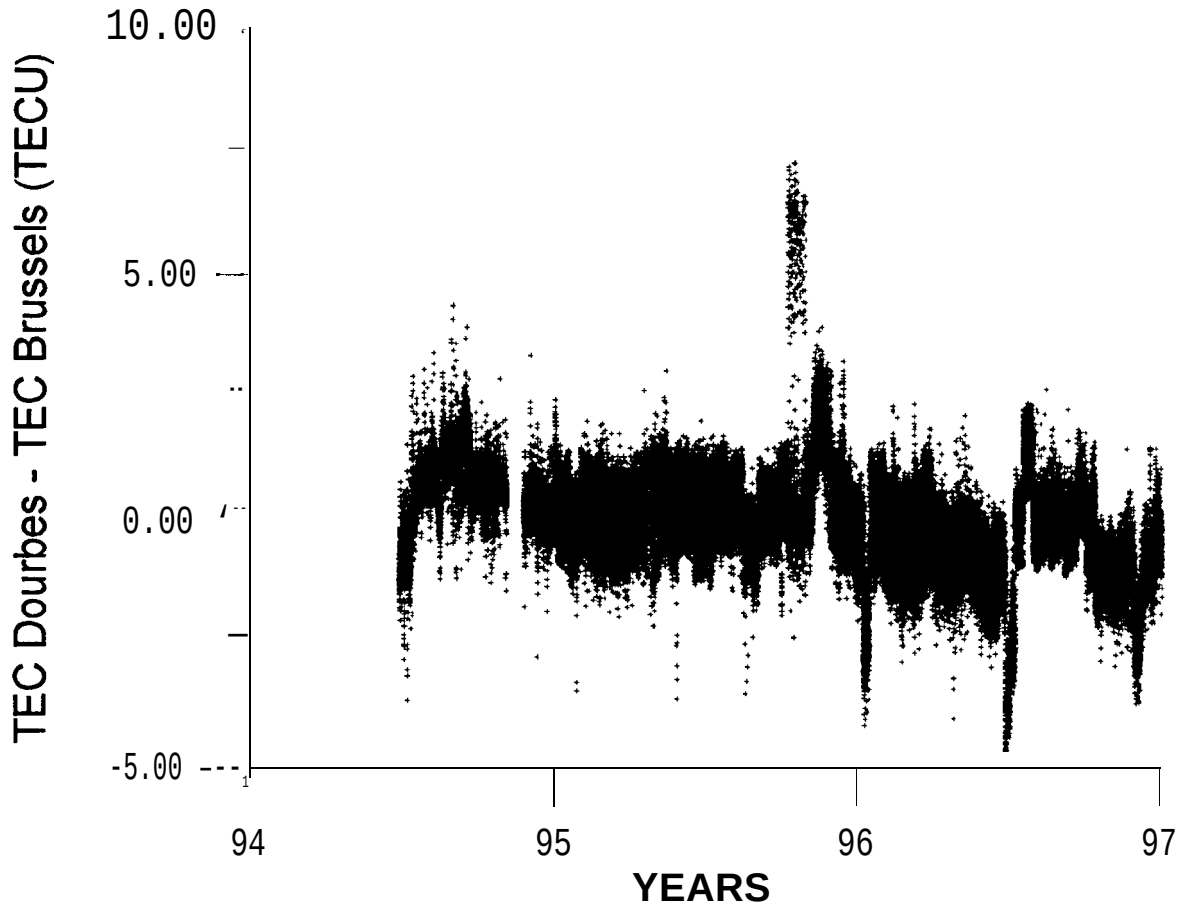

*Figure 6. Difference between the **value** of the TEC computed at **Dourbes** and Brussels.*

2. **Accuracy: at Dourbes, an ionosonde which is the property of the Royal Meteorological Institute of Belgium is collocated** with our GPS station. This ionosonde produces an electron concentration profile up to the maximum of the F2-layer. The ionosonde measurements are used to compute the Total Electron Content above Dourbes:

- in a first step, numerical integration of the measured bottomside electron concentration profile gives the bottomside part;

- in a second step, analytical integration of a Chapman function modelling the topside electron concentration profile gives the topside part; the parameters of the Chapman function are evaluated using the information contained in measured bottomside profile; we assume that the electron concentration is constant in the protonosphere.

This TEC has been compared with the TEC obtained by GPS on a period of 2 years (1995 and 1996). The results of both methods are in very good agreement: in most of the cases, the difference between "GPS" TEC and "ionosonde" TEC remains within 2-3 TECU; the mean and the standard deviation of the difference computed on this period are respectively 0.46 TECU and 1.72 TECU. More details can be found in Warnant and Jodogne (1997).

DETECTION OF IRREGULARITIES IN THE TOTAL ELECTRON CONTENT

From equation (4), it can be seen that the geometry-free combination also allows to monitor the evolution of the TEC in function of time, A $TEC_p^i(t_k)$:

$$\text{A } TEC_p^i(t_k) = 9.5241016 \; \frac{(\Phi^i_{p,GF}(t_k) - \Phi^i_{p,GF}(t_{k-1}))}{(t_k - t_{k-1})} \tag{6}$$

where A $TEC_p^i(t_k)$ *is* defined as:

$$\text{A } TEC_p^i(t_k) = \frac{TEC_p^i(t_k) - TEC_p^i(t_{k-1})}{(t_k - t_{k-1})} \tag{7}$$

It is important to stress that the computation of A $TEC_p^i(t_k)$ does not require the estimation of the real ambiguity, $N^i_{p,GF}$, as long as no cycleslip occurs.

The TEC variations in function of the time can be divided in 2 classes:

- the *regular gradients:* the usual gradients observed in the TEC; for example, the TEC has a minimum value during the night and reaches its maximum around 14hO0 (local time). Consequently, there is a gradient depending on local time;

- the *irregular gradients:* gradients due to irregular ionospheric phenomena such as Traveling Ionospheric Disturbances and scintillation effects.

Traveling Ionospheric Disturbances (or TIDs) appear as waves in the electron density (and consequently in the TEC) due to interactions between the neutral atmosphere and the ionosphere. They have a wavelength ranging from a few tens of kilometres to more than thousand kilometres. Their occurrence often cause important gradients in the TEC even on short distances. ***Scintillation*** effects are variations in phase and amplitude of a radio signal passing through small scale irregularities in the ionosphere. Scintillation effects are very often observed in the polar and equatorial regions and are sometimes detected in the mid-latitude regions.

In this paper, we present a method allowing to detect medium-scale Traveling Ionospheric Disturbances (MSTIDs) and scintillation effects using GPS measurements. MSTIDS have horizontal wavelengths of several hundreds of kilometres, periods ranging from about 12 minutes to about 1 **hour and horizontal phase speeds ranging from 100 to 300 m/s (Van Velthoven, 1990).**

Traveling Ionospheric Disturbances and scintillation effects cause high frequency changes in the TEC. Consequently, these phenomena can be studied by detecting such changes in A TEC_p^i.
In order to do that, we filter out the low frequency changes in the TEC by modelling A TEC_p^i using a low order polynomial. The residuals R_I of this adjustment (i.e. A TEC_p^i- polynomial) contain the high frequency terms.

In a similar way as Wanninger (1994), we define the *ionospheric variability, VI,* using the standard deviation of the residuals R_I (table 1):

$$V_I = O \text{ when } 0.00 \le \sigma_{R_I} < 0.08 \text{ TECU/min}$$

$$V_I = 1 \text{ when } 0.08 \le \sigma_{R_I} < 0.10 \text{ TECU/min}$$

V_I	σ_{R_I} (TECU/min)
0	$0.00 \le \sigma_{R_I} < 0.08$
1	$0.08 < \sigma_{R_I} < 0.10$
2	$0.10 \le \sigma_{R_I} < 0.15$
...	...
8	**0.40< (JR,< 0.45**
9	$\sigma_{R_I} \ge 0.45$

Table 1. Definition of the ionospheric variability

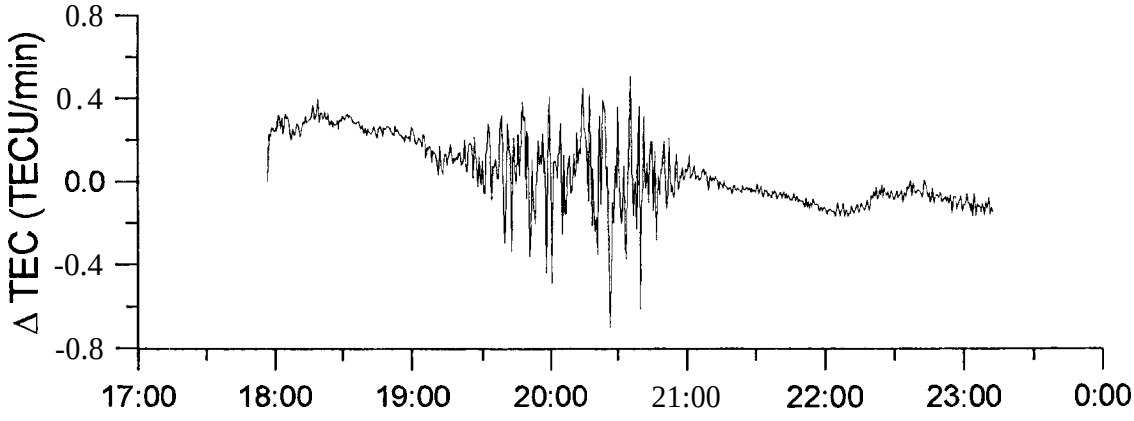

Figure 7. Scintillations observed at Brussels on May 281993.

In practice, the ionospheric variability is computed for every observed satellite, using periods of 15 minutes of measurements. When V_I is different from zero, we decide that an ***"event"*** is detected. Such an "event" is presented in figure 7. This figure displays the TEC gradients, A *TEC*, observed at Brussels on May 281993. These gradients are caused by scintillations effects. Figure 8 shows the gradients observed in 3 GPS stations operated by the Royal Observatory of Belgium. These effects are due to a (Medium-Scale) Traveling Ionospheric Disturbance. In fact, most of the "events" detected in Belgium are due to TIDs.

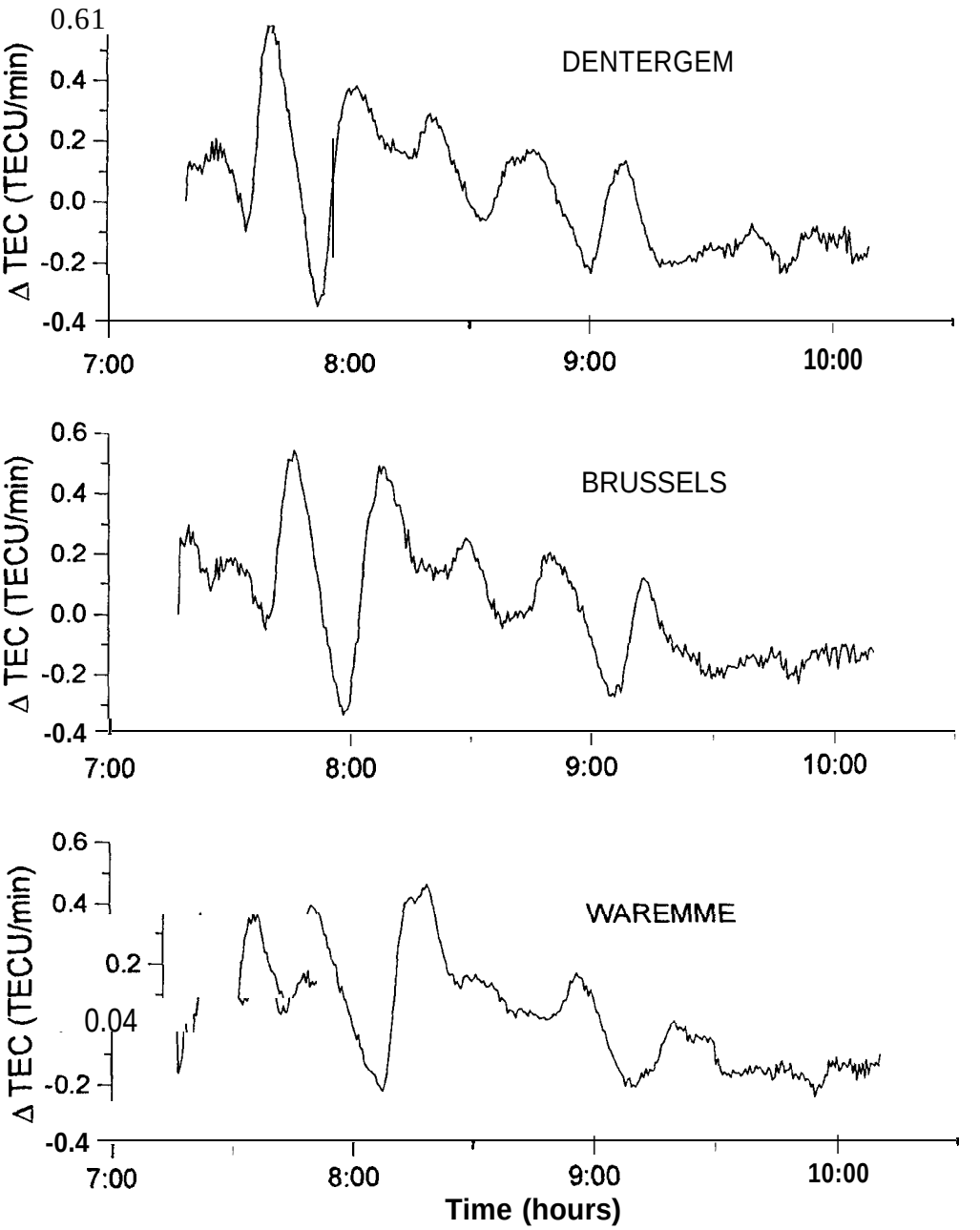

*Figure 8. TEC gradients due to a **TID** observed on October 301994 in 3 **Belgian stations.***

With a sampling interval of 30 seconds, 24 hours of GPS measurements in the RINEX format are stored in a file of which the size is ranging from 1.5 Mb to more than 2 Mb. To perform any long term study based on GPS measurements, it is thus indispensable to develop automatic data processing procedures. In particular, it is not realistic to imagine that an operator could screen the residuals to decide "manually" if a TID is present or not. For this reason, we must choose threshold values which will be used by the computer to take an automatic decision. The choice of 0.08 TECU/min as threshold value to decide if a an event is taken into account comes from the fact that the multipath also gives rise to high frequency changes in the geomet~-free combination. This site-dependent effect can reach several centimetres on phase measurements and has periods

ranging from a few minutes to several hours depending on the distance separating the reflecting surface from the observing antenna (if this distance is shorter, the period is longer). The multipath effect being more frequent at low elevation, we have chosen an elevation mask of 20°. In the case of the Belgian permanent GPS network, a threshold value of 0.08 TECU/min is large enough to avoid to interpret multipath effects as ionospheric phenomena. This value should be valid for most of the GPS sites but should be applied with care in locations where the multipath is particularly important. An additional verification is then performed: the comparison of the ionospheric variability observed in neighboring GPS stations allows also to distinguish between multipath and ionospheric phenomena: indeed, large residuals observed at the same time in different stations cannot be due to multipath.

Two other error sources can affect our method: cycles slips and phase surges. ***Cycle slips are*** jumps of an integer number of cycles which occur when the receiver loses lock on the satellite signal. In an automated data processing procedure, an uncorrected cycle slip could result in a σ_{R_1} above the threshold value even if no ionospheric perturbation is present.

Phase surges give rise to several successive jumps in the GPS phase measurements. These jumps are not integer numbers of cycles. For this reason, this error is much more difficult to detect. In addition, this effect is related to the receiver-to-satellite geometry: it means that a similar effect can be observed in several neighboring GPS stations at the same time (Sleewaegen, 1997). Nevertheless, these jumps can be identified because their period is always shorter (a few minutes) than the periods of ionospheric disturbances.

The choice of 15 minute periods to compute the ionospheric variability is due to the fact that most of the MSTIDs have periods ranging from 5 to 30 minutes. If we choose a too short period, the TID will not have the time to cause TEC changes large enough to be detected. On the other hand, if the period is too long, the large residuals in A TEC_p' due to the TID will be lost among the other residuals and the resulting σ_{R_1} will remain under the threshold of 0.08 TECU/min.

STATISTICS CONCERNING THE OCCURRENCE OF TIDs

The procedure outlined here above has been applied to the Belgian GPS network. This experiment has allowed us to compute statistics concerning the occurrence of TIDs above Belgium (i.e in a mid-latitude European station) and to answer the following questions: are TIDs unusual phenomena, do they appear during specific periods in the day, in the year, in the solar cycle, ..?

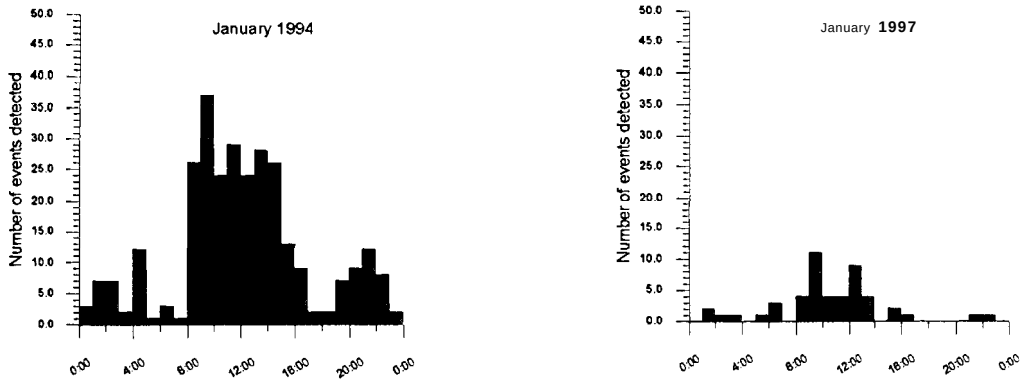

Figure 9. Number of events detected in function local time in January 94 and January97,

Figure 9 shows the statistics of the observed TIDs for two month: January 1994 and January 1997. This figure displays the number of TIDs encountered during these month in function of the time in the day. It means that a sum of all events occuring at a specific time (for example between 10hOO and 11h00) during a whole month is made.

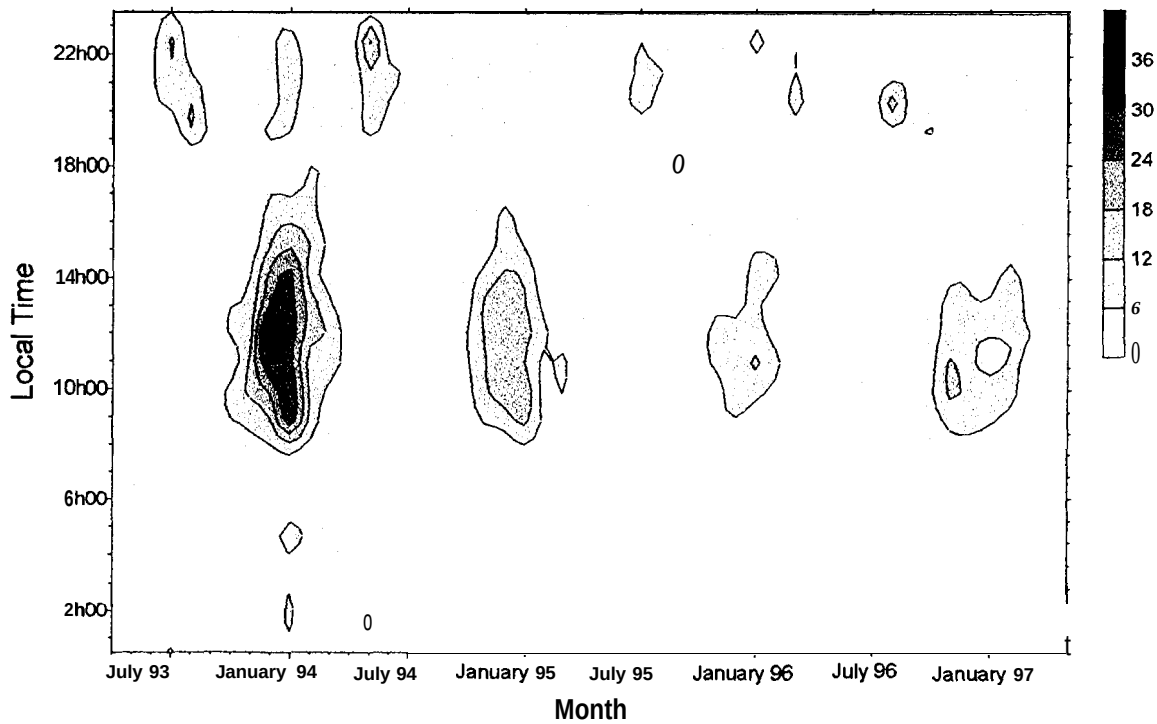

Figure 10. Number of TIDs detected from April 93 to May 97 in function of local time.

Figure 10 shows the number of events (TIDs) detected from April 93 to May 97 in function of the local time. The different levels of grey represent the number of events detected. By looking at this figure, several conclusions can be drawn concerning the number of detected TIDs :

- there is a main maximum between 10hOO and 16hO0 (local time) during the winter;
- there is a secondary maximum during the night;
- it decreases with decreasing solar activity.

The case of scintillation effects is different: only a few "events" are observed in one year. These results confirm the conclusions of previous studies performed by means of other independent techniques (see for example, Van Velthoven (1 990)).

CONCLUSIONS

The paper has outlined the method developed at the Royal Observatory of Belgium in order to compute the Total Electron Content. This method requires the determination of the receiver and satellite differential group delays. The combined biases (receiver + satellite) are obtained on a daily basis from the geometry-free combination of code observations. The computed biases undergo day-to-day and seasonal variations; in most of the cases these variations are "artificial": they are due to ionospheric residual errors. For this reason, we adopt the mean value of all the computed biases on a long period to reduce the influence ofthese errors. Nevertheless, the biases also undergo "real" changes: they are sometimes due to the temperature (during hot summer days) but we have not been able to explain all these variations. For this reason, the receiver bias has to be regularly controlled.
The precision (internal consistency) and the accuracy of our method has also been verified:

- the TEC computed at Brussels has been compared to the TEC obtained at Dentergem, Dourbes and Waremme: they agree within 2-3 TECU;

- the GPS TEC has been compared with the TEC computed from ionosonde measurements: the mean and the standard deviation of the differences "GPS" TEC - "ionosonde" TEC computed on two years (1995 and 1996) are respectively 0.46 TECU and 1.72 TECU.

In addition, the paper has presented a very simple method allowing to detect medium-scale Travelling Ionospheric Disturbances and scintillation effects using the geometry-free combination of GPS carrier phase measurements. This method has been applied to the GPS measurements gathered in the Belgian GPS network since 1989. This experiment has allowed to compute statistics concerning the occurrence of TIDs and scintillations above Belgium. The results which are in good agreement with previous independent studies show that TIDs are very common phenomena at Brussels but only a few scintillation effects have been detected.

REFERENCES

Lanyi G. E., T. Roth (1988), ***"A comparison of mapped and measured total ionospheric electron content using global positioning system and beacon satellite observations",*** Radio Science, 23, 483-492.

Sleewaegen J-M.. (1997), Personal communication Royal Observatory of Belgium,

Van Velthoven P. J. (1990), ***"Medium-scale irregularities in the ionospheric electron content",*** Ph. D. Thesis, Technische Universiteit Eindhoven.

Wanninger L. (1994), ***"Der*** *Einfluß der Ionosphere* ***auf die*** *Positionierung mit GPS"*, Ph. D. Thesis, Wissenschaftliche Arbeiten der Fachrichtung Vermes-sungswesen der Universität Hannover, Nr. 201, 137p.

Wanninger L., E. Sardon,R.Warnant(1994), *"Determination of the Total Ionospheric Electron Content with GPS - Difficulties and their Solution"*, Proceedings of Beacon Satellite Symposium '94, ed. By Dept. of Physics of University of Aberystwyth, 13-16.

Warnant R. (1996), ***"Etude du comportement du Contenu Electronique Total et de ses irregularities dans une station de latitude moyenne. Application aux calculs depositions relatives par le GPS"***, Ph. D. Thesis (in French), Série Géophysique (N° Hors-Série) de 1' Observatoire Royal de Belgique, Bruxelles.

Warnant R., ***J.-C.Jodogne(1997), "A Comparison between the TEC Computed using GPS and Ionosonde Measurements",*** paper presented at the Beacon Satellite Symposium '97, to be published in Acts Geodaetica et Geophysics Hungarica.

Wilson B. D. , A. J. Mannucci (1993), ***"Instrumental Biases in Ionospheric Measurements derived from GPS data"***, Proceedings of ION GPS'93, Salt Lake City.

MONITORING THE IONOSPHERE OVER EUROPE AND RELATED IONOSPHERIC STUDIES

N. Jakowski, S. Schlüter and A. Jungstand

Deutsches Zentrum für Luft- und Raumfahrt e. V.
Femerkundungsstation Neustrelitz
Kalkhorstweg 53, D-17235 Neustrelitz

ABSTRACT

The rather dense network of GPS ground receivers of the IGS geodetic community is used to monitor the total electron content (TEC) of the ionosphere on a routine base. TEC maps are generated by combining GPS-derived TEC data with a well-qualified regional TEC model. Taking into account the achieved RMS accuracy of TEC in the order of 2x10] $^{6}m^{-2}$ the TEC maps provide a lot of information for more detailed ionospheric studies. So the TEC monitoring data will help to develop and improve ionospheric models, to study complex solar-terrestrial relationships and to explore large scale ionospheric perturbations. The mapping technique is also recommended for real time applications in navigation and geodesy.

INTRODUCTION

Space based radio navigation systems such as the US Global Positioning System (GPS) and the Russian Global Navigation Satellite System (GLONASS) offer the unique opportunity to monitor the ionosphere on global scale.

Due to the dispersive nature of the ionosphere the total electron content (TEC) can be derived from code and carrier phase measurements on L1/L2 frequencies by difference methods. The same technique is applied to compensate ionospheric propagation errors in space based navigation satellite systems.

Since first-order ionosphere induced range errors are proportional to TEC, ionospheric TEC maps are helpful in different geodetic and navigation applications especially for single frequency GPS and GLONASS users to enhance the accuracy and reliability y of measurements.

Ionospheric TEC maps are generated in DLR/DFD Femerkundungsstation Neustrelitz since February 1995 on a regular base. Corresponding hourly maps are available in the Internet via *http://www.nz.dlr.de/gps/gps-ion.html with* a time delay of about two days,

TEC MONITORING OVER EUROPE

The algorithm for TEC estimation from GPS measurements is described by Sardon et al. (1994). Assuming a second-order polynomial approximation for TEC variations over the observing GPS ground station, both TEC as well as the instrumental satellite-receiver biases are estimated by a Kalman filter run over 24 hours. The 30s data of GPS stations of the European IGS network thus allow the determination of slant TEC values along more than 100 satellite-receiver links over the European area with high time resolution. The slant TEC data are then mapped to the vertical by applying a mapping function which is based on a single layer approximation at hsp=400km (Jakowski et al., 1996a).
Ionospheric maps are generated by combining the observed TEC data with the regional TEC model (Neustrelitz TEC Model-NTCM) in such a way that the map represents measured values near measuring points and model values at regions without measured data. This procedure has the advantage that also in case of a low number of measurements physically reasonable TEC data are provided to users. So this method is strongly recommended for application in real time ionosphere monitoring systems.
The NTCM model is described elsewhere (e.g. Jakowski et al., 1996, a, b). It has to be mentioned that the TEC maps cover the area of 32.5 °≤ϕ≤70°N and -20 °≤λ≤60°E in latitude and longitude, respectively. The grid resolution is 2.5° in latitude and 5° in longitude resulting in 272 grid values for one map.
Due to the low data density in the eastern part of the area, the eastward border of the maps is temporarily fixed at 40°E.

COMPARISON WITH IONOSPHERIC MODELS (IRI95)

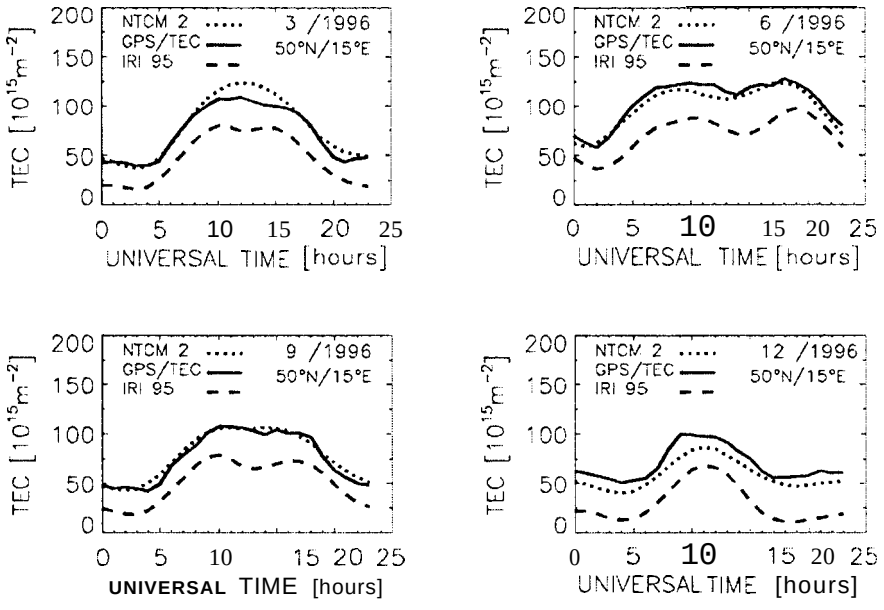

Fig. 1: Diurnal variation of TEC derived from NTCM2, IRI95 and GPS measurements for different seasons at 50 °N/15 °E.

Long-term observations of TEC over large areas are well suited for the development and check of ionospheric models. Thus, GPS-derived TEC monitoring data over Europe have been used to derive the regional TEc model NTCM2. On the other hand, the TEC monitoring data can be used to

check and/or improve well-known ionospheric models such as IRI95 or Bent. A comparison between monthly averaged TEC monitoring data, NTCM2 and corresponding IRI95-derived TEC data is made in Fig. 1 at a fixed grid point at 50°N/ 15°E for different seasons. It has to be mentioned that the IRI95-TEC data were derived by integrating IRI95 electron density profiles up to 1000km height, i.e. these values doesn 't include the plasmaspheric electron content. Indeed, the permanent difference between TEC monitoring/NTCM2 data and IRI95-TEC in the order of 1-4x$10^{16}$$m^{-2}$ could be explained by the plasmaspheric content not considered in IRI95-TEC. This fits quite well with plasmaspheric content estimations made by Kersley and Klobuchar (1 978) using ATS 6 radio beacon observations.

Taking into account the growing solar activity during the next years, it is evident that regional and global TEC monitoring activities by several groups will contribute to essential improvements of already well-prepared ionospheric models. On the other hand the development of special TEC models should be possible on a high standard.

SOLAR CONTROL OF TEC

It is a well-known fact that the solar extreme ultraviolet radiation (EUV) is the major source of ionospheric ionization. Several studies have indicated that there exist a nearly linear relationship between the solar flux $F_{10.7}$ (rough measure of the EUV intensity) and TEC (e.g. Jakowski and Paasch, 1984; Davies et al., 1992). The sensitive response of TEC to solar activity variations becomes evident in its solar rotation dependence (Jakowski et al., 1991). To check these relationships, the cross correlation function was computed between the $F_{10.7}$ index and corresponding TEC data obtained at fixed grid points during 1996. The results illustrated in Fig. 2 indicate again a certain delay between the solar radio flux index $F_{10.7}$ and the ionospheric response up to 2 days with some interesting features related to the geographic latitude. The increasing level of solar activity and improved knowledge of the EUV-$F_{10.7}$ relationships are good conditions to explore this phenomenon in the near future.

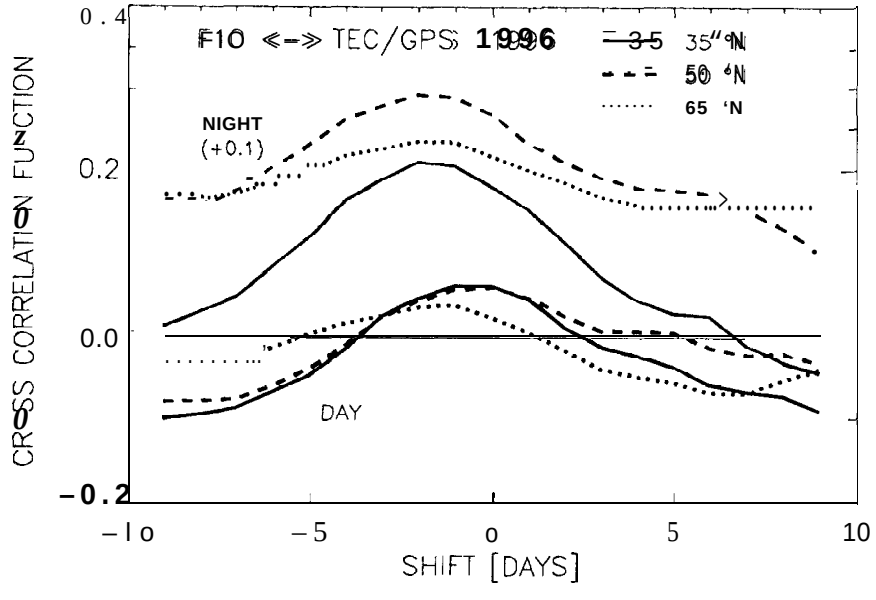

Fig. 2: Cross correlation between GPS based 3-hourly averaged TEC data at 15 'E longitude and the solar radio flux index $F_{10.7}$ (Day-time: 11-13 UT; night-time: 1-3 UT).

LARGE SCALE PERTURBATIONS IN THE IONOSPHERE

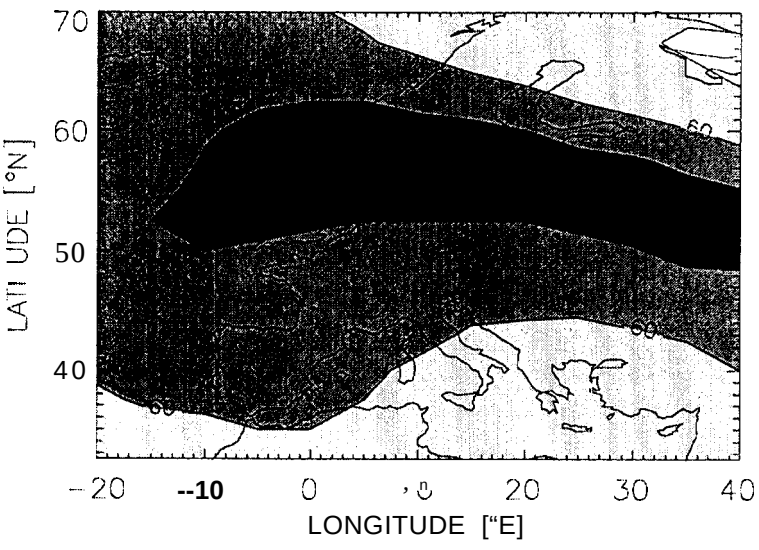

Fig. 3: Electron density trough over Europe in the coarse of the ionospheric perturbations on 11 April 1997, 00:00 UT (Difference between contour lines is $15x10^{15}m^{-2}$).

GPS based ionospheric monitoring provides an outstanding tool to study large scale processes in the ionosphere (e.g. Jakowski, 1995). So the horizontal extension of large scale structures can easily be detected as it is shown in Fig. 3 for the mid-latitude trough. This trough has been developed in the coarse of a geomagnetic/ionospheric storm on April 11, 1997, 00:00 UT. As a consequence of various coupling processes, ionospheric perturbations are closely related to geomagnetic activity. The competing character of these magnetosphere-ionosphere-thermosphere interactions leads to a rather stochastic behaviour of the ionosphere during ionospheric storms. Nevertheless, ionospheric storms indicate some common features as f.i. the so-called „positive" and „negative" phases of ionization when referring to the mean behaviour. The variation with time of TEC deviations from corresponding mean or „normal" values is called storm pattern.

Since common signatures of the storm behaviour should be pronounced in storm statistics, we have superposed such storm periods whose geomagnetic activity or its time gradient exceeds certain critical levels. The synchronization of storm pattern is reached by simple local time dependence (LTV) or by defining a selected geomagnetic activity phase (maximum of three-hourly Ap values or Ap-increase during the onset phase) as the reference storm time (ST=0). So local time controlled effects might be separated from storm time driven effects. In agreement with former studies (Jakowski et al., 1990) the preliminary analysis of 23 storm periods over Europe indicate a clear seasonal dependence of storm pattern. Superposed storm time pattern for summer (May-August) and winter months (November-February) illustrate this phenomenon in Figs. 4-6. Summer storms over Europe are characterized by a rather short positive phase (about 10 hours) which is followed by a well-pronounced negative phase starting at high latitudes. In contrast to this behaviour, winter storms over Europe are characterized by a well-developed positive phase lasting more than 24 hours. As Fig. 6 indicates, the positive phase is more pronounced at high latitudes in winter and at lower latitudes in summer. These seasonal differences can be explained by the global thermospheric circulation directed from the summer to the winter hemisphere in an average sense (Jakowski et al.,

1990). Collecting more and more TEC data during the next years, the statistical analysis of storm pattern can essentially be improved.

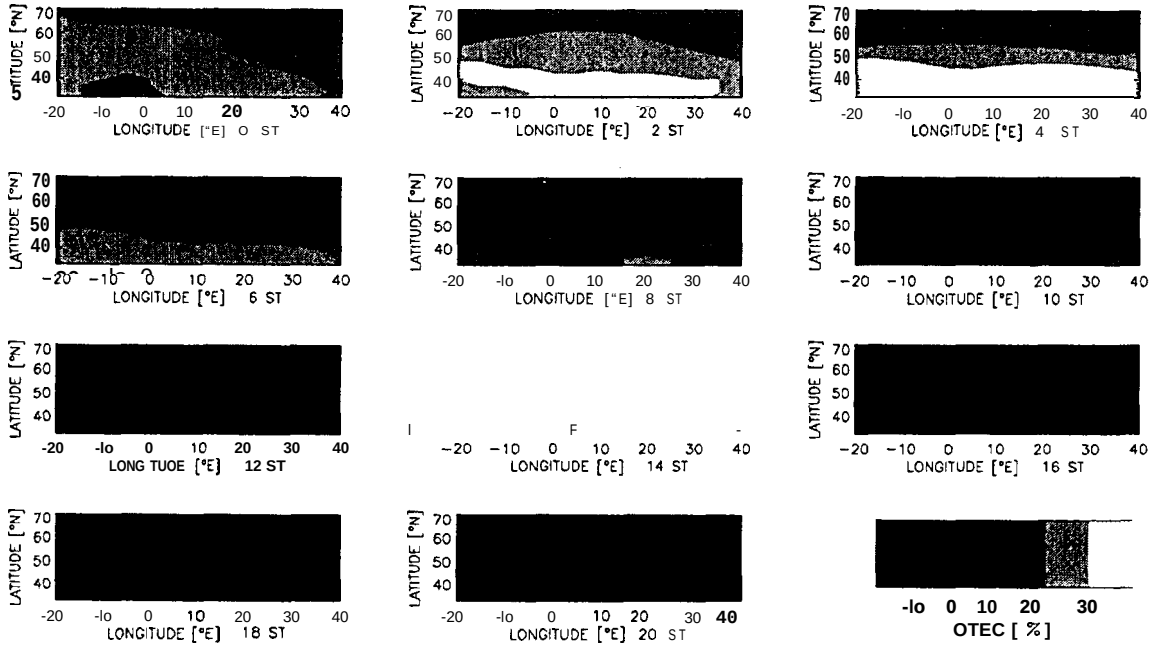

Fig. 4: Two-hourly maps of percentage TEC perturbation pattern for summer storms (May-August during 1995-1997).

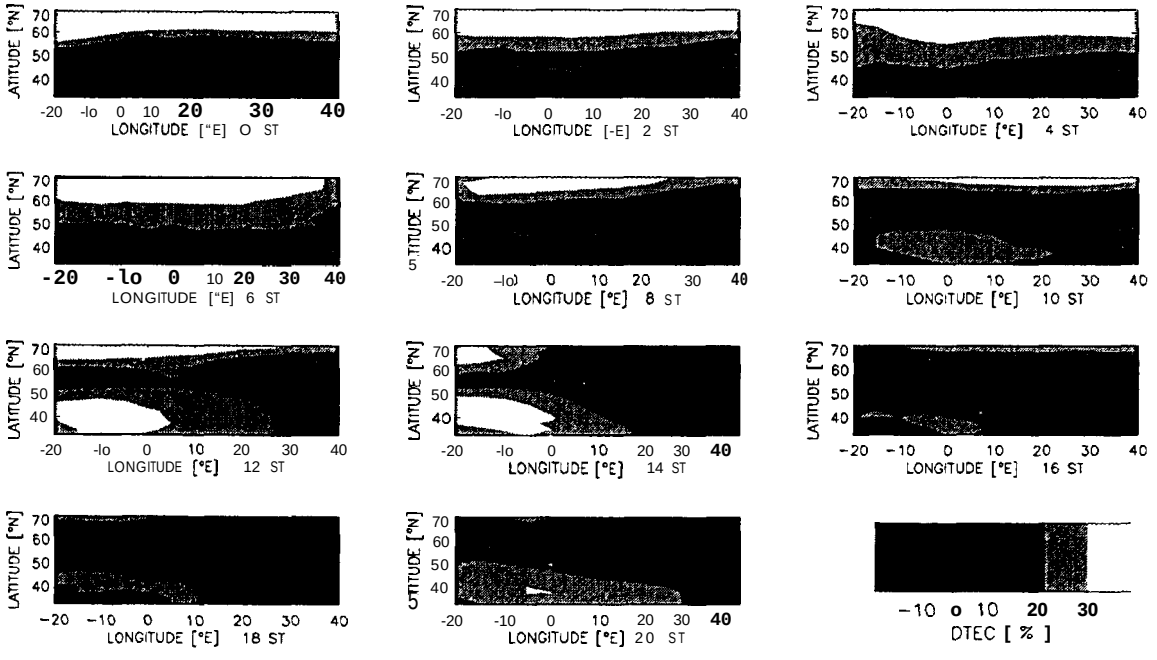

Fig. 5: Two-hourly maps of percentage TEC perturbation pattern for winter storms (November-February during 1995 -1997)._

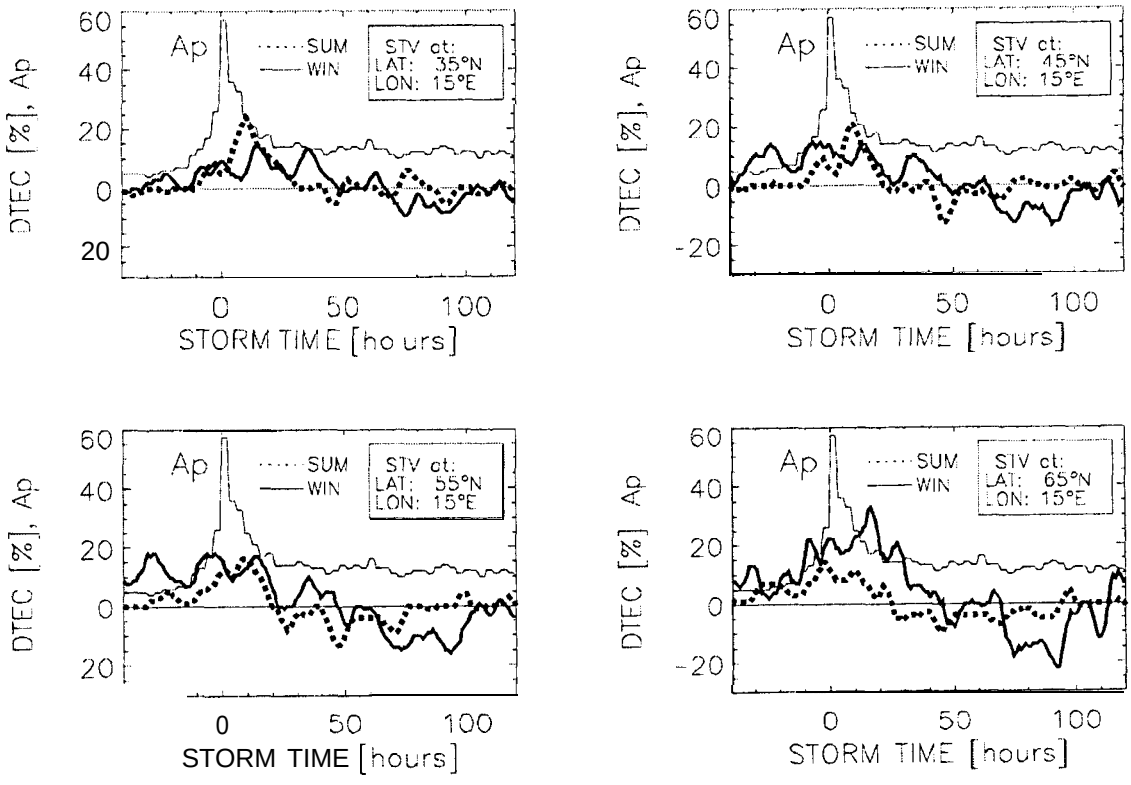

Fig. 6: Superposition of percentage TEC perturbation pattern for summer and winter storms selected from the time interval 2/95-8/97. Storm time ST=00 is defined by Ap_{max} , selection criteria for storm periods are: $Ap_{max}>30$, $Ap<20$ for prestorm conditions (3 days).

CONCLUSIONS

It has been shown that the rather dense network of well-qualified GPS ground stations of the IGS network provides a unique opportunity for reliable ionospheric monitoring. Considering a RMS error of TEC in the order of 2x10 tGm-2 the described mapping technique is suited to reconstruct large scale horizontal structures in the ionosphere. Real time ionospheric monitoring and the delivery of TEC maps to GPS and/or GLONASS users should enhance accuracy and integrity of navigation satellite systems.

The ionospheric monitoring technique based on global and regional GPS measurements contributes directly to „Space Weather" reports and predictions.

Furthermore it becomes evident that GPS based ionospheric monitoring is a powerful tool for developing and/or checking ionospheric models, for studying solar-terrestrial relationships and for exploring large-scale ionospheric perturbations.

Acknowledgement

The authors are grateful to the international IGS community for making available the high-accurate GPS data sets.

References

Davies K., W. Degenhardt, G.K. Hartmann, N. Jakowski, R. Leitinger , Relationship between Ionospheric Electron Content and Solar Fluxes, Proc. of the Int. Beacon Sat. Symp. (Ed.: Min-Chang Lee), Cambridge, July 6.-10,188-191, 1992.

Jakowski N. and E. Paasch, Report on the observations of the total electron content of the ionosphere in Neustrelitz/GDR from 1976 to 1980, Ann. Geophys. 2,501-504, 1984.

Jakowski N., E. Putz, and P. Spalla, Ionospheric storm characteristics deduced from satellite radio beacon observations at three European stations, Ann. Geophys. 8, 343-352, 1990.

Jakowski N., B. Fichtelmann, and A. Jungstand, Solar activity control of ionospheric and thermospheric processes, J. Atmos. Terr. Phys., 53, 1125-1130, 1991.

Jakowski N., Ionospheric Research and Future Contributions of the IGS Network, Proc. IGS Workshop, Potsdam, 15.-17.05.1995, 17-29, 1995.

Jakowski N., E. Sardon, E. Engler, A. Jungstand, and D. Klähn, About the use of GPS Measurements for Ionospheric Studies, GPS Trends in precise Terrestrial Airborne, and Spaceborne Applications", IAG Symposium 115, (Eds.: Beutler, Hein, Melbourne, Seeber), Springer-Verlag, 248-252, 1996a.

Jakowski N., E. Sardon, E. Engler, A. Jungstand, D. Klähn, Relationships between GPS-signal propagation errors and EISCAT observations, Ann. Geophys. 14, 1429-1436, 1996b.

Kersley L. and J.A. Klobuchar, Comparison of protonospheric electron content measurements from the American and European sectors, Geophys. Res. Lett. 5, 123-125, 1978.

Sardon E., A. Rius, N. Zarraoa, Estimation of the transmitter and receiver differential biases and the ionospheric total electron content from Global Positioning System observations, Radio Science, VO1.29, N. 3,577-586, 1994.

ROUTINE PRODUCTION OF IONOSPHERE TEC MAPS AT ESOC - FIRST RESULTS

J. Feltens[1], J.M. Dow [2], T.J. Martín-Mur [2],
C. García Martinez [3] and P. Bernedo[3]
1. EDS at Flight Dynamics Division,
ESA, European Space Operations Centre,
Robert-Bosch-Str. 5, D-64293 Darmstadt, Germany
2. ESOC
3. GMV at ESOC

ABSTRACT

The first version of ESOC'S Ionosphere Monitoring Facility (IONMON) software has become operational. The routine production of TEC maps and receiver/satellite differential code bias values has started in January 1998. ESOC intends to contribute with these products to an IGS ionosphere service as well as to use the ionosphere maps for the support of other ESA-missons, e.g. ERS and ENVISAT.

This paper condenses the results obtained from the first month of routine IGS ionosphere processing at ESOC with different kinds of TEC modeling. A comparison between TEC maps obtained from these distinct mathematical TEC models is made in order to assess the internal accuracy that can be achieved. A verification with TEC maps provided by other Analysis Centers will be possible when the IONEX format (Schaer et al., 1997) has been commonly implemented. The ESOC TEC maps are available in IONEX format. Verification of satellite differential code biases was done by comparison with values obtained from some other centers.

Based on the experiences made with the first month of operational ionosphere maps production, a fine-tuning of the models and last improvements could be made in order to optimize routine ionosphere processing.

INTRODUCTION

It is the task of this paper to give an overview on how routine IGS ionosphere processing is done at ESOC and to present an analysis of the first results obtained.

The paper will start with an overview over ESOC'S ionosphere processing under the aspects of observation data used, geographical extent, mathematical models invoked, number of TEC maps produced daily, time resolution and delay of availability.

The main part of the paper will thereafter concentrate on the results achieved during the first month of routine ionosphere processing at ESOC. Until now, validation had to be restricted to internal comparisons only. The implementation of the Ionosphere Map EXchange Format (IONEX) (Schaer et al., 1997) at the other Analysis Centers will enable an easy exchange of ionosphere products and thus allow for intercomparisons. The assessment of internal accuracy was done by the comparison of TEC maps obtained from different mathematical models. For the verification of estimated satellite differential code biases, corresponding values from some other Analysis Centers were available and could be used.

Finally this paper will conclude with an outlook on intended future activities and software extensions planned at ESOC in the area of the ionosphere.

ROUTINE IONOSPHERE PROCESSING AT ESOC

The operational evaluation of ionosphere products at ESOC is currently coupled to the final orbit processing. If a certain routine and experience has been achieved, the provision of ionosphere products in rapid mode can be taken into consideration. The software's structure and environment allows principally for a rapid processing.

Carrier phase leveled to code measurements - so called "TEC observable" - enter into the Ionosphere Monitoring Facility (IONMON) software. The sampling rate is 6 minutes.

Currently 4 IONMON runs are made per day, using TEC observable collected from a global net of about 50 stations, 24 hours of observation data enter into each fit. The 4 daily runs are:

1) Determination of a set of receiver/satellite differential code bias values. In order to cleanly extract the influence of the differential code biases from the TEC observable, only nighttime tracking data is enter into that fit. The ionosphere's part (which is expected to be quite small over nighttime) is absorbed by a low degree and order spherical harmonic of $n = 4, m = 2$, **with the degree and order 1 coefficients kept fixed to zero. The differential code bias values thus obtained serve then as reference values for the other 3 fits of that day, and are introduced with a constraint of 0.5 ns there.**

2) Global TEC model by fitting a GE-function (Feltens et al., 1996) of degree and order $n = 10, m = 8$ **to the TEC** observation data. In the GE-function fit the ionosphere's electron density is assumed to be condensed within an infinitesimal thin layer enclosing the Earth as hollow sphere in a height of 450 km. The mapping function is $1/\cos z$. **In the analyses of next chapter this fit will be denoted as "GE".**

3) Global 3-d Chapman Profile model (Feltens, 1998). The maximum electron density N_0 is represented by a degree and order $n = 10, m = 8$ GE-function, and the height of maximum electron density h_0 is modeled with an extended sin-function. The allowed height range is 400 $km \leq h_0 \leq$ 450 km. The output of this Chapman Pro-

file model are 6 maps: A TEC map obtained by integration over the Chapman Profile, a N_0 map, a h_0 map and maps of electron density at heights of 250, 500 and 750 km. In the analyses of next chapter this fit will be denoted as "CP".

4) Global 3-d Chapman Profile model. The maximum electron density No is represented by a degree and order $n = 10, m = 8$ GE-function, and h_0 is estimated as global constant. The output are also a TEC map, a No map and maps of electron density at h = 250, 500, 750 km. A h_0 **map does not make sense in this case, since h_0 is constant. In the analyses of next chapter this fit will be denoted as** "CP1".

All fits use a 20^o elevation cutoff, and elevation-dependent weights are applied to the observables. The internal evaluation of all these models is done in the solar-magnetic reference frame.

Polynomial models to represent the TEC within the local area around a single ground station can be evaluated upon special request and over limited time for ESOC-internal use only. It is not intended to deliver these local polynomial models to the IGS. 6 hours of observation data enter into such a polynomial fit.

Once a certain routine has been achieved, the ionosphere products processing can be enhanced, e.g. every 6 hours a global model with 24 hours of TEC data.

FIRST RESULTS

TEC Maps

As already pointed out above, no access to TEC maps from outside ESOC was available for the analysis of the first results of operational processing. So only an ESOC-internal verification between the TEC maps originating from the different mathematical models could be done so far. An application of GE-function TEC models to ERS altimeter and S-band data during a period covering February '97 provided corrections for ionospheric signal delays with accuracies comparable to that obtained from the IRI-95 model (Feltens et al., 1997). The GE-functions shall thus serve here as reference with respect to which the 3-d Chapman Profile models shall be compared. The results presented here were obtained over the period from 28 December 1997 (97362) to 23 January 1998 (98023).

One indicator of accuracy is the daily repeatability of statistical parameters, such as %-age of measurements used and ***rms,*** in the one and in the other TEC model fit. Figures 1a and lb show these two parameters for the three fits GE, CP and CP1:

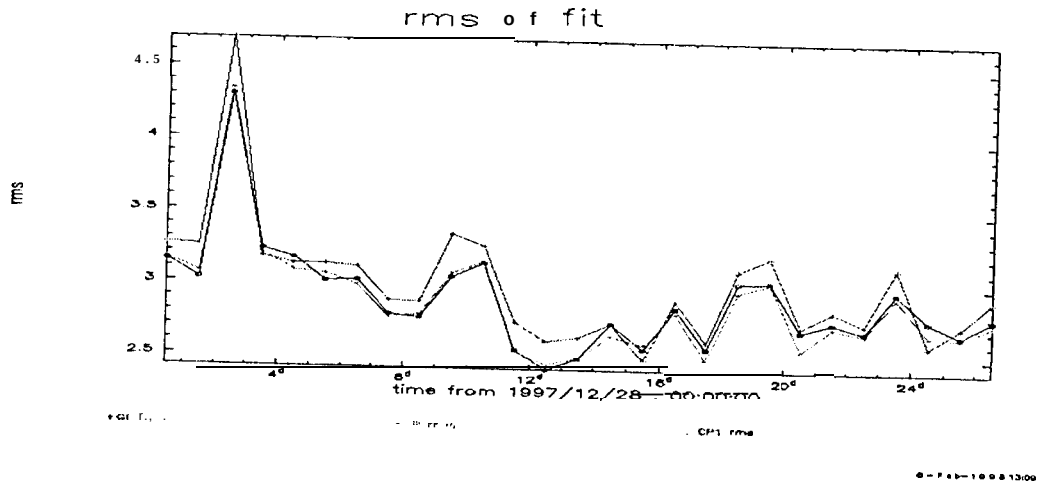

Figure la: Daily ***rms*** obtained for the GE, CP and CP1 fits.

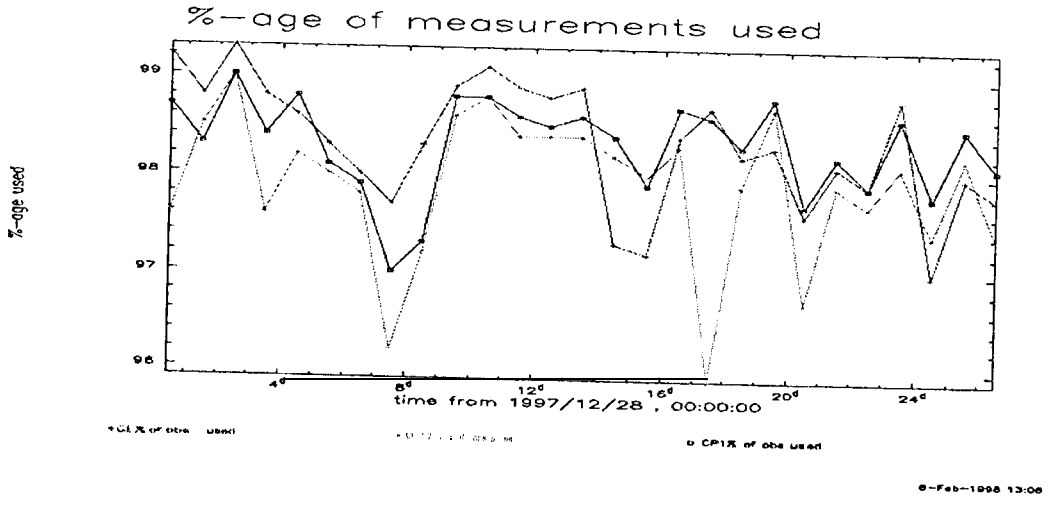

Figure lb: Daily %-age of measurements used in the GE, CP and CP1 fits.

The curves of Figures 1a and 1 b seem to indicate that GE-function fits and Chapman Profile fits are of comparable accuracy, with the Chapman Profile models showing a tendency to be slightly better. The **CP** fits show the lowest ***rms,*** but also the lowest 96-age of measurements used. **The *rms*** of the CPI **fits are** slightly higher, but more observations were taken. When comparing GE-functions with Chapman Profile models it must be kept in mind, that the Chapman Profile models show more flexibility because of more unknowns that are estimated.

The next Figure 2 presents the daily variation of estimated height h_0 of maximum electron density from the CPI fits.

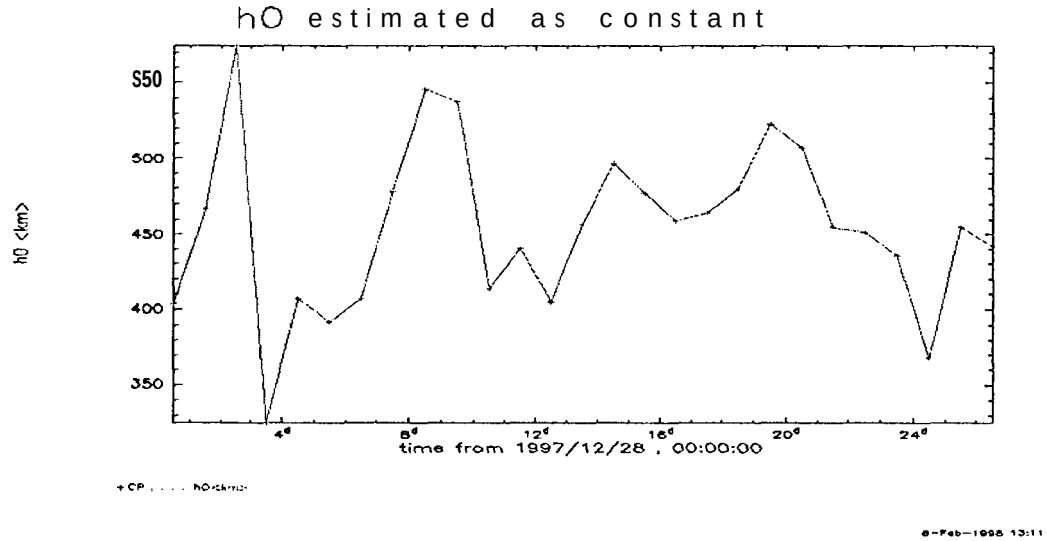

Figure 2: Daily estimated h_0 values from the CP1 fits [km].

Figure 2 shows a quite strong variation of the daily estimated h_0 values. But, as is pointed out in (Feltens, 1998), h_0 is only weakly estimable from pure TEC observable. The inclusion of satellite-to-satellite tracking (SST) data into the Chapman Profile model fits might improve this situation. Because for lack of such data, this could not be done yet, A combination of TEC data with other kinds of data, e.g. ionosonde data, might improve the situation too.

Figures 3 to 5 show a sequence different maps obtained for one day from the GE, CP and CP1 fits. All Figures have a vertical range from $+90^o$ to -90^o in geographic latitude and a horizontal range from 0^h local time (-18@) to 24^h local time (+18@) and are centered at 12^h local time (0^o).

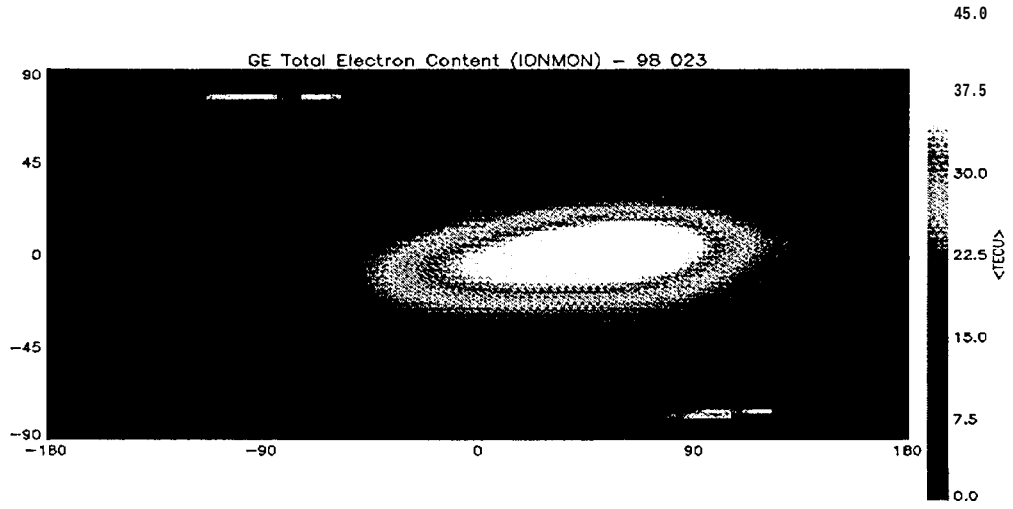

Figure 3: Global *TEC* map from GE fit for doy 98023,

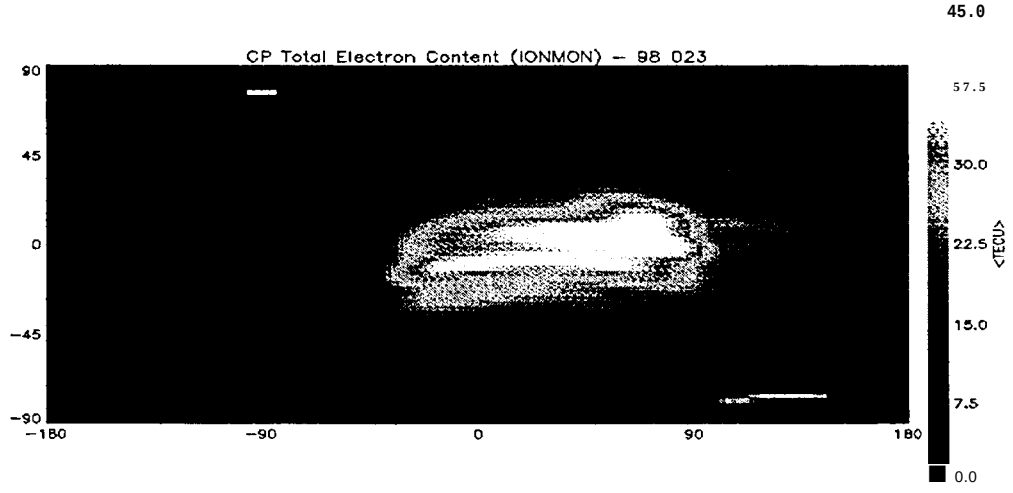

Figure 4a: Global *TEC* map from CP fit for doy 98023,

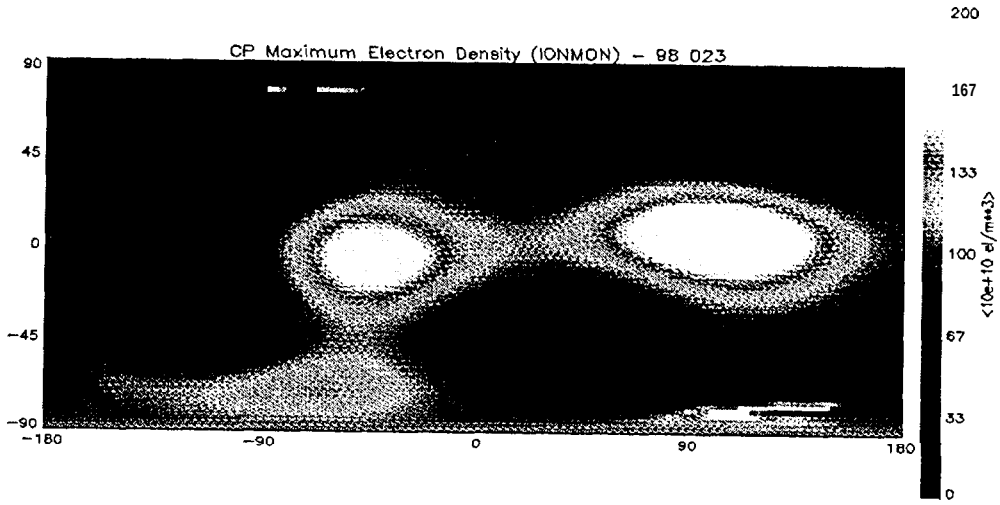

Figure 4b: Global N_0 map from CP fit for doy 98023.

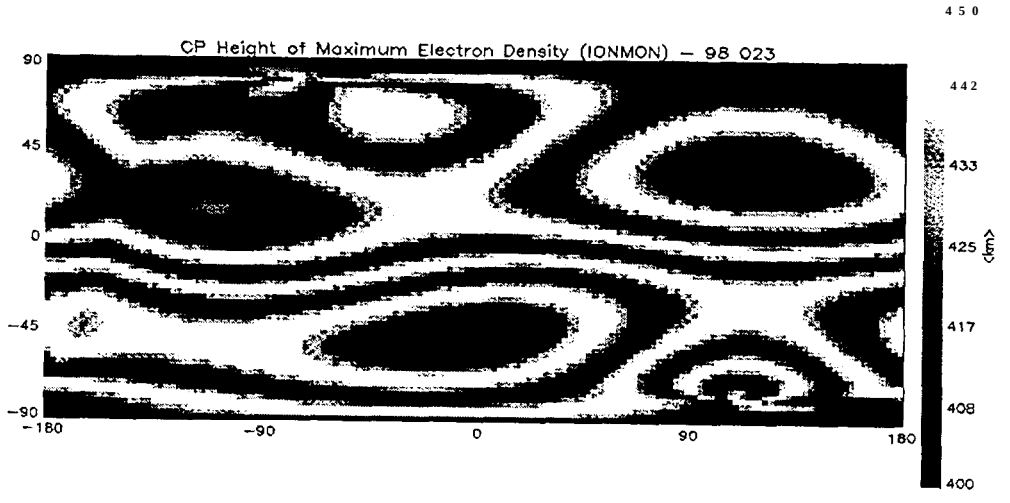

Figure 4c: Global h_0 map from CP fit for doy 98023.

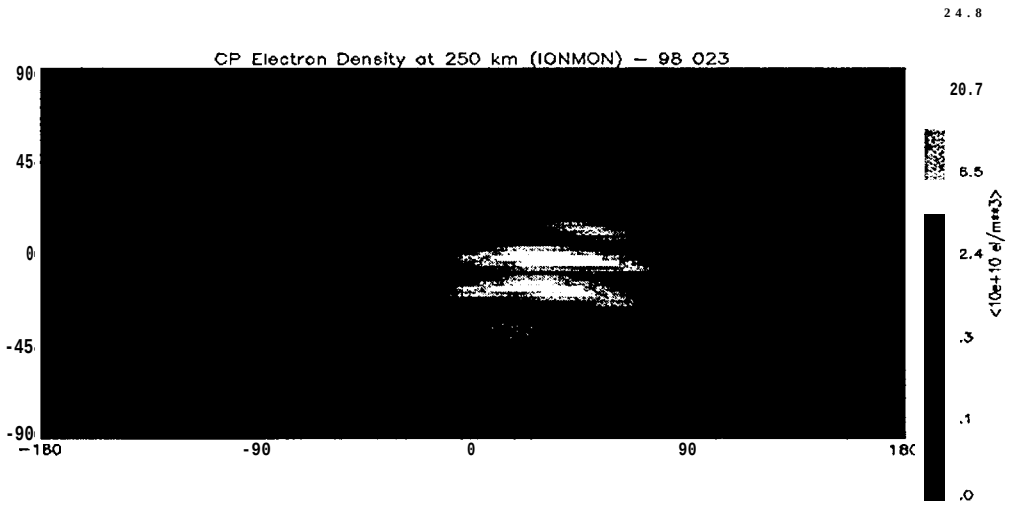

Figure 4d: Global electron density map at h = 250 km from CP fit for doy 98023.

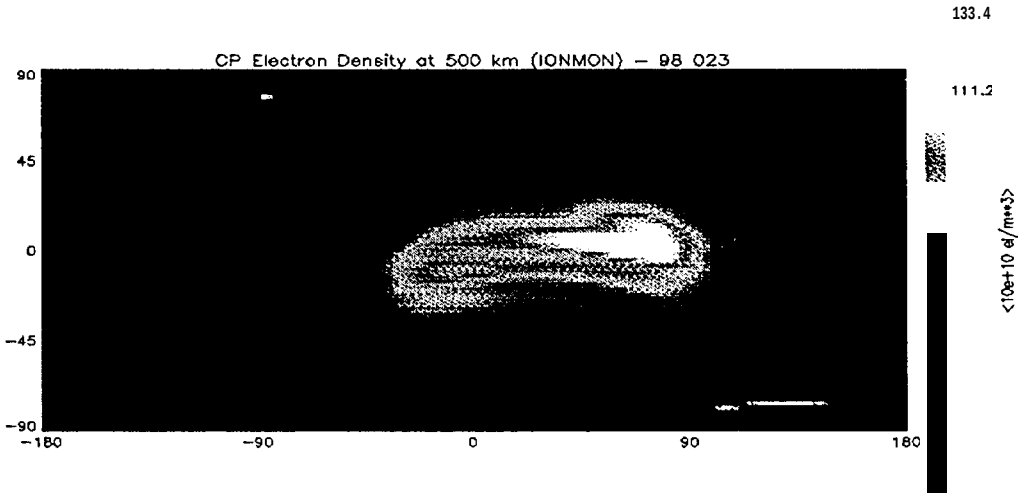

Figure 4e: Global electron density map at h = 500 km from CP fit for doy 98023.

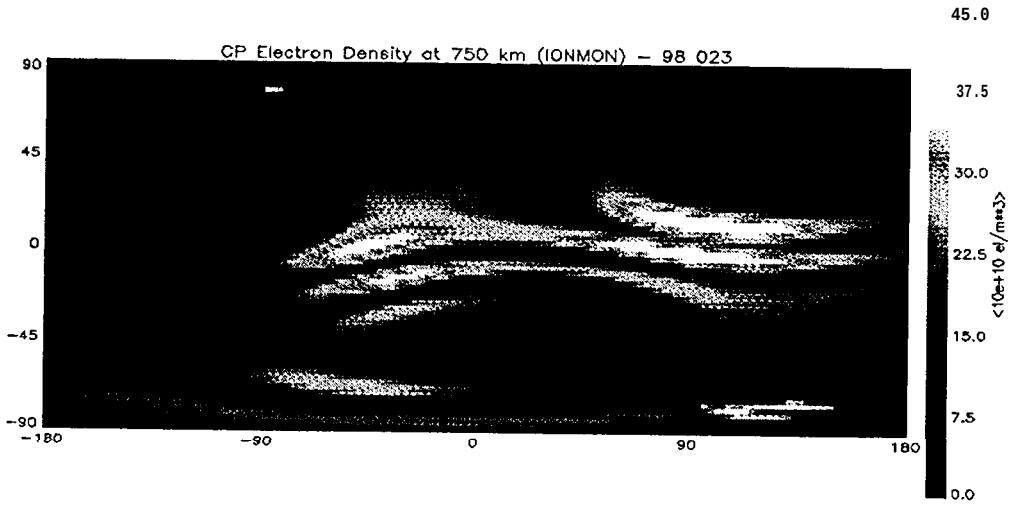

Figure 4f: Global electron density map at h = 750 km from CP fit for doy 98023.

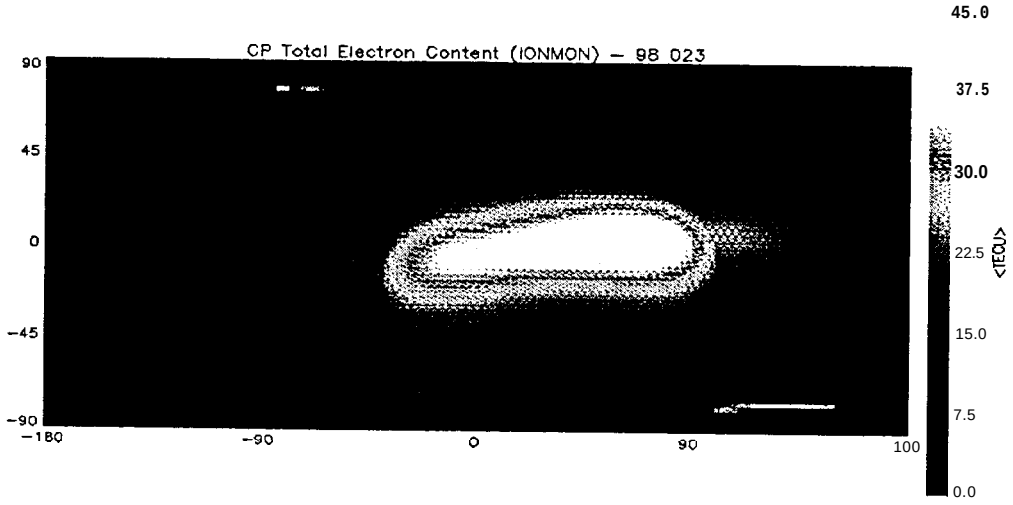

Figure 5: Global *TEC* map from CP1 fit for doy 98023.

When comparing the TEC maps in Figures 3, 4a and 5, one recognizes an overall good agreement between the GE , CP and CP1 fit. Compared with the GE map, the two Chapman Profile maps present finer structures. This is especially valid for the map from the CP fit, since the height h_0 is not treated as constant but as extended sin-function single layer in this case. The estimation of both, N_0 and h_0, makes the Chapman Profile models more flexible than the GE-function, thus allowing a better adaption to the TEC observation data. Additionally the 3-d geometry being intrinsic in the Chapman Profile models may enhance this flexibility. This 3-d geometry is ruled by the Sun's zenith angle χ (see Feltens, 1998).

The h_0 map shown in Figure 4c should not so strongly be interpreted as the real h_0 distribution, but more as the result of absorbing unmodeled effects in the CP fit.

Figures 4d to 4f present the electron density at different heights. Apart from the N_0 map of Figure 4b, the map for h = 500 km shows the **heighest electron density values, since it is closest to the height of maximum electron density. The lowest electron density can be seen in the map for h = 250 km,** indicating a strong decrease of ionization by the solar radiation after having passed h_0. The map for h = 750 km shows an overall lower niveau of electron density than the map for h = 500 km, which can be expected from theory - but at the borders the electron density can be heigher at 750 km than at 500 km. This effect is also explained by Chapman Profile theory: Close to the terminator the height of maximum electron density is larger than at noontime (Feltens, 1998), and this effect propagates upwards and can be felt in 750 km altitude.

The above maps show abnormal peaks at high latitudes. Because of holes in the station net and the arrangement of orbital inclinations in GPS satellite constellation, there is a bad coverage around the poles. As consequence there are no observation data in these zones to which the TEC models could fix. This problem can only be overcome by densifying the station net in the polar regions (as far as new stations become available) - especially on the southern hemisphere.

Differential Code Biases

DLR Femerkundungsstation **Neustrelitz** had provided differential code bias values with respect to which the **ESOC/IONMON** differential code biases could be compared. As example the values for four satellites are presented Figure 6 over the time span from 28 December 1997 to 23 January 1998:

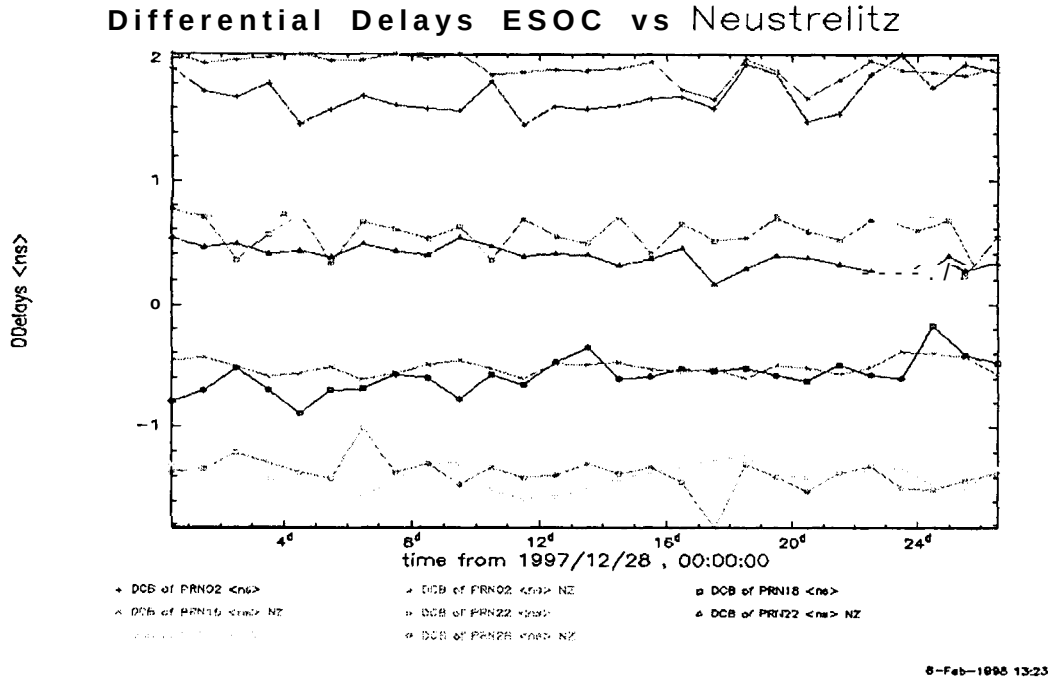

Figure 6: ESOC versus DLR Neustrelitz differential code bias values for PRNs 02, 18, 22,26.

Figure 6. shows an agreement between the Neustrelitz and the ESOC values within 0.3 *ns* over the whole period. An agreement of the same order was also found for the other GPS satellites. Additional comparisons with differential code bias values from the Astronomical Institute of the University of Beme comfirmed this order of agreement,

CONCLUSIONS

ESOC has started with the routine evaluation of ionosphere products at the beginning of this year 1998. Three different kinds of global TEC maps and a set of receiver/satellite differential code bias values are produced daily. Of the three **TEC** maps two are based on a

Chapman Profile approach, thus providing also information on the ionosphere's electron distribution with respect to height.

Validation of achieved TEC map accuracy could so far only be done by analysis of ESOC-internal products. The common implementation of the IONEX software at all Analysis Centers will then allow for an easy and efficient intercomparison of ionosphere products.

Verification of internal accuracy was basically done with two methods:

1) By examination of the daily continuity of statistical parameters.

2) By comparison of TEC maps from different mathematical models for identical days.

Both methods confirmed stable and accurate IONMON model and software performance.

For the approval of estimated differential code biases, external values were available for comparison and showed an overall agreement in the order of 0.3 ns.

All in all ESOC'S operational ionosphere processing looks accurate and stable. The products are output in the IONEX format. ESOC is ready to contribute to an IGS ionosphere product.

REFERENCES

Feltens, J., J.M. Dow, T.J. Martín-Mur, C. García Martinez and M.A. Bayona-Pérez, 1996, Verification of ESOC Ionosphere Modeling and Status of IGS Intercomparison Activity, IGS Presentation, in ***Proceedings of the 1996 IGS Analysis Centers Workshop,*** **Silver Spring, MD, U. S.A., March 19-21, 1996, pp 205-219.**

Feltens, J., J.M. Dow, T.J. Martín-Mur, C. Garcia Martinez, F. Martínez-Fadrique and R. Piriz, 1997, Using GPS for Ionospheric Corrections of ESA Tracking Data, in ***Proceedings*** *of* ***the 12th International Symposium on Space Flight Dynamics,*** ESOC, **Darrnstadt, Germany, June 2-6, 1997, pp 121-125.**

Feltens, J., 1998, Chapman Profile Approach for 3-d Global TEC Representation, IGS Presentation, in ***Proceedings of the 1998 IGS Analysis Centers Workshop,*** **ESOC,** Darmstadt, Germany, February 9-11, 1998.

Schaer, S., W. Gurtner and J. Feltens, 1997, IONEX: The Ionosphere Map EXchange Format Version 1, February 25, 1998, in ***Proceedings*** *of the* ***1998 IGS Analysis Centers Workshop,*** **ESOC,** Darmstadt, Germany, February 9-11, 1998.

CHAPMAN PROFILE APPROACH FOR 3-D GLOBAL TEC REPRESENTATION

J. Feltens
EDS Industries (Deutschland) GmbH, based at
Flight Dynamics Division,
ESA, European Space Operations Centre,
Robert-Bosch-Str. 5, D-64293 Darmstadt, Germany

ABSTRACT

Until now, ESOC employed single layer algorithms to describe ionospheric TEC 2-dimensionally. Since the real ionosphere is a 3-dimensional phenomenon but not a 2-dimensional one, the idea arose to establish a physically more realistic 3-dimensional model, based on a Chapman Profile approach. The presentation of this new 3-dimensional TEC model will be the task of this paper.

The new 3-dimensional TEC model represents the ionosphere's electron density by a simple Chapman Profile, whereby the layer of maximum electron density N_0 acts as scaling factor and its height h_0 as profile parameter. N_0 and h_0 in turn are modeled as global single layers. The 3-dimensional TEC model uses so called "leveled TEC observables", derived from dual-frequency GPS tracking data, for the determination of its model parameters in a least squares fit. Beyond the evaluation of ground-based tracking data, the processing of SST data is possible too.

INTRODUCTION

This paper will concentrate on the presentation of the basic mathematical algorithms that were worked out to realize a 3-dimensional Chapman Profile TEC model. Numerical results and analyses obtained during an application of the new model to TEC observation data over a longer period of time, are presented in the paper *"Routine Production of Ionosphere TEC Maps at ESOC - First Results"* (Feltens et al., 1998), which is also part of these IGS workshop proceedings.

The presentation of mathematical algorithms in this paper had to be limited to on overview only. A complete mathematical description of the 3-dimensional Chapman Profile TEC model with all its background is given in (Feltens, 1998), and everything what can only be shown roughly here, is described in (Feltens, 1998) in detail.

This paper will start with the attempt to express GPS-derived leveled TEC observable mathematically in terms of a 3-dimensional TEC model based on a Chapman Profile. Since TEC observable do not stand for discrete ionospheric electron density values at certain

points, but represent the integral over all electron densities along the satellite signal path, solutions of the analytical integral over several forms of the Chapman Profile function will be presented, The basic Chapman Profile model parameters are the maximum electron density N_0 and its height h_0. They will be modeled as global single layers. Key points of numerical applicability for practical use are geometrical aspects, the setting up of linearized observation equations and the establishment of initial values needed for least squares fits. Finally this paper will give some remarks on the estimability of N_0 and h_0 from pure TEC observable and then close with a conclusion.

CONCEPTION OF A CHAPMAN PROFILE MODEL

A TEC observable can mathematically be described as follows:

$$S \cdot (\tilde{\Phi}_1 - \tilde{\Phi}_2)_j^i = TEC_j^i + S \cdot c \cdot (d_j + d^i) + \varepsilon \qquad (1)$$

$S \cdot (\tilde{\Phi}_1 - \tilde{\Phi}_2)_j^i$	carrier phase leveled to code observable or "TEC observable" measured between satellite i and ground station (or second satellite) j,
	S= 9.52 $[TECU/m]$, multiplication factor for GPS signals, for details see Equation (4.5) of TN-08 (Feltens, 1995a),
TEC_j^i	slant range TEC along signal path from satellite i to station (satellite) j,
$S \cdot c$	$S \cdot c = 2.85$ $[TECU/s]$ multiplication factor to convert from [nanoseconds] into $[TECU]$, for details see Equation (4.11) of TN-08,
d_j	differential hardware delay of station (or second satellite) j, normally given in [nanoseconds],
d^i	differential hardware delay of satellite i, normally given in $[nanoseconds]$,
&	TEC observation noise.

The Total Electron Content TEC is the integral of ionospheric electron density N_e along signal path:

$$TEC = \int_j^i N_e(s)\, ds \qquad (2)$$

According to (Cappellari et al., 1976, page 7-46), the electron density N_e can at any point be represented as a function of height h_m and peak electron density N_m using a Chapman Profile:

$$N_e(z) = N_m \cdot e^{(1 - z - e^{-z})} \quad \text{with } z = \frac{h - h_m}{H} \qquad (3)$$

where

N_e	electron density at any arbitrary point along the Chapman Profile,
h	height above Earth surface at which N_e is wanted,
N_m	maximum electron density of the Chapman Profile,
h_m	height of maximum electron density N_m above Earth surface.
H	*scale* height.

N_m and h_m vary with the zenith angle χ of the Sun, i.e. with day time (see e.g. Ratcliffe, 1972). At noon N_m reaches its maximum and h_m its minimum. And during the time from sunset to sunrise h_m has its maximum and N_m its minimum. To achieve more generality it's convenient to refer Equation (3) to the values that N_m and h_m would reach at noon time. With $N_m(\chi = 0^o) = N_0$ and $h_m(\chi = 0^o) = h_0$ Equation (3) can be expressed as follows in terms of N_0 and h_0 (Ratcliffe, 1972):

$$N_e(z) = N_0 \cdot e^{(1 - z - \sec\chi \cdot e^{-z})} \quad \text{with} \quad z = \frac{h - h_0}{H} \tag{4}$$

where

χ	solar zenith distance,
NO	maximum electron density of the Chapman Profile referred to $\chi = 0^o$,
h_0	height of maximum electron density NO above Earth surface at χ = (F'.

The Chapman Profile theory assumes the scale height to be constant along the whole profile (Ratcliffe, 1972). According to (Cappellari et al., 1976) the scale height can be expressed as a function of h_0 as follows:

$$H = \frac{5}{3} \cdot \{30 + 0.2 \cdot (ho - 200)\} = \frac{ho - 50}{3} \quad [km] \tag{5}$$

Once N_0 and h_0 are known, Equation (4) can be used to calculate the electron density at any point and height along the Chapman Profile. Putting Equation (4) into Equation (2) and this into Equation (1) gives finally Equation (6) relating the Chapman Profile to the TEC observable:

$$S \cdot (\tilde{\Phi}_1 - \tilde{\Phi}_2)_j^i = N_0 \int_j^i e^{(1 - z - \sec\chi \cdot e^{-z})} ds + S \cdot c \cdot (d_j + d^i) + \varepsilon \tag{6}$$

Next a relation between the integrand ds and the profile variable z must be established: The differential triangle in Figure 1 indicates the following relation between differential increments dh in height and ds in slant range direction:

$$ds = \frac{dh}{\cos Z} \tag{7}$$

where

$\cos Z$ cosine of slant range zenith distance.

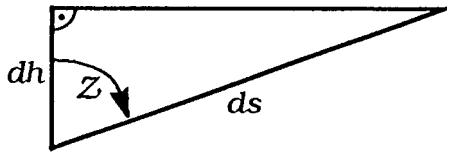

Figure 1: Differential triangle - relation between differential increment dh in height and differential increment ds in slant range direction.

And from Equation (4) the following relation between dz and dh can be derived:

$$dh = H \cdot dz \tag{8}$$

With the Relations (7) and (8) Equation (6) can thus be modified according to:

$$S \cdot (\tilde{\Phi}_1 - \tilde{\Phi}_2)_j^i = N_0 \cdot H \cdot \frac{1}{\cos Z} \cdot \int_{z_j}^{z_i} e^{(1 - z - \sec\chi \cdot e^{-z})} dz + S \cdot c \cdot (d_j + d^i) + \varepsilon \tag{9}$$

The $1/\cos Z$-term can be understood as counterpart to the mapping functions used for single layer models (see e.g. Feltens, 1995a).

For several versions of the Chapman Profile function analytical integrals were found. The establishment of these integrals is presented in detail in (Feltens, 1998). Since such formulae developments are out of the scope of this paper, only the final integral functions can be presented here.

Analytical integral over the simplest form of the Chapman Profile function:

$$\int e^{(1 - z - e^{-z})} dz = e^{(1 - e - z)} \tag{10}$$

The Integral (10) was also comfirmed by (Cappellari et al., 1976), where it is inherent in the Equations (7-146).

Analytical integral over the $\sec\chi$-form of the Chapman Profile function:

$$\int e^{(1 - z - \sec\chi \cdot e^{-z})} dz = \cos\chi \cdot e^{(1 - \sec\chi \cdot e^{-z})} \tag{11}$$

Analytical integral over the $\sec\chi$-form of the Chapman Profile function in terms of height h above ground:

$$\int e^{\left(1 - \left(\frac{h - h_0}{H}\right) - \sec\chi \cdot e^{-\left(\frac{h - h_0}{H}\right)}\right)} dh = H \cdot \cos\chi \cdot e^{\left(1 - \sec\chi \cdot e^{-\left(\frac{h - h_0}{H}\right)}\right)} \tag{12}$$

Only the $\sec\chi$-form of the Chapman Profile function is of relevance for further considerations. Regarding the Integrals (11) and (12), Equation (9) can finally expressed as follows:

$$S \cdot (\tilde{\Phi}_1 - \tilde{\Phi}_2)_j^i = N_0 \cdot H \cdot \frac{\cos\chi}{\cos Z} \cdot e^{(1 \,-\, \sec\chi \cdot e\text{-}z)_{z_j}^{z_i}} + S \cdot c \cdot (d_j + d^i) + \varepsilon \qquad (13)$$

Equation (13) is that final equation which relates TEC observable to the integral over the Chapman Profile. Equation (13) is thus the base upon which the observation equations will be set up.

REPRESENTATION OF N_0 AND h_0 AS SINGLE LAYERS

N_0 and h_0 are clearly coupled with $\chi = 0^o$, i.e. with noon time (see Equation (4) above). So the coordinate origin for N_0 / h_0 single layer development should be positioned at 12^h local time, i.e. at the Sun's maximum elevation above horizon. However, from ionosphere observations it is well known, that the diurnal maximum of electron density appears with a delay of about 2 hours. This effect has been accounted for in the software by calculating the Sun's psition vector with a delay of 2 hours in such a way, that at 14^h the Sun's position of 12^h enters into the processing.

The software tests have shown that N_0 can be best modeled with a GE-function (Feltens, 1995 b). And these software tests also confirmed the method of computing the solar ephemerides with a 2 hours delay, since the maxima of the fitted No-GE-function and the Chapman Profile geometry ruled by χ did coincide under these conditions, thus causing the *rms* to minimize.

To model h_0, special functions had to be worked out which force h_0 to get values in a predefine height range only. Two basic aspects had to be considered: 1) h_0 shall be modeled as smooth surface. 2) The surface functions should be designed so, that they can only reach values within predefine height limits. Since h_0 is referred $\chi = 0°$, i.e. noontime, of the daily height variation, only the noontime values are of relevance for h_0. Thus ignoring the daytime dependency, h_0 should only show variations depending mostly on solar activity. Expressed in numbers, these variations are in the range of $250 < h_0 \leq 400\ km$. However, the software tests have shown that the allowed height range should be set even narrower and slightly higher than 400 *km*:

$$ho_{min} = 400km \quad , \quad ho_{max} = 450km \qquad \text{Ah.} = ho_{max} - ho_{min} = 50km \qquad (14)$$

In operational use the allowed height range, as defined above in (14), should be adapted to the actual solar activity from time to time.

Of several candidates tried out, only the following approach, which appeared to be the most promising function to represent h_0, is shown here. (Feltens, 1998) gives a complete overview over all candidates that were tried out for h_0-modeling. The best candidate is a Sin-function enclosing another function $f(x,y)$ as its argument. The sin-function restricts the output values always to the range $-1 \leq value \leq 1$, and the internal function $f(x,y)$ causes -

if not linear - the unknown parameters not to be a affected by a 2π-bias, the period of the sin-function, which could make convergence unstable. h_0 is then established by a proper scaling of the extended sin-function:

$$h_0 = \xi(x, y) = h_{0_{min}} + \frac{\Delta h_0}{2} \cdot \{1 + \sin[f(x, y)]\} \tag{15}$$

Instead of a sin-function, a cos-function could have been used too. But, since both should be equivalent, only the sin-function approach was implemented into the software.

Of several candidates the one **shown in Equation (16) was chosen for the inner function** $f(x,y)$. **The** first term $c \cdot \sin(x + y)$ has been included to enhance numerical stability:

$$f(x, y) = C \cdot \sin(x + y) + \nu_x \cdot \sin^2 x \cdot \cos x + \mu_x \cdot \sin x \cdot \cos^2 x + \nu_y \cdot \sin 2y \cdot \cos y + \mu_y \cdot \sin y \cdot \cos^2 y \tag{16}$$

with

$C = 0.001$ numerically small constant

And the arguments x and y are defined as follows:

$$+90^o \geq x \geq -90^o \quad , \quad x = \varphi_m$$
$$0^o \leq y \leq 180^o \quad , \quad y = \tau/2 \tag{17}$$

where

φ_m geomagnetic latitude,

τ local time.

The extended sin-function approach in the form presented above allows for the estimation of exactly 4 coefficients $\nu_x, \mu_x, \nu_y, \mu_y$. A generalization of Function (16) appears possible, but was not considered further. This might be a subject of future model extensions.

NUMERICAL REALIZATION

Integration of the Chapman Profile Formulae

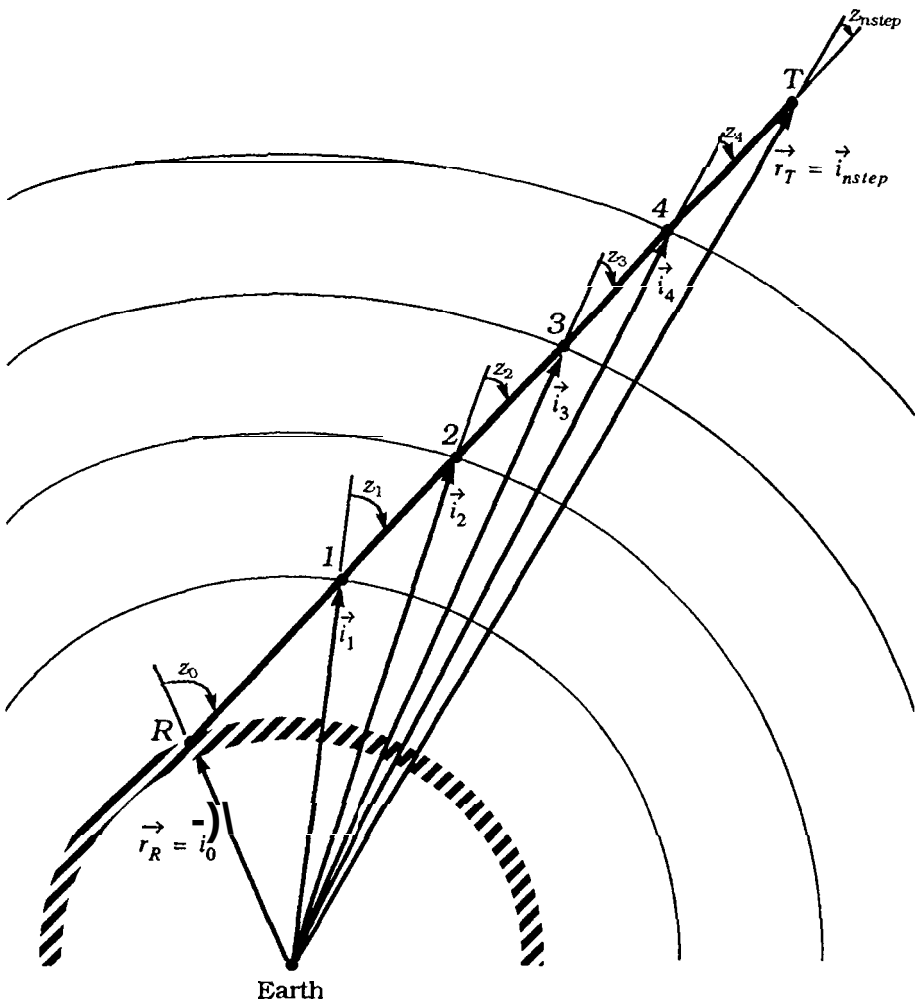

Figure 2: Change of zenith distance Z with height h.

In order to prepare the formulae of the preceding chapters for practical use, several aspects had to be considered:

1) The Integrals (11) and (12) were established under the assumption of **plane stratified** ionosphere layers, i.e. the satellite and solar zenith angles Z and χ were-assumed to be constant and independent of height - but the real ionosphere is, like the Earth, in first approximation a sphere.

2) The 3-dimensional TEC model shall also be usable for satellite-to-satellite tracking (SST) data. In the case of ground-based GPS tracking it is obvious that ionospheric signal delays can be expressed by one Chapman Profile. - However, at SST applications

geometrical conditions can arise, at which an ionospheric delay must be expressed by the sum of two Chapman Profiles.

3) (Feltens, 1995a, Section 5.3) presents a method to determine position vectors of satellite signal intersection points through the layer of maximum electron density. This algorithm assumes the shell height to be globally constant. However, the new model treats h_0 as single layer, i.e. there are variations in height, depending on geographic position. So the formulae of (Feltens, 1995a) must here be used in an iteration loop to find an intersection point through the No-layer.

Figure 2 shows how the satellite zenith distance Z changes with height h. The signal path is described by the range vector $\vec{p} = \vec{r}_T - \vec{r}_R$. In order to account for the changing satellite zenith distance Z, the following integration rule is exploited for Chapman Profile integration (see e.g. Bronstein and Semendjajew, 1979):

$$\int_a^d f(x)dx = \int_a^b f(x)dx + \int_b^c f(x)dx + \int_c^d f(x)dx \quad , \qquad a < b < c < d \tag{18}$$

The signal path s along which to be integrated is thus subdivided into equidistant intervals AS. However, the signal path length is normally not an integer number of a predefine interval AS. So the "actual integration step width" As is defined as follows:

$$nstep = int\left(\frac{s}{\Delta S}\right) + 1 \qquad \text{and} \qquad \Delta s = \frac{s}{nstep} \qquad [km] \tag{19}$$

where

s	slant range, identical with the amount $\lvert\vec{\rho}\rvert$ of the range vector above,
AS	"nominal integration step width",
nstep	number of integration steps,
int	function corresponding to Fortran INT, i.e. cutting off the decimal digits.
As	"actual integration step width".

Integration is now done, starting at the lowest point of integration path and going upwards in steps of As to the highest point, in the way that at the beginning and ending of each interval As the position vectors $\vec{i}_p$ on the slant range are determined:

$$\vec{i}_p = \vec{i}_0 + \frac{p \cdot \Delta s}{|\vec{\rho}|} \cdot \vec{\rho} \qquad p = 1,2, \ldots, nstep \tag{20}$$

where (see Figure 2)

$\vec{i}_p$	position vector of an integration step beginning/ending point on slant range,
$\vec{i}_0$	position vector of the lowest point of the integration path,
$\vec{i}_{nstep}$	position vector of the highest point of the integration path,
$\vec{\rho}$	range vector defining slant range signal path $\vec{p} = \vec{r}_T - \vec{r}_R$,

As "actual integration step width",

P *running* **integration** step number,

nstep total number of integration steps.

Making the dot product of a position vector $\vec{i}_p$ with the range vector $\vec{\rho}$ gives the cosine of the satellite's zenith distance z_p at that point ***p*** on the slant range:

$$\cos z_p = \frac{\vec{i}_p \cdot \vec{\rho}}{|\vec{i}_p| \cdot |\vec{\rho}|} \tag{21}$$

And from the cosine values of two successive points ***p*** and ***p-1*** the means are built:

$$\cos z_{p-1,p} = \frac{1}{2} \cdot (\cos z_{p-1} + \cos z_p) \tag{22}$$

What was shown in Figure 2 for the satellite zenith distance is in a similar way also valid for the Sun's zenith distance χ. So the solar zenith distance is handled in the same way as the satellite zenith distance was treated above: At each point $\vec{i}_p$ where $\cos z_p$ is computed, $\cos \chi_p$ **is calculated too:**

$$\cos \chi_p = \frac{\vec{i}_p \cdot (\vec{r}_o - \vec{i}_p)}{|\vec{i}_p| \cdot |\vec{r}_o - \vec{i}_p|} \tag{23}$$

where

$\vec{r}_o$ ***the Sun's*** position vector,

The mean value being valid for the integration step between two successive points ***p*** and ***p-l*** **is then:**

$$\cos \chi_{p-1,p} = \frac{1}{2} \cdot (\cos \chi_{p-1} + \cos \chi_p) \quad \text{and} \quad \sec \chi_{p-1,p} = 1/\cos \chi_{p-1,p} \tag{24}$$

On the other hand there is a significant difference between handling satellite zenith distances Z and solar zenith distances χ: Close to the terminator the Sun's zenith angle becomes $\chi = 90°$, and beyond on the **nightside** $\chi > 90^o$. This causes the $\sec\chi$-term to become infinite at 90° and to change its sign beyond. The software tests have shown, that, when χ is approaching 90°, it should be frozen from a certain limit on for the whole nightside to a constant value. Of several values tried out $\chi = 70°$ was found to be the best limit angle, i.e. for TEC modeling it is assumed that the electron content enclosed by the Chapman Profile does not go below that of $\chi = 70°$ for the whole nighttime:

$$\textit{if} \quad \chi > 70^o \quad \rightarrow \quad \text{set } \chi = 70° \tag{25}$$

The software tests have shown that the Chapman Profile integration **should** be restricted to a height range of **60-2000** ***km.*** As appropriate step width AS = 50 ***km was*** identified. Before starting the integration, the software reduces integration path to that part of the whole slant range from ground station to satellite, which lies in that height range.

Establishment of Linearized Observation Equations

In order to obtain the partials with respect to the unknows Equation (13) is written here again, now with the functional dependencies explicitly expressed:

$$S \cdot (\tilde{\Phi}_1 - 52); = N_0 \cdot H(h_0) \cdot \frac{\cos\chi}{\cos Z} \; e^{(1 - \sec\chi \cdot e^{-z(h_0, H(h_0))})}\Big|_{z_1} + S \cdot c \cdot (d_j + d^i) + \varepsilon$$

and

$$z(h_0, H(h_0)) = \frac{h - h_0}{H(h_0)} \qquad H(h_0) = \frac{h_0 - 50}{3} \; [km] \tag{26}$$

The unknowns to be estimated in Equation (26) are the single layer coefficients N_{kl} and h_{nm} to represent $N_0(N_{kl})$ and $h_0(h_{nm})$, and the differential code bias values d_j and d^i. For the single layer coefficients N_{kl} and h_{nm} the partials $\partial\{S \cdot (\tilde{\Phi}_1 - \tilde{\Phi}_2)\}/\partial N_0$ and $\partial\{S \cdot (\tilde{\Phi}_1 - \tilde{\Phi}_2)\}/\partial h_0$ *are* needed anyway, and then the partials $\partial N_0/\partial N_{kl}$ and $\partial h_0/\partial h_{nm}$ are attached via chain rule to obtain the required partials $\partial\{S \cdot (\tilde{\Phi}_1 - \tilde{\Phi}_2)\}/\partial N_{kl}$ and $\partial\{S \cdot (\tilde{\Phi}_1 - \tilde{\Phi}_2)\}/\partial h_{nm}$ *with* respect to the unknowns needed for the observation equations. Knowledge of the partials $\partial\{S \cdot (\tilde{\Phi}_1 - \tilde{\Phi}_2)\}/\partial N_0$ and $\partial\{S \cdot (\tilde{\Phi}_1 - \tilde{\Phi}_2)\}/\partial h_0$ thus allows for the establishment of the partials for coefficients of any single layer model by applying the chain rule. Exploiting this fact, any single layer model can extended for 3-dimensional Chapman Profile applications.

Regarding the geometrical aspects treated in the previous section and Equation (26), the TEC and its partial with respect to h_0, which are both obtained via integration along the profile, can be expressed by the following summation formulae for practical use:

$$TEC(h) = N_0 \cdot H \cdot \sum_{p=1}^{nstep} \frac{1}{\cos Z_{p-1,p}} \cdot \left\{ \cos\chi_{p-1,p} \cdot e^{(1 - \sec\chi_{p-1,p} \cdot e^{-z_p})} - \cos\chi_{p-1,p} \cdot e^{(1 - \sec\chi_{p-1,p} \cdot e^{-z_{p-1}})} \right\} \tag{27}$$

and

$$\frac{\partial TEC(h)}{\partial h_0} = \frac{1}{3} \cdot \sum_{p=1}^{nstep} \frac{1}{\cos Z_{p-1,p}} \cdot \left\{ \cos\chi_{p-1,p} \cdot e^{(1 - \sec\chi_{p-1,p} \cdot e^{-z_p})} - \cos\chi_{p-1,p} \cdot e^{(1 - \sec\chi_{p-1,p} \cdot e^{-z_{p-1}})} \right\}$$
$$+ N_0 \cdot H \cdot \sum_{p=1}^{nstep} \frac{1}{\cos Z_{p-1,p}} \cdot \left\{ e^{(1 - 2\sec\chi_{p-1,p} \cdot e^{-z_p})} \cdot \frac{\partial z_p}{\partial h_0} - e^{(1 - z_{p-1} - \sec\chi_{p-1,p} \cdot e^{-z_{p-1}})} \cdot \frac{\partial z_{p-1}}{\partial h_0} \right\} \tag{28}$$

and the partials $\partial z_{p-1}/\partial h_0$ and $\partial z_p/\partial h_0$, being needed for Summation Formula (28):

$$\frac{\partial z_{p-1}}{\partial h_0} = \frac{-1}{H} \cdot \left\{ 1 + \frac{z_{p-1}}{3} \right\} \qquad \text{and} \qquad \frac{\partial z_p}{\partial h_0} = \frac{-1}{H} \cdot \left\{ 1 + \frac{z_p}{3} \right\}$$

The partial $\partial TEC(h)/\partial N_0$ *is* trivial:

$$\frac{\partial TEC(h)}{\partial N_0} = \frac{TEC(h)}{N_0} \tag{29}$$

If, for a SST measurement, the total integration path must be sub-divided into two sub-pathes, two Chapman Profiles have to be integrated, and the final partials with respect to N_0 and h_0 are then obtained by summing up the partials of each Chapman Profile.

The partials for the receiver and satellite differential code bias d_j and d^i are simply:

$$\frac{\partial\{S\cdot(\tilde{\Phi}_1-\tilde{\Phi}_2)\}}{\partial d_j} = S\cdot c = 2.85 \text{ (for GPS)}\ , \qquad \frac{\partial\{S\cdot(\tilde{\Phi}_1-\tilde{\Phi}_2)\}}{\partial d^i} = S\cdot c = 2.85 \text{ (for GPS)} \tag{30}$$

Getting Initial Values for the Unknowns

Since N_0 appears linear in the Chapman Profile function (see Equation (26)), its value needs not to be known a priori to establish the partial for it. Equation (29) shows that its partial is the TEC value normalized to N_0. So using Equation (27) and summing up the TEC with No = 1 gives the partial for N_0 without necessity of explicit knowledge of No itself. However, a h_0-value is needed to do this summation. During the first iteration h_0 is thus kept fixed to some initial values, and only values for the No-single layer coefficients are estimated. If No is represented by a GE-function, this first iteration must be done in logarithmic mode (Feltens,1995b and Feltens, 1998). From the second iteration on the h_0-parameters are then estimated together with the No-parameters, using the No-coefficient values obtained from the first (or the previous) iteration as initial values. In the case h_0 is represented by an extended sin-function, the h_0-coefficients are kept fixed with one $(\nu_x)_0, (\mu_x)_0, (\nu_y)_0, (\mu_y)_0 = 1$ (with respect to the predefine height range given in Equation (14)) during the first iteration.

h_0's role is twofold: On one hand it is estimated as an unknown, on the other hand it is used to fix the intersection points through the No-layer in order to evaluate AJ_o- and scale height El-values there, and to compute the argument z of the Chapman Profile function. To evaluate the intersection points, N_0, Eland z, the h_0-single layer parameters of the previous iteration must thus be used. To make No finally conform with h_0, a last iteration is made with keeping h_0 again fixed, now to its recently estimated values, only estimating the N_0-parameters and the differential code bias values.

ESTIMABILITY OF N_0 AND h_0 FROM TEC OBSERVABLE

The software tests have shown, that the Chapman Profile fits are rather insensitive against h_0-variations, and estimated h_0-parameters show only weak significance. This is obvious when keeping in mind that TEC observable are measurements of the integral over the electron density, and this integral is the area under the electron density profile. A TEC observable thus corresponds to such an area value. And an area value alone gives only the area's amount, saying nothing about the area's shape, i.e. the profile peak at h_0 can be extracted from the information provided by pure TEC observable only from effects caused by the varying elevations under which these observable were made. Because for lack of corre-

spending tracking data, the SST option could not be included into the software tests so far. It is hoped that the inclusion of SST data will improve the situation, since SST measurements are affected, depending on the geometrical conditions, by more varying parts of the ionosphere than ground-based tracking data. Inclusion of SST data might thus improve the resolution of profile parameters, such as h_0.

The determination of No-parameters is stable, and No-single layer coefficients are estimated significantly. TEC models obtained when modeling N_0 with GE-functions appear to have the same order of accuracy as pure single layer GE-function fits - with the *rms* tending to be slightly better, i.e. Chapman Profile fits are of comparable accuracy as pure GE-function fits, but provide information on the ionosphere's third dimension - the height.

CONCLUSIONS

A mathematical model has been worked out allowing for the 3-dimensional representation of ionospheric TEC from TEC observation fits. These TEC measurements can be derived from GPS dual-frequency tracking data. The ionospheric TEC is modeled as the integral over simple Chapman Profiles with the layer of maximum electron density N_0 acting as scaling factor and its height h_0 as profile parameter. Both, N_0 and h_0, are in turn represented as global single layers. For the modeling of h_0 special single layer functions were developed.

Since GPS-derived TEC observable represent the ionosphere's total electron content along signal path, no discrete electron density values are observed, but the integral over all electron densities along the signal path. Analytical solutions for the integral over several versions of the Chapman Profile function were found and implemented into the model. In order to account for certain geometrical aspects, the integral over the Chapman Profile function is finally evaluated by a mixture of analytical and numerical approach.

From its conception this Chapman Profile-founded model allows the evaluation of ground-based data as well as of SST data. However, for lack of SST data, software tests had so far to be restricted to the evaluation of ground-based data.

All in all the whole 3-dimensional TEC model is built up by simple mathematical formulae. From the model's and the software's conception and structure it is possible to combine it with every single layer and to include more complex ionosphere profiles in future steps of software extension.

The task of this paper was the presentation of the basic mathematical algorithms realizing the 3-dimensional TEC model. Analyses of numerical results, that came out when applying this model to TEC data fits, are presented in (Feltens et al., 1998), which is also published in these IGS workshop proceedings.

REFERENCES

Bronstein, I.N. and K.A. Semendjajew, 1979, Taschenbuch der Mathematik, *Verlag Harri Deutsch, Thun und Frankfurt/Main*, Vol 1+2.

Cappellari, J.0, C.E. Velez and A.J. Fuchs, 1976, Mathematical Theory of the Goddard Trajectory Determination System, Goddard Space Flight Center, X-582-76-77, Greenbelt, MD, U. S.A., April 1976, Section 7.6.2 'Ionosphere Models', pp 7-44-7-52.

Feltens, J., 1995a, GPS TDAF Ionosphere Monitoring Facility, Mathematical Model Developments, in GTDAF-TN-081s.s *1/- 11 Sep-95* (ESOC-internal document).

Feltens, J., 1995b, GPS TDAF Ionosphere Monitoring Facility, Examination of the Applicability of Gauß-Type Exponential Functions to Ionospheric Modeling, in *GTDAF-TN-09 Iss* 1/- *11 Sep-95* (ESOC-internal document).

Feltens, J., 1998, GPS TDAF Ionosphere Monitoring Facility, Chapman Profile Model for the IONMON, in *GTDAF-TN-14 Iss 1/-* 04 *Mar-98* (ESOC-internal document).

Feltens, J., J.M. Dow, T.J. Martín-Mur, C. García Martinez and P. Bernedo, 1998, Routine Production of Ionosphere TEC Maps at ESOC - First Results, IGS Presentation, in *Proceedings of the 1998 IGS Analysis Centers Workshop,* ESOC, Darmstadt, Germany, February 9-11, 1998.

Ratcliffe, J. A., 1972, An introduction to the ionosphere and magnetosphere, *Cambridge University Press, Great Britain, 1972.*

THE ROLE OF GPS DATA IN IONOSPHERIC MODELLING, MAPPING AND NOWCASTING

R. Leitinger,
Institut fur Meteorologic und Geophysik,
Universität Graz, A-801O GRAZ, Austria

ABSTRACT

The classical sources for ionospheric electron content (TEC) data are disappearing quickly. The ionospheric research community has to shift to Global Navigation Satellite Systems (GNSS, presently GPS and GLONASS) to gain TEC data from the plasma influence on the GNSS signals. This means a serious shift in policies and a necessity for enhanced research into the capabilities and the shortcomings of the „new" systems. One of the most serious consequences is the loss of temporal continuity. It has to be overcome by incorporation of ionosonde observations. The so-called „plasmasphere" problem also is a serious one if one is interested in long-term studies of ionospheric electron content or if TEC data are needed for correction of the ionospheric influence (e.g., ground to a height of 800 km).
Already now GNSS derived TEC data play a major role in ionospheric modelling, mapping and nowcasting. The importance of GNSS data for these purposes will increase quickly in the near future. Therefore close co-operation of institutions with ionospheric research and application capabilities with other users of GNSS signals is a necessity.

INTRODUCTION

The quantity of interest is the vertical ionospheric electron content (TEC). It is derived from the electron content along a slant ray path from the satellite transmitter (S) to the ground receiver (R):

$$I_I = \int_R^S N \, ds = \int_0^z N \, \frac{dh}{\cos\beta}$$

(N: electron density; ds: ray path element; dh: height element; β: zenith angle along ray; z is a „ceiling height" which depends on the observation method: for GPS observations it is the height of the satellite).

I/is not an observable: conversion of measured data (from a technical point of view phase differences) into I_I values involves a „calibration" process.

Projection onto the vertical gives the (vertical) electron content (TEC):

$$I_{/} = \overline{\frac{1}{\cos\beta}} \int_0^z N \, dh = \overline{\frac{1}{\cos\beta}} \; I_{\perp} = \frac{1}{\cos\chi} \; I_{\perp}$$

Since the electron density distribution along the ray RS is not known the projection is done in the following way: instead of the true mean for $(1/\cos\beta)$ an approximate value is taken ($1/\cos\chi$,; $\chi = \beta(h_i)$: zenith angle in the „mean ionospheric height" or „shell height" hi). If a fixed value is assumed for hi , it is recommended to use 400 km. (At least in periods of high solar activity this value is too low in lower latitudes - in the vicinity of the crests of the equatorial anomaly and over the dip equator).

DATA SOURCES

In the past we had the following types of „satellite beacons" and could make use of three different ,,propagation effects", namely the Faraday effect, the Group Delay effect (plasma influence on the modulation phase) and the Differential Doppler effect (plasma influence on carrier phase). Table 1 shows two „long-term" opportunities, namely the VHF beacons of the older types of geostationary communication satellites and the 150/400 MHz coherent beacons of the (US) Navy Navigation Satellite System (NNSS). The communication satellites needed the VHF beacons for navigation in the transfer phase and some were kept in continuous operation to allow observations of the Faraday effect (provided the polarisation of the beacon was elliptical and not nearly circular). A geostationary beacon provides a time constant ray path and therefore time continuous observations of ionospheric electron content with a „ceiling height" z of 2000 km (weighting because of the height dependence of the longitudinal component of the geomagnetic field, see, e.g., Titheridge, 1972). The NNSS satellites allow observations of the Differential Doppler effect (carrier phase difference; see, e.g., Leitinger et al., 1975). Since the satellites are in nearly circular and nearly polar orbits (in heights around 1100 km) evaluation of the observations essentially gives the latitude dependence of electron content. The transit time (around 20 minutes for an overhead pass) is short enough to neglect temporal variations of the ionization.

Table 1 also contains hints at the only two dedicated ,,experiments" which were available to the beacon satellite community: S-66 (Beacon Explorers B and C - A was a failure). BE-B provided global coverage for Faraday effect observations on two signals (40 and 41 MHz) and gave opportunity to construct the first regional models for electron content (see, e.g., Ebel et al., 1969). They suffered from the shortcomings one has with one satellite only, namely the coupling of local time variations and seasonal variations. The operation of the Beacon Explorers did not cover high solar activity. As far as it is known an other opportunity provided by S-66 was not used on a wider basis, namely the observation of carrier phase differences

(e.g., using the 40 and 360 MHz signals), The Beacon Explorers also had a 20 MHz beacon but because of interference problems (man mad noise) it could not be used from most locations.

The Radio Beacon Experiment on board of the geostationary communication research satellite ATS-6 was a very ambitious one (see Davies, 1980). One of the crucial achievements was the successful separation of (slant) plasmaspheric electron content from the total electron content. Thanks to ATS -6 RBE we have clear ideas about the plasmaspheric contribution for low solar activity.

Presently we are in a transition phase: The geostationary VHF beacons are faded out (they already have disappeared for Europe). NNSS has been decommissioned as a navigation system. Three to four satellites are kept in operation for ionospheric research purposes, hopefully for several more years. More and more the beacon satellite community has to shift to GPS (and GLONASS) data. This shift means a serious change in policy: most of the ionospheric research institutions will not be able to make their own GPS or GLONASS observations, they rel y (and will have to continue to rely) on data collected for other purposes. It is very important to ensure that ionospheric expertise and research capabilities are preserved over the transition phase and that a multitude of comparisons of TEC data from all available sources are made.

Table 1: beacon opportunities of the past

Beacon satellites	**frequencies (MHz)**	**propagation effects**	**properties & remarks**
geostationary communication satellites	**136...138**	**Faraday**	fixed ray path, continuity in time, very good temporal resolution
polar orbiting NNSS	150/400	Diff. Doppler	scan in latitude, very good latitudinal resolution
Special Experiments:			
orbiting 1965-1969: S-66 (Beacon Explorers)	40/41	Faraday	
geostationary 1974-1977: ATS-6 RBE	40,41,140, 360 + modulation	Faraday, Diff. Doppler, Group Delay	separation of total content from ground to ATS-6 into ionospheric and plasmaspheric part

In the near future we will have GNSS plasma data only for long-term investigations which need observations conditions which remain as homogeneous as possible. Probably NNSS type beacons will be available from time to time on ,,experimental" basis.

It is important to note that continuos data collection and preservation is necessary not only for long-term investigations but for research into „geophysical events" as well. Presently the occurrence of such events (e.g., of ionospheric storms, large amplitude Traveling Ionospheric Disturbances, regional disturbances of other types) cannot be predicted and this author doubts very much that all „events" of importance will be predictable in the future. „Events" are studied after their occurrence (case studies with data from the data base).

TEC DATA COLLECTIONS AND THEIR USE

Ionospheric physics (and other branches of external geophysics) as well as many important applications need collections of ionospheric data. These data bases are used for typical „long-term" investigations (mapping, modelling, system planning) and retrospectively for case studies and applications like corrections for propagation errors (first order errors in single frequency applications of satellite signals) and other uses of nowcasting procedures, Tables 2 and 3 give an overview.

'able 2: **Use of TEC data bases for ionospheric physics**

(1) „Long-term"	Modelling, Mapping
	Solar cycle dependence
	Global Change
(2) „Events" (effects of)	Geomagnetic Storms
	Atmospheric Gravity Waves ⇒ TIDs
	Solar Flare Effects
	Others ? (Unexplained TEC excursions)

Table 3: Applications of TEC data

Geophysics: Ionization is important „tracer" for	Neutral atmosphere processes
	Magnetospheric processes
	Solar--terrestrial relations
Retrospective Applications:	TEC maps (testing, improving, refining)
	Correction of propagation errors (e.g., for single frequency altimetry)

	Retrospective nowcasting
	Retrospective updating of maps

The desired data density differs from application to application. Table 4 gives an overview for regional applications. Typical sizes of „regions“ are in the order of 30 to 50 degrees in latitude times 60 to 90 degrees in longitude. For lack of homogeneous coverage global studies are usually made by combining regional results (e.g., from Europe, the Americas, Australia, East Asia). Global TEC maps even with a much coarser resolution in latitude and longitude than regional ones would be of great value for global studies. From the point of view of geophysics and of applications for users the minimum would be one map per day for a given Universal Time („snapshot" maps) if temporal development can be assessed by means of data from a selection of observing points which are considered „typical“ for a region of importance. Ionosonde parameters (especially foF2 the maximum plasma frequency of the ionosphere and maximal electron density derived from it) are very well suited for monitoring of the temporal development of ionospheric disturbances. If more than one global map is produced per day it is recommended to construct the maps in Local Time (TEC over a grid in latitude and longitude for fixed LT). The minimum LT resolution would be 6 hours (4 maps per day, e.g., for 00 LT, 06 LT, 12 LT, 18 LT) but major improvements could be gained if the number of maps per day is larger. (8 maps per day already gives a very good impression on the temporal development of global storm disturbances.) However, it is important to note that global maps cannot replace regional ones.

Table 4: Desired data density (regional applications):

	At	As	$\Delta\varphi$	$\Delta\lambda$
Regional Mapping	1 h	500 km	5“	15°
Most applications	15 min	500 km	5“	15°
Events:				
storms	15 min	200 km	2°	4°
LSTIDs	5 min	200 km	2°	4“

LSTIDs: Large Scale TraveHing Ionospheric Disturbances

For ambitious applications like navigation of aircraft, land vehicles, ships in coastal waters and on rivers, etc., near real time regional maps are a necessity. The data behind such regional maps should be preserved for retrospective purposes.

Presently it is not realistic to assume that the hole globe will be covered with GNSS based regional maps with the resolution needed for ambitious applications. From the point of view of ionospheric physics important gaps will remain, e.g., over the oceans, and probably for many years over parts of Africa and Asia. One possibility to gain ionospheric data over remote areas is the use of GNSS occultation combined

with information on horizontal gradients of TEC. Global maps could help to bridge the gaps in the horizontal gradient information which is very scarce in the regions with poor coverage with ground stations.

From a geophysical point of view „higher latitudes" (Europe: N of 60°N) and „lower latitudes" (European/African sector: S of 35°N) are more important than the comparatively well known „mid latitudes".

REMARKS AND CONCLUSIONS

(1) There is no doubt that GNSS data (ground based as well as occultation derived) will be the most important source of ionospheric „mass data" in the near future. This does not mean that these data can replace important research instruments like the Incoherent Scatter Radars. Furthermore optimal use of GNSS derived data makes it necessary to maintain the ionosonde network in operation. For many purposes electron content information is not sufficient. The ionosondes provide very valuable additional profile information and they provide temporal continuity for fixed locations which cannot be obtained from GNSS observations.

(2) For several reasons it is very important to continue NNSS observations as long as this is possible. They provide independent data and therefore possibilities to check the integrity of GNSS derived data, GNSS receiver calibration, etc. The spatial resolution of NNSS derived TEC is excellent and better than what can be gained from all other remote and in-situ measurements, Furthermore the „plasmasphere" problem is not yet solved for GNSS derived TEC: we know what to expect for times of low solar activity (mainly from ATS-6 RBE) but we have a lack of experience from high solar activity. Comparison of GPS data with NNSS data gives very valuable information about the plasmaspheric contribution in GNSS TEC.

(3) The transition from the classical TEC sources to GNSS means an important change in working conditions for the ionosphere research community: most of the research groups will not have their own receiving equipment but will have to rely on data collections (like IGS) and on close co-operation with other users of GNSS signals. It will be necessary to provide help and assistance to research groups in less developed countries. Regional data centers for GNSS derived TEC are a possible solution to data access problems in less developed countries.

(4) Close co-operation between international (global and regional) organisations for the use and application of ionospheric information is necessary to ensure optimal use of the novel data sources based on ground and space reception of GNSS signals. Since 1971 the International Beacon Satellite Group (presently Working Group G2 of the International Union for Radio Science - URSI) is an organisation which brings together scientists and engineers from different fields and from different regions

(chairman: R. Leitinger, Austria, co-chairmen: J.A. Klobuchar, USA, PVS Rama Rae, India). It is an important forum for the exchange of relevant information and experiences. It organizes Symposia in distances of two to three years (see Kersley, 1994 and Bencze and Leitinger, 1998 for the Proceedings of the two most recent Beacon Satellite Symposia). In recent years members of the Beacon Satellite Group have been involved extensively in assessing GPS as a data source for ionospheric research and for propagation errors in the application of transionospheric radio signals.

REFERENCES

Bencze, P, and R. Leitinger (editors), 1998, Proceedings of the International Beacon Satellite Symposium 1997, Sopron, Hungary, 30 June-5 July, 1997. In print: *Acts Geodetica et Geophysics Hungarica*

Davies, K., 1980, Recent progress in satellite Radio Beacon studies with particular emphasis on the ATS-6 Radio Beacon Experiment, *Space Sci. Rev.* 25, pp 357-430

Ebel, A., G. Hartmann, R. Leitinger, G. Schmidt, J.P. Schödel, 1969, Vergleichende Auswertung von Faraday-Effekt-Beobachtungen zweier Empfangsstationen. *Zs. Geophysik 35,* pp. 373-411

Kersley, L. (editor), 1994, Proceedings of the International Beacon Satellite S ympo sium, University of Wales, Aberystwyth, UK, 11-15 July 1994

Leitinger, R., G. Schmidt, A. Tauriainen, 1975, An evaluation method combining the Differential Doppler measurements from two stations that enables the calcula tion of the electron content of the ionosphere. *J. Geophysics (Zs. Geophysik) 41, pp. 201-213*

Titheridge, J. E., 1972, Determination of ionospheric electron content from the Fara day rotation of geostationary satellite signals. *Planet. Space Sci. 20,* pp. 353-369

MAPPING AND PREDICTING THE IONOSPHERE

Stefan Schaer, Gerhard Beutler, Markus Rothacher
Astronomical Institute, University of Berne
CH-3012 Berne, Switzerland

ABSTRACT

The Center for Orbit Determination in Europe (CODE) produces daily maps of the Earth's ionosphere on a regular basis since January 1, 1996. These global ionosphere maps (GIMs) are derived from exactly the same GPS tracking data — doubly difference carrier phase measurements — as those used for the determination of CODE core products delivered to the IGS like precise GPS orbits, earth orientation parameters (EOPs), station coordinates and velocities. For the ionospheric product we have to analyze the so-called *geometry*-free linear combination (LC), which primarily contains ionospheric information, as opposed to the ionosphere-free LC, which contains the "geometrical" information and completely eliminates the influence of the ionospheric refraction (ignoring higher-order terms). At present (March 1998), the GPS tracking network processed at CODE consists of more than 110 globally distributed stations of the International GPS Service for Geodynamics (IGS).

After reprocessing all 1995 IGS data using the "Bernese Processing Engine" [Rothacher et al., 1996a], a long-time series of daily GIM parameters covering a time span of about 3.2 years is at our disposal. On the one hand this ionosphere time series reveals the evolution of the total electron content (TEC) on a global scale, on the other hand it indicates that short-term as well as long-term predictions for CODE GIM parameters are possible. We discuss the time series for a few selected TEC parameters and develop a method to predict the TEC parameters. Furthermore, we describe how the temporal resolution can be increased when using spherical harmonic (SH) expansions to model the global TEC. First attempts estimating 2-hour maps are encouraging.

CODE'S IONOSPHERE PRODUCTS — AN OVERVIEW

The principles of the TEC mapping technique used at CODE were described in [Schaer et at., 1995] and [Schaer et al., 1996a].

At present the following ionosphere products are generated on a routine basis:

- 24-hour global ionosphere maps (GIMs) are produced using double-difference phase *or* phase-smoothed code observations. The phase-derived TEC maps proved their usefulness for ambiguity resolution (AR) on long baselines [Rothacher et al., 1996b].
- *Rapid* global maps are available with a delay of about 12 hours, the *final* ones after 3 days (in the IONEX format [Schaer et al., 1998]).
- Regional (European) maps are produced as well and are also used to support AR. On the average 90% of the initial carrier phase ambiguities can be resolved reliably —- without making use of code measurements. Daily IONEX files containing hourly snapshots of the ionosphere are made available via anonymous ftp.
- Daily sets of differential code biases (DCBs) for all GPS satellites (and the contributing receivers) are estimated at CODE since October 1997.

Figure 1 shows the daily DCB estimates (dots) for 27 GPS satellites from day 022, 1998, to day 071, 1998, and the combined DCBs (circles) aligning all satellite-specific DCBS in the sense that the overall mean becomes *zero* (to obtain a virtual, but very stable reference). However, there are a couple of PRNs with *drifting* DCBS with respect to the remaining PRNs. PRN 08, which was launched few months ago, shows a significant drift of almost –0.5 ns over 50 days. We observe an increased root-mean-square error (RMS) for this satellite when assuming and modeling the DCBS as constant quantities (see Figure 1 and Table 1).

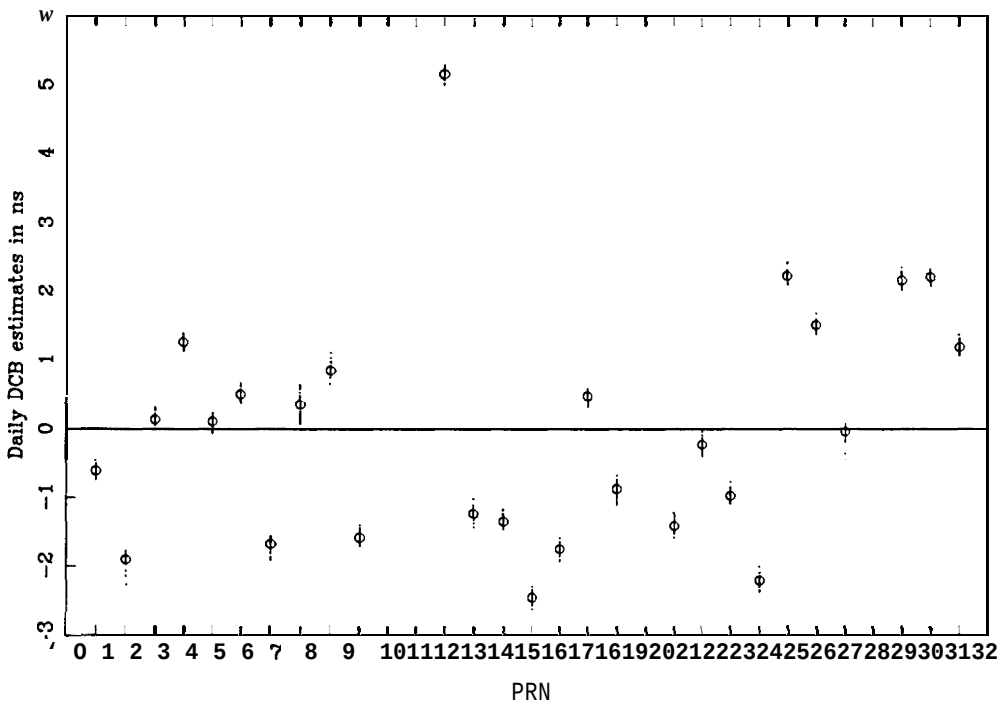

Figure 1. Daily PRN-specific DCB estimates (dots) for 27 GPS satellites from day 022, 1998, to day 071, 1998, and combined DCBS (circles)

The *combined* values of the satellite-specific DCBS taking into account the variance information of the individual solutions are listed in Table 1. In addition, the weighted RMS (WRMS) of the daily estimation is given for each PRN. The total WRMS of the 50-day DCB combination amounts to 0.08 ns. Let us mention that the estimated receiver-specific DCBs are of the order of ±15 ns and show a day-to-day scattering highly depending on the station considered, Note that the DCB results presented here originate from a special solution where we simultaneously estimate n station-specific TEC models leading to 16 n TEC plus n +27 DCB parameters per day in total, where n is the number of stations processed.

Table 1. Combined DCBS and weighted RMS errors of daily estimation

PRN	DCB (ns)	WRMS (ns)	PRN	DCB (ns)	WRMS (ns)
01	–0.63	0.06	*17*	–1.74	0.06
02	–1.90	0.07	*18*	+0.49	0.07
03	+0.14	0.06	*19*	–0.87	0.08
04	+1.26	0.06	*21*	–1.41	0.08.
05	+0.11	0.07	*22*	–0.23	0.06
06	+0.51	0.07	*23*	–0.97	0.06
07	–1.68	0.11	*24*	–2.19	0.06
08	+0.35	0.16	*25*	+2.23	0.05
09	+0.86	0.07	*26*	+1.51	0.09
10	–1.57	0.07	*27*	–0.04	0.08
13	+5.16	0.06	*29*	+2.17	0.07
14	–1.22	0.07	30	+2.22	0.06
15	–1.34	0.07	31	+1.19	0.07
16	–2.43	0.08			

Figure 2 shows snapshots of (a) a phase-derived and (b) a code-derived 24hour TEC map for day 017, 1998 (taken at 12:00 UT). The number of contributing stations was 79 on that particular day. Light fields indicate small TEC, dark ones large TEC (up to 37.6 and 39.0 TECU here). The level lines are drawn at intervals of 2.5 TECU. There is no significant difference between the two maps.

LONG-TIME SERIES OF GLOBAL TEC PARAMETERS

The long-time series of global TEC parameters available at CODE covers over 1168 days and includes (8 + 1)2 = 81 SH coefficients (the SH expansion was truncated at degree and order 8). The zero-degree SH coefficient representing the mean TEC on a global scale characterizes the ionospheric activity pretty well. The evolution of this particular TEC parameter during a period of low solar activity is shown in Figure 3. The daily estimates (dots) and a smoothed curve to better visualize the behavior are given. One recognizes a long-term trend caused by the 1 l-year solar cycle, annual and semi-annual variations, and relatively strong short-term fluctuations with periods of the order of 27 days due to the Sun's rot ation. We clearly see maxima at equinox and minima at solstice, however, the minima in summer are more pronounced than those in winter. The recent ionospheric minimum was observed in summer 1996.

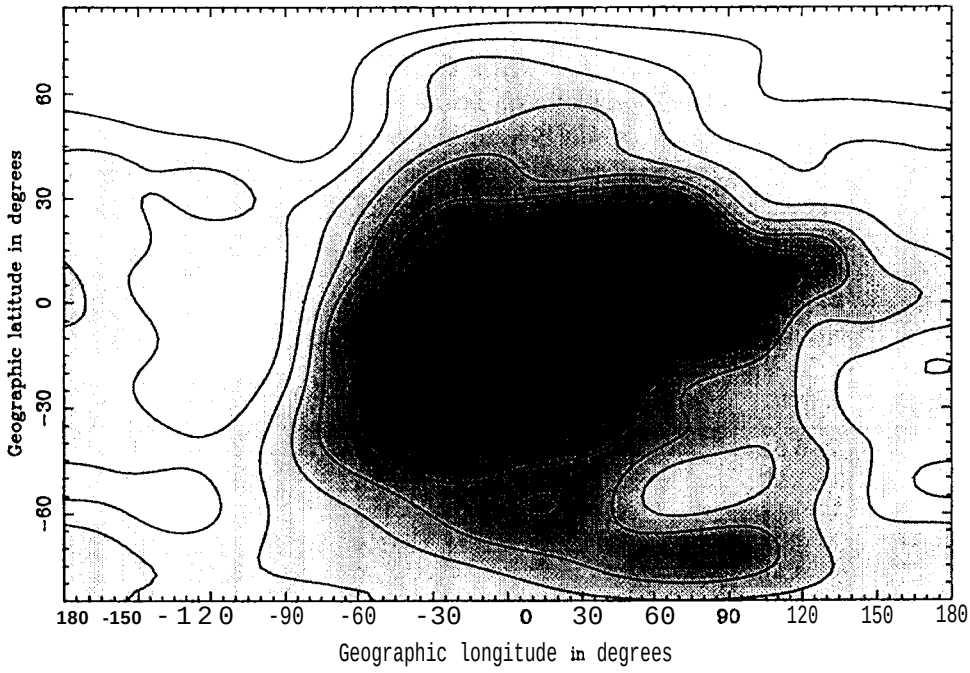

(a) *Phase*-derived TEC map

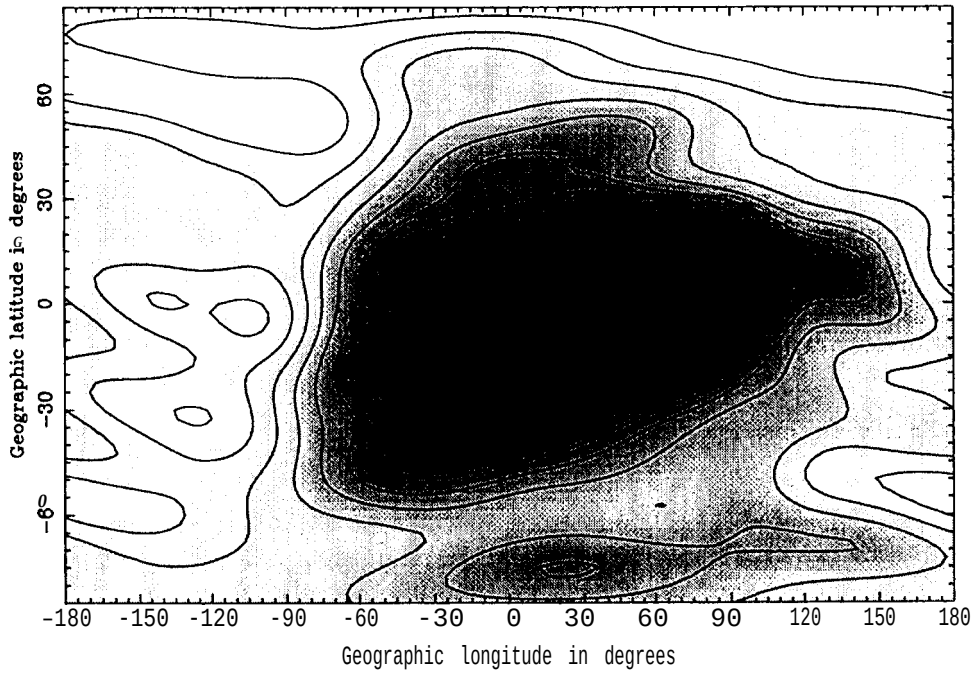

(b) Code-derived TEC map

Figure 2. 24-hour TEC maps for day 017, 1998

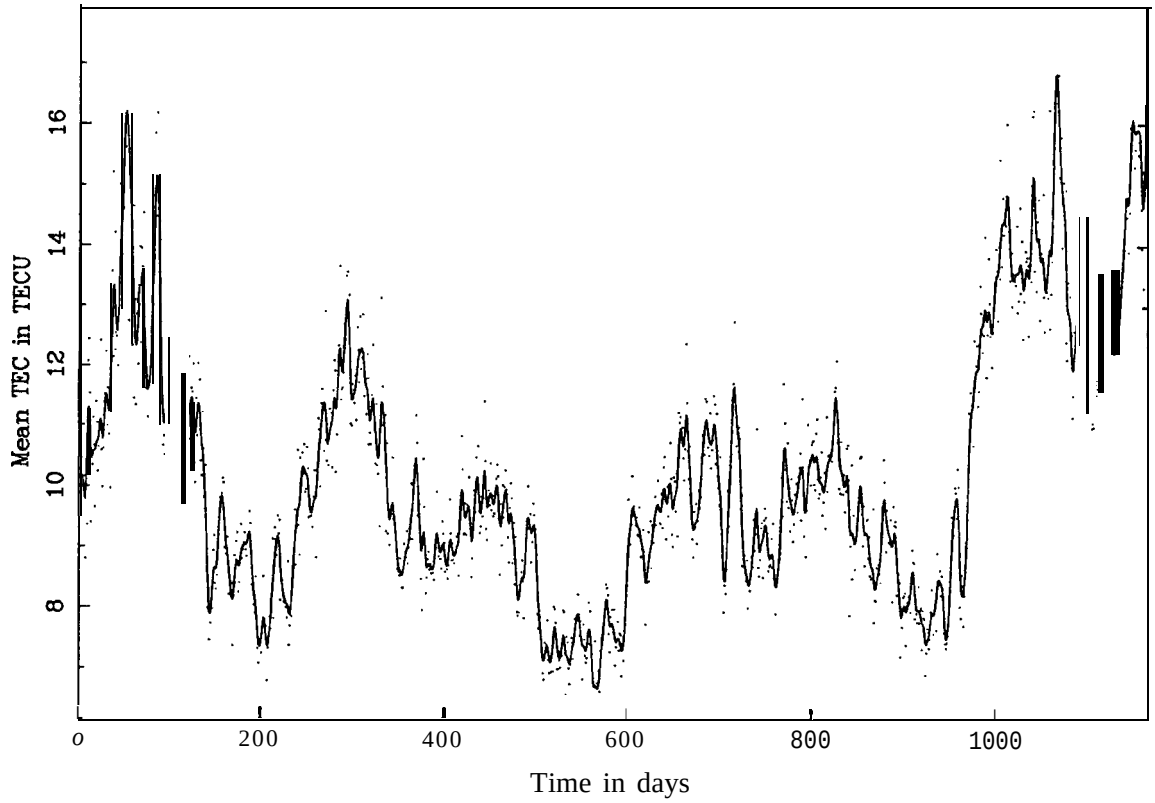

Figure 3. Zero-degree coefficient (mean TEC) from day 001, 1995 to day 072, 1998

Figures 4 and 5 illustrate a few other SH coefficients showing similar periodicities and features as mentioned above.

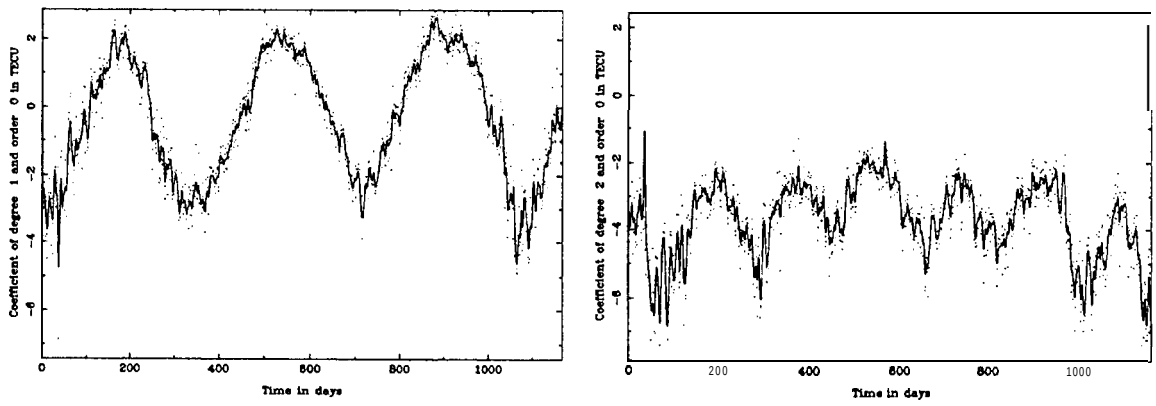

(a) Term of degree 1 (and order 0)

(b) Term of degree 2 (and order O)

Figure 4. Zonal SH terms

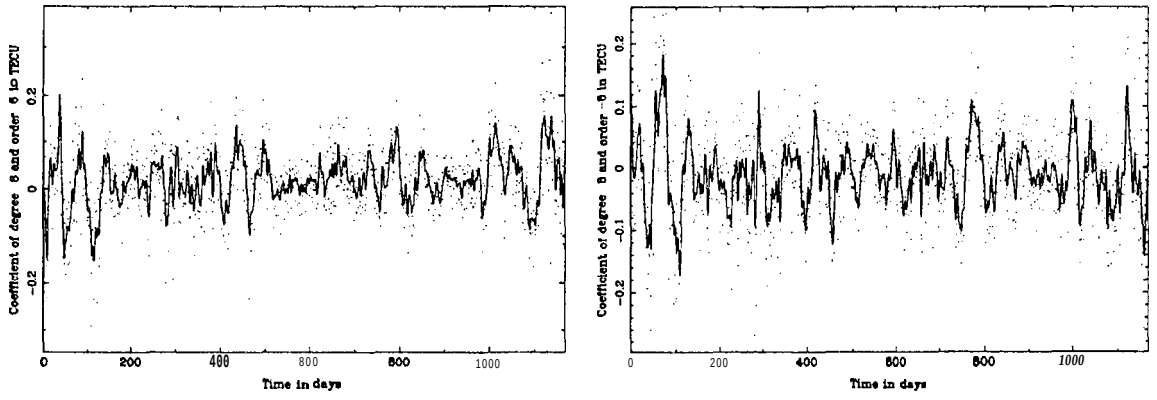

(a) Cosine term of degree 8 and order 6

(b) Sine term of degree 8 and order 6

Figure 5. Tesseral SH terms

When correlating the mean TEC values and the 10.7-cm solar flux, the correlation factor is almost 0.8, reaching its maximum at a lag of 1 day.

PREDICTING THE IONOSPHERE

Let us split up the "ionospheric signal" $\boldsymbol{l}$ — a time series of SH TEC parameters $e_{ij}(t_k)$ · into a *deterministic* component $\boldsymbol{d}$, which can be represented by a so-called trend function @(t), a *stochastic* component $\boldsymbol{s}$, and a noise component $\boldsymbol{n}$:

$$\boldsymbol{l} = \boldsymbol{d} + \boldsymbol{s} + \boldsymbol{n} \quad \text{or} \quad \boldsymbol{l} - \boldsymbol{\Phi}(\boldsymbol{x}_0) = \boldsymbol{A}\,\boldsymbol{x} + \boldsymbol{s} + \boldsymbol{n}. \tag{1}$$

As our trend function we use a harmonic expansion with a few prominent periods (11, 1, and 1/2 years)

$$\Phi(t) = a_0 + \sum_{i=1}^{m} (a_i \cos(\omega_i t) + b_i \sin(\omega_i t)) \quad \text{with} \quad \omega_i = \frac{2\pi}{\tau_i}. \tag{2}$$

The unknown parameters $\boldsymbol{x}$ of the trend function are estimated in a least-squares adjustment

$$\boldsymbol{x} = \left(\boldsymbol{A}^T \boldsymbol{C}_{zz}^{-1} \boldsymbol{A}\right)^{-1} \boldsymbol{A}\boldsymbol{T}\ \boldsymbol{C}_{zz}^{-1}(\boldsymbol{l} - \boldsymbol{\Phi}(\boldsymbol{x}_0)), \tag{3}$$

where

$$\boldsymbol{x}^T = [a_0, a_1, b_1, \ldots, a_n, b_n] \text{ and } \boldsymbol{C}_{zz} = \boldsymbol{C}_{ss} + \boldsymbol{C}_{nn}. \tag{4}$$

C_{ss} and C_{nn} are the covariance matrices for the actual "signal" and the pure "noise", respectively. Finally, if we perform short-term predictions (or interpolations), the *stochastic* component s is of interest, too:

$$\begin{bmatrix} s \\ n \end{bmatrix} = \begin{bmatrix} C_{ss} \\ C_{nn} \end{bmatrix} C_{zz}^{-1} \, (l - \Phi(x)) \, . \tag{5}$$

The autocovariance function γ, which is used to set up the covariance matrices C_{ss} and C_{zz}, may be evaluated as

$$\gamma(h\,\Delta t) = \frac{1}{n} \sum_{k=1}^{n-|h|} (e_{ij}(t_k) - \Phi(t_k))(e_{ij}(t_{k+|h|}) - \Phi(t_{k+|h|})). \tag{6}$$

h At denotes the lag; $\gamma(0)$ is the variance of the stochastic component.

The autocovariance function (ACF) of the mean TEC, i. e., the SH coefficient coo, is given in Figure 6. We notice that the ACF mainly reflects the Sun's rotation period of approximately 27 days.

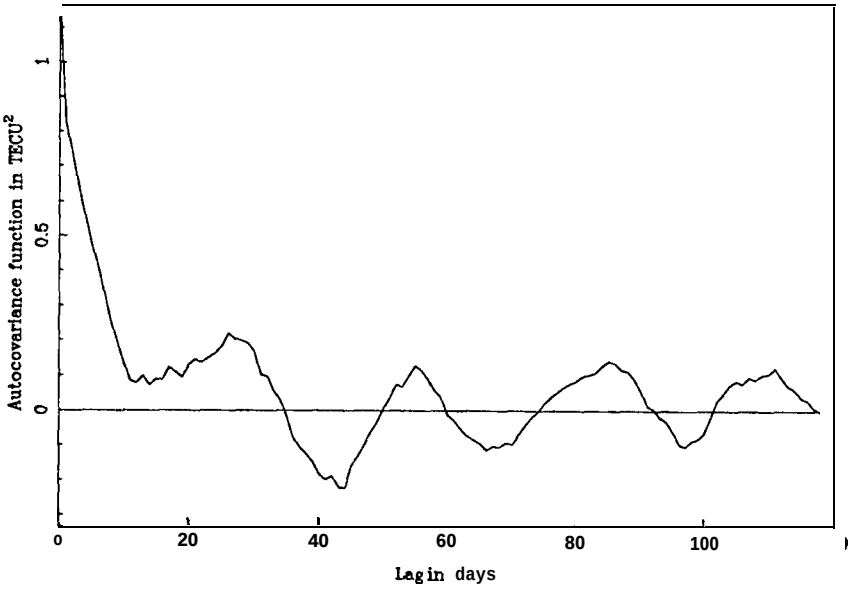

Figure 6. Autocovariance function of zero-degree coefficient for lags up to 120 days

Figure 7 shows the results when predicting (and interpolating) the mean TEC based on (a) a two-year time series *only* and (b) the complete time series. The daily GIM estimates are represented by dots. The trend function $\Phi(t)$ is given by the solid, smooths line and follows the general signal pretty well. It is amazing, considering that the time span of two years is quite short compared to a solar cycle, how well the extrapolated trend function shown in Figure 7a matches the real TEC observations shown in Figure 7b. The rapidly varying line also includes the *stochastic* component covering a prediction length of 30 days.

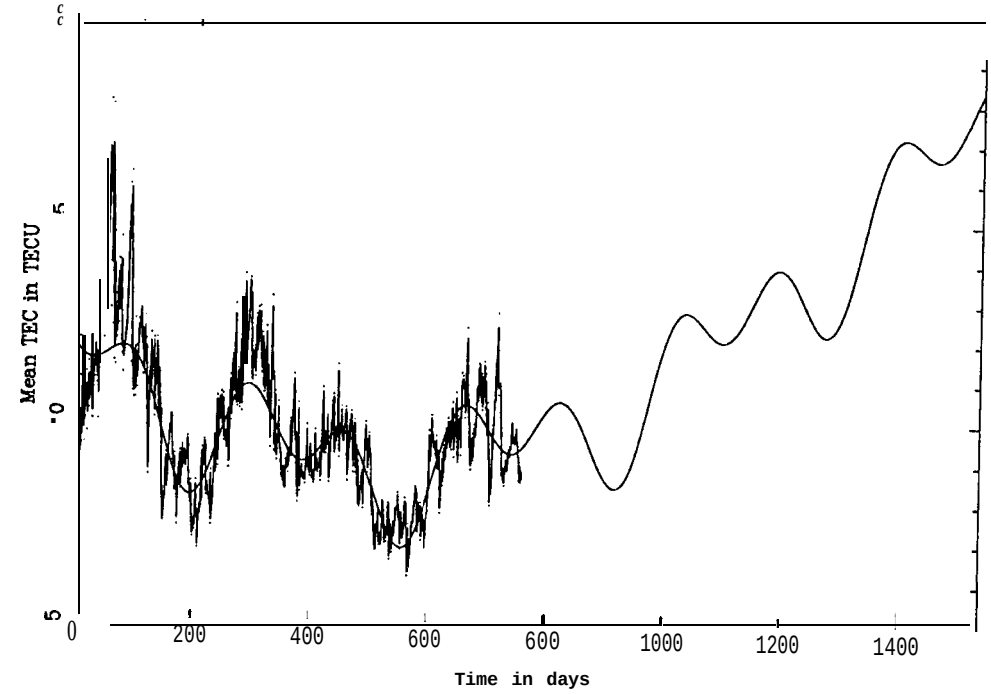

(a) 1995-1996 GIM data

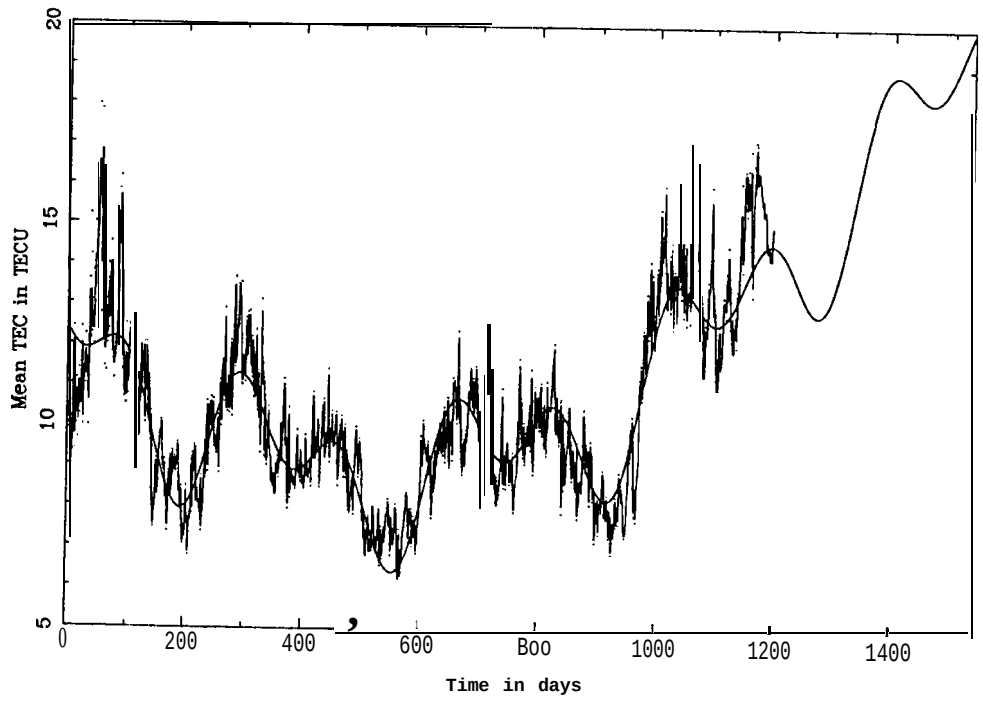

(b) All GIM data

Figure 7. Prediction of mean TEC based on (a) a two-year time series and (b) the complete time series

When inspecting Figure 7 we see that the prediction consisting of $\boldsymbol{d} + \mathbf{s}$ does not exactly match the daily estimates because the matrix $\boldsymbol{C}_{nn}$ is not a zero matrix but contains the variances provided by the primary ionosphere parameter estimation.

By performing the least-squares collocation step for each SH coefficient using the same prediction length, merging the predicted TEC coefficients to a full set of SH parameters, and writing a corresponding GIM file, we get a procedure that allows us to predict entire CODE GIMs! A software tool solving that task has been developed.

HIGH TEMPORAL RESOLUTION TEC USING SPHERICAL HARMONIC EXPANSIONS

In this section we discuss a method on how to increase the temporal resolution of the TEC representation when using spherical harmonic (SH) expansion.

SH expansions are well suited to model time-independent quantities given on a spherical surface. When dealing with the ionosphere, the entire sphere is probed by GPS stations when deriving one-day TEC maps. The disadvantage is a poor temporal resolution because of the assumption of a "frozen" ionosphere co-rotating with the Sun, However, the general ionospheric behavior may well be described with daily TEC maps. When generating several TEC maps per day, one has to expect at times unreasonable — very high or negative — TEC estimates in regions where no stations are located. One may avoid such problems by limiting the variations between consecutive TEC maps with "relative" a priori constraints between consecutive maps by adding "relative" pseudo-observations of the type

$$\Delta e_{ij} = e_{ij}(t_k) - e_{ij}(t_{k-1}) = 0 \quad \text{for} \quad k = 2, \ldots, n \tag{7}$$

to the system of normal equations stemming from actual observations. Note that the a priori sigmas $\sigma_{\Delta e_{ij}}$ used for the pseudo-observations Δe_{ij} do not affect the "absolute" TEC determinations. Optimal values for these sigmas have to be found experimentally. Due to the fact that we deal with *normalized* SH coefficients, we may simplify this problem by setting $\sigma_{\Delta e_{ij}} \approx \sigma_{\Delta e}$.

A series of 12 2-hourly TEC maps (taken at 01:00, 03:00, ... 23:00 UT) is shown in Figure 8a. The typical double-peak structure co-rotating with the Sun fairly well follows the geomagnetic equator, even when referring the TEC representation to a solar-geographic coordinate system. Nevertheless, Figure 8a indicates that a solar-geomagnetic reference frame is more appropriate.

The associated RMS maps shown in Figure 8b describe the formal accuracy of the TEC as a function of earth-fixed coordinates and basically reflect the station coverage. "Light" regions indicate small RMS (see, e. g., Europe or North America), "dark" regions mean large RMS (see, e. g., the region around the station O'Higgens, Antarctica). The ratio of the largest and smallest RMS is about 11. Such RMS maps may be included in IONEX files [Schaer et al., 1998].

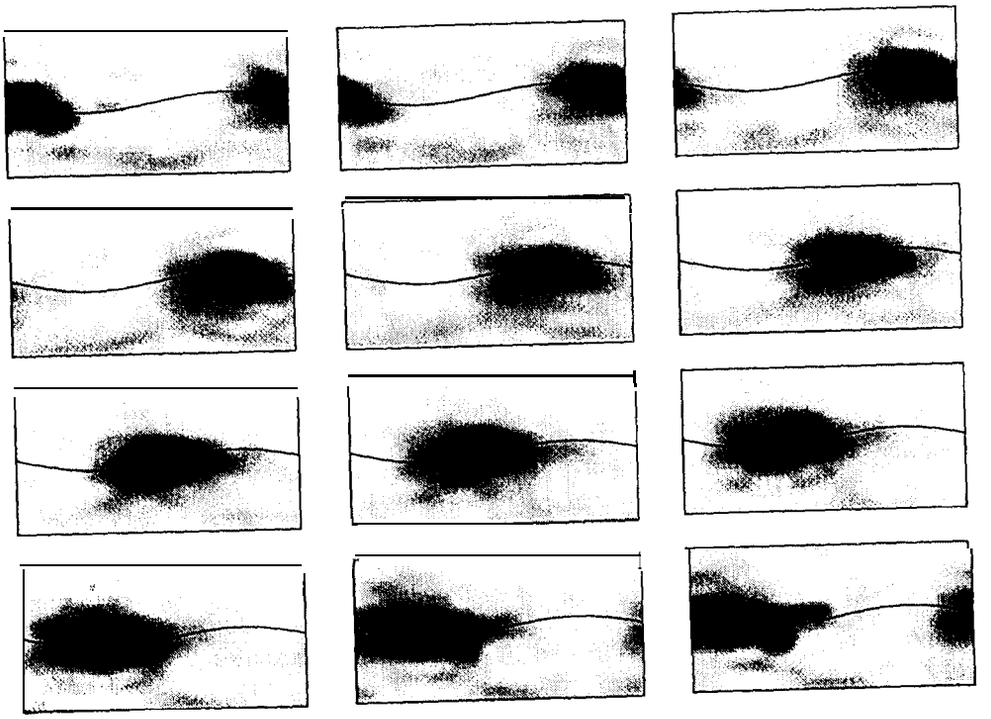

(a) TEC maps

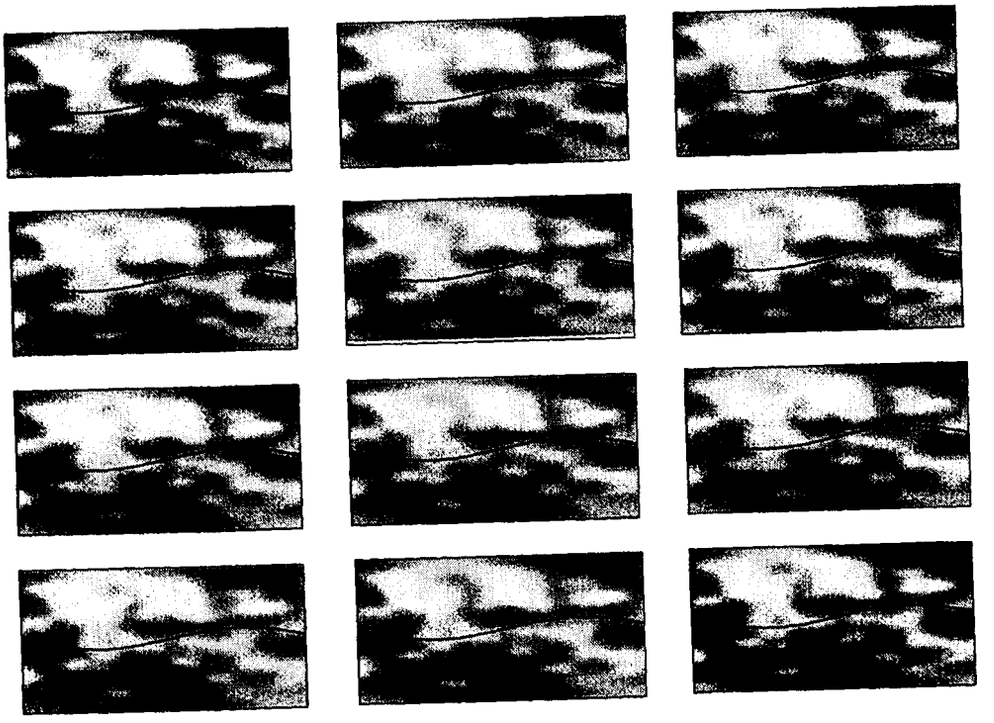

(b) RMS maps

Figure 8. 2-hourly TECand RMSmaps forday O17,1998

SUMMARY

The CODE Analysis Center produces global and European ionosphere maps by analyzing double-difference phase observations (using an interferometric processing technique) *and* phase-smoothed code observations (processing one-way observations) on a regular basis. Some changes were recently made in our processing scheme: The elevation cut-off angle was decreased from 20 to 10 degrees and at the same time the elevation-dependent observation weighting defining $\cos^2 z$ as weight on the zero-difference level, where z is the zenith distance, was activated. The maximum degree of the SH expansion was increased from 8 to 12 in order to be able to resolve smaller TEC structures like, e. g., the equatorial anomaly.

A higher temporal resolution when using SH expansions is possible by limiting the variations in time with slight '(relative" constraints between consecutive sets of SH coefficients. The 2-hour results obtained are very encouraging. The higher the temporal resolution, the less important it is whether a solar-geographic or a solar-geomagnetic reference frame is used.

Daily sets of differential code biases for the GPS satellites (and receivers) are estimated at CODE since October 1997. The day-today scatter of the satellite-specific DCBS is about 0.08 ns. Finally, an approach based on a least-squares collocation to predict global TEC was developed. Approaching the next solar maximum, the knowledge of the ionosphere becomes more and more import ant. The access to *fast* and *up-to-date* ionospheric information is required by many applications.

OUTLOOK

We will start to produce global ionosphere maps with a 2-hour resolution in the near future. Furthermore we intend to derive predicted ionosphere maps on a regular basis (e. g., 2-day predictions).

The generation of global maps statistically describing the fluctuations of the TEC as presented in [Schaer et al., 1996b] is planned. Reprocessing all global data since 1995 becomes more and more important in view of the progress made in the ionosphere modeling.

It is our declared goal to continuously map the ionosphere for (at least) the next period of high solar activity and to study in particular the impact of the ionosphere on the IGS core products. The establishment of a future IGS ionosphere product as discussed at the IGS AC Workshop in Darmstadt, Germany [Feltens and Schaer, 1998] is another reason to continue these efforts.

REFERENCES

Feltens, J. and S. Schaer, 1998, IGS Products for the Ionosphere, *Proceedings of the IGS AC Workshop,* Darmstadt, Germany, February 9-11, 1998.

Rothacher, M., G. Beutler, E. Brockmann, S. Fankhauser, W. Gurtner, J. Johnson, L. Mervart, S. Schaer, T. A. Springer, and R. Weber, 1996a, *The Bernese GPS Software Version 4.O,* September 1996, Astronomical Institute, University of Berne, Switzerland.

Rothacher, M., G. Beutler, E. Brockmann, L. Mervart, S. Schaer, T. A. Springer, U. Wild, A. Wiget, C. Boucher, and H. Seeger, 1996b, Annual Report 1995 of the CODE Analysis Center of the IGS, *1995 Annual Report of the IGS*, September 1996, IGS Central Bureau, JPL, Pasadena, CA, USA, pp. 151-173.

Schaer, S., G. Beutler, L. Mervart, M. Rothacher, and U. Wild, 1995, Global and Regional Ionosphere Models Using the GPS Double Difference Phase Observable, *Proceedings of the IGS Workshop on Special Topics and New Directions,* Potsdam, Germany, May 15-17, 1995, pp. 77-92.

Schaer, S., G. Beutler, M, Rothacher, and T. A. Springer, 1996a, Daily Global Ionosphere Maps Based on GPS Carrier Phase Data Routinely Produced by the CODE Analysis Center, *Proceedings of the IGS A C Workshop,* Silver Spring, MD, USA, March 19-21, 1996, pp. 181-192.

Schaer, S., M. Rothacher, T. A. Springer, and G. Beutler, 1996b, Mapping the Deterministic and Stochastic Component of the Ionosphere Using GPS, *EOS Transactions of the 1996 AGU Fall* Meeting, Vol. 77, No. 46, p. 142.

Schaer, S., W. Gurtner, and J. Feltens, 1998, IONEX: The Ionosphere Map EXchange Format Version 1, February 25, 1998, *Proceedings of the IGS AC Workshop,* Darmstadt, Germany, February 9–11, 1998.